HELLENIC REPUBLIC
UNIVERSITY OF IOANNINA
FACULTY OF SCIENCE
DEPARTMENT OF MATERIALS SCIENCE

Design and development of novel layered nanostructured hybrid materials for environmental, medical, energy and catalytic applications

Georgia Potsi

DOCTORAL THESIS

Ioannina, 2017

ΕΛΛΗΝΙΚΗ ΔΗΜΟΚΡΑΤΙΑ
ΠΑΝΕΠΙΣΤΗΜΙΟ ΙΩΑΝΝΙΝΩΝ
ΣΧΟΛΗ ΘΕΤΙΚΩΝ ΕΠΙΣΤΗΜΩΝ
ΤΜΗΜΑ ΜΗΧΑΝΙΚΩΝ ΕΠΙΣΤΗΜΗΣ ΥΛΙΚΩΝ

Ανάπτυξη και μελέτη καινοτόμων υβριδικών και σύνθετων υλικών με ανόργανες φυλλόμορφες νανοδομές

Γεωργία Πότση

ΔΙΔΑΚΤΟΡΙΚΗ ΔΙΑΤΡΙΒΗ

Ιωάννινα, 2017

HELLENIC REPUBLIC
UNIVERSITY OF IOANNINA
FACULTY OF SCIENCE
DEPARTMENT OF MATERIALS SCIENCE

Design and development of novel layered nanostructured hybrid materials for environmental, medical, energy and catalytic applications

Georgia Potsi

DOCTORAL THESIS

Ioannina, 2017

«Η έγκριση της διδακτορικής διατριβής από το Τμήμα Μηχανικών Επιστήμης Υλικών της Σχολής Θετικών Επιστημών του Πανεπιστημίου Ιωαννίνων δεν υποδηλώνει αποδοχή των γνωμών του συγγραφέα Ν. 5343/32, άρθρο 202, παράγραφος 2».

Ημερομηνία αίτησης της κ. Γεωργίας Πότση:21/09/2012

Ημερομηνία ορισμού Τριμελούς Συμβουλευτικής Επιτροπής: 28/09/2012 και 06/02/2013

Μέλη Τριμελούς Συμβουλευτικής Επιτροπής:

Επιβλέπων
Δημήτριος Γουρνής, Καθηγητής του ΤΜΕΥ του ΣΘΕ του Πανεπιστημίου Ιωαννίνων

Μέλη
Δημήτριος Γουρνής, Καθηγητής του ΤΜΕΥ του ΣΘΕ του Πανεπιστημίου Ιωαννίνων
Μιχαήλ Καρακασίδης, Καθηγητής του ΤΜΕΥ του ΣΘΕ του Πανεπιστημίου Ιωαννίνων
Αθανάσιος Μπουρλίνος, Επίκουρος Καθηγητής του τμήματος Φυσικής του Πανεπιστημίου Ιωαννίνων

Ημερομηνία ορισμού θέματος: 28/09/2012
Ανάπτυξη και μελέτη καινοτόμων υβριδικών και σύνθετων υλικών με ανόργανες φυλλόμορφες νανοδομές

ΔΙΟΡΙΣΜΟΣ ΕΠΤΑΜΕΛΟΥΣ ΕΞΕΤΑΣΤΙΚΗΣ ΕΠΙΤΡΟΠΗΣ : 28/11/2016

Δημήτριος Γουρνής,	Καθηγητής του ΤΜΕΥ της ΣΘΕ του Π.Ι.
Μιχαήλ Καρακασίδης	Καθηγητής του ΤΜΕΥ της ΣΘΕ του Π.Ι.
Αθανάσιος Μπουρλίνος	Επίκουρος Καθηγητής του Τμήματος Φυσικής του Π.Ι.
Petra Rudolf	Καθηγήτρια του Zernike Institute for Advanced Materials, RUG
Αλκιβιάδης Παϊπέτης	Καθηγητής του ΤΜΕΥ της ΣΘΕ του Π.Ι.
Χαράλαμπος Σταμάτης	Καθηγητής του Τμήματος Βιολογικών Εφαρμογών και Τεχνολογιών της Σχολής Επιστημών Υγείας του Π.Ι.
Αλέξιος Δούβαλης	Αν. Καθηγητής του Τμήματος Φυσικής του Π.Ι.

Έγκριση Διδακτορικής Διατριβής με βαθμό **«ΑΡΙΣΤΑ»** στις **21/12/2016**

Ο Πρόεδρος του Τμήματος

Καρακασίδης Μιχαήλ
Καθηγητής

Η Γραμματέας του Τμήματος

Ξανθή Τουτουνζόγλου

Date of application Mrs. Georgia Potsi, 21/09/2012

Date of appointing Three Membered Advisory committee: 28/09/2012 and 06/02/2013

Three Membered Advisory committee:

Supervisor

Dimitrios Gournis, Professor of Department of Materials Science & Engineering of the University of Ioannina

Members

Dimitrios Gournis, Professor of Department of Materials Science & Engineering of the University of Ioannina

Michael Karakassides, Professor of Department of Materials Science & Engineering of the University of Ioannina

Athanasios Bourlinos, Assistant Professor of The Physics Department of the University of Ioannina

Date of thesis definition: 28/09/2012

Design and development of novel layered nanostructured hybrid materials for environmental, medical, energy and catalytic applications

SEVEN MEMBERED COMMITTEE ASSIGNATION: 28/11/2016

Dimitrios Gournis	Professor of Department of Materials Science & Engineering, School of Natural Sciences of UOI
Michael Karakassidesς	Professor of Department of Materials Science & Engineering, School of Natural Sciences of UOI.
Athanasios Bourlinos	Assistant Professor of Physics Department, School of Natural Sciences of UOI
Petra Rudolf	Professor of Zernike Institute for Advanced Materials of RUG
Alkiviadis Paipetis	Professor of Department of Materials Science & Engineering, School of Natural Sciences of UOI.
Haralambos Stamatis	Professor of Department of Biological Applications and Technologies BAT, School of Medical Sciences of UOI
Alexios Douvalis	Associate Professor of Physics Department, School of Natural Sciences of UOI

Approval Dissertation with grade "EXCELLENT" on 21/12/2016

The President of the Department	**The Secretary of the Department**
Professor Karakasidis Michael	**Xanthi Toutounzoglou**

• Περίληψη

- Ο τομέας των φυλλόμορφων νανοδομημένων υβριδικών υλικών επικεντρώνεται κυρίως στη σύνθεση και στις πιθανές εφαρμογές υλικών που συνδυάζουν τις ιδιότητες των δομικών τους μονάδων σε κλίμακα νανομέτρων. Συνδυάζοντας αυτές τις δομικές μονάδες μπορούμε να βελτιώσουμε ή και να δημιουργήσουμε νέες ιδιότητες οι οποίες δεν ήταν παρούσες στα επιμέρους αρχικά μας υλικά. Στόχος της παρούσας διατριβής είναι ο σχεδιασμός και η ανάπτυξη ολιγοστρωματικών νανοδομημένων υβριδικών υλικών για περιβαλλοντικές, βιο-ιατρικές ενεργειακές και καταλυτικές εφαρμογές. Πιο συγκεκριμένα, στο πόνημα αυτό περιγράφεται η σύνθεση, ο χαρακτηρισμός και οι πιθανές εφαρμογές μια πληθώρας υλικών που έχουν σαν βάση αλλοτροπικές δομές του άνθρακα ή άλλα ανόργανα υλικά όπως οι φυλλόμορφοι άργιλοι.

- Το κεφάλαιο 3 περιγράφει την σύνθεση πολυλειτουργικών υποστυλωμένων υλικών τα οποία έχουν αναπτυχθεί μέσω της ενσωμάτωσης μορίων αμινοαδαμαντίνης στον ενδοστρωματικό χώρο οξειδίου του γραφίτη και φυλλόμορφων αργιλοπυριτικών αργίλων. Οι διάφορες τεχνικές χαρακτηρισμού που χρησιμοποιούνται αποδεικνύουν την επιτυχή ενσωμάτωση της αμινοαδαμαντίνης καθώς και ότι τα τελικά υποστυλωμένα υλικά παρουσιάζουν αυξημένη ειδική επιφάνεια. Επιπροσθέτως τα υβριδικά υλικά βρέθηκαν να έχουν σημαντική προσροφητική ικανότητα οργανικών ρύπων γεγονός που τα καθιστά κατάλληλα για χρήση σε περιβαλλοντικές εφαρμογές. Επιπλέον παρουσιάζουν βελτιωμένη κυτταροτοξική ικανότητα σε καρκινικά κύτταρα (A549) σε σχέση με υγιή κύτταρα (MRC-5) στα οποία η δράση τους είναι ελάχιστη γεγονός που τα καθιστά κατάλληλα να χρησιμοποιηθούν ως ανασταλτικοί παράγοντες ανάπτυξης σε βιο-ιατρικές εφαρμογές.

- Στο κεφάλαιο 4 περιγράφεται η χημική οξείδωση νανοδίσκων άνθρακα που έχουν παραχθεί βιομηχανικά μέσω της πυρολυτικής διαδικασίας Kværner Carbon Black & H_2 και ο σχηματισμός ενός υδρόφιλου αναλόγου. Περιγράφεται ο λεπτομερής χαρακτηρισμός τόσο του αρχικού όσο και του

οξειδωμένου υλικού καθώς και μελέτη των κυτταροτοξικών ιδιοτήτων του οξειδωμένου υλικού. Κατά την οξείδωση των νανοδίσκων επιτυγχάνεται ο διαχωρισμός τους από το μίγμα νανοδίσκων/νανοκώνων/καταλοίπων του αρχικού υλικού και η δημιουργία λειτουργικών ομάδων οξυγόνου (επόξυ-, υδρόξυ-, καρβόξυ-) στην επιφάνεια τους βελτιώνοντας την διαλυτότητα τους σε πολικούς διαλύτες ώστε να μπορούν να χρησιμοποιηθούν σε διάφορες εφαρμογές. Η μελέτη των κυτταροτοξικών ιδιοτήτων τους έδειξε ότι οι οξειδωμένοι νανοδίσκοι δρουν ως κυτταροτοξικοί παράγοντες και αποτελούν ένα πολλά υποσχόμενο υλικό για την ανάπτυξη νανο βιοκαταλυτικών συστημάτων.

- Στο κεφάλαιο 5 παρουσιάζεται μια ανασκόπηση διαφόρων πειραματικών μελετών πάνω στην σύνθεση και τις ιδιότητες νανοδομών άνθρακα που περιέχουν οργανικά-ανόργανα πολυεδρικά ολιγομερή σιλοξάνια (POSS) (cage-like). Στόχος είναι να τονιστεί η βελτίωση των φυσικοχημικών ιδιοτήτων που επιτυγχάνεται με προσθήκη τους επικεντρώνοντας στον αντίκτυπο που μπορεί να έχουν τα υβριδικά αυτά υλικά σε διάφορες τεχνολογικές εφαρμογές.

- Στο κεφάλαιο 6 αναφέρεται η ενσωμάτωση υποκατεστημένων κυβικών σιλοξανίων του σιδήρου (Fe^{+3}), σε νατριούχο μοντμοριλλονίτη καθώς και στο όξινα ενεργοποιημένο ανάλογό του με σκοπό την δημιουργία καινοτόμων καταλυτικών υποστυλωμένων δομών. Μια πληθώρα τεχνικών χαρακτηρισμού εφαρμόστηκε ώστε να αποδειχθεί η επιτυχής ενσωμάτωση των σιλοξανίων στις αργιλικές μήτρες καθώς και ο σχηματισμός υποστυλωμένων δομών μέσω τις θέρμανσης τους. Τα τελικά παραγόμενα υλικά βρέθηκαν να διαθέτουν μεγάλη ειδική επιφάνεια ενώ η παρουσία νανοσωματιδίων αιματίτη (α-FeO_3) επιβεβαιώθηκε μέσω της φασματοσκοπία Mössbauer. Καταλυτικές πειραματικές μετρήσεις έδειξαν ότι τα τελικά υβριδικά υλικά καταλύουν την αφυδάτωση της ισοπροπανόλης σε προπένιο και διισο-προπυλαιθέρα λόγω της μεγάλης ειδικής επιφάνειας και των ενεργών καταλυτικών κέντρων στην επιφάνεια τους ενώ η εκλεκτικότητα προς την διάσπαση της ισοπροπανόλης επηρεάζεται από στερεοχημικές παραμέτρους

- Στο κεφάλαιο 7 παρουσιάζεται η δημιουργία λεπτών ολιγοστρωματικών υμενίων υποκατεστημένων με μέταλλα (Cu^{2+} και Fe^{+3}) πολυεδρικών ολιγομερικών σιλοξανίων (POSS) μέσω της μεθόδου Langmuir –Schaefer ή με συνδυασμό της με τη μέθοδο αυτο-οργάνωσης (self-assembly) με τη χρήση μιας απλής τασιενεργής ένωσης όπως το αραχιδικό οξύ (AA). Ο χαρακτηρισμός με διάφορες τεχνικές απέδειξε την επιτυχή εναπόθεση των στρωμάτων της τασιενεργής με αποτέλεσμα την δημιουργία περιοδικών δομικών μονάδων που αποτελούνται αντίστοιχα από στρώματα αραχιδικού οξέος και υποκατεστημένων με μέταλλα (Cu^{2+} και Fe^{+3}) POSS. Επιπλέον, η ενδοστρωματική απόσταση μεταξύ των δομικών μονάδων εξαρτάται από την γεωμετρία και τον αριθμό ένταξης των μεταλλικών ιόντων. Επιπροσθέτως η σύγκριση των δύο πειραματικών πρωτοκόλλων σύνθεσης έδειξε ότι τα υβριδικά υμένια που έχουν εναποτεθεί με τη συνδυασμένη συνθετική διαδικασία που περιλαμβάνει το στάδιο της αυτό-οργάνωσης των μορίων οδηγούν σε καλύτερα οργανωμένες δομές.

Summary

The field of layered nanostructured hybrid materials focuses on the synthesis and possible applications of materials that combine the properties of building blocks of nanometer size dimensions. Bringing together the building blocks can enhance their properties or generate new properties not present in either of the constituents alone.

The aim of this thesis centred on layered nanostructured hybrid materials for environmental, medical, energy and catalytic applications, is to describe the synthesis, characterization and possible applications of a number of hybrid layered materials based on carbon allotropes or different inorganic matrices like clay minerals.

Chapter 3 presents the synthesis of multi-functional pillared layered materials synthesized by the intercalation of adamantylamine into the interlayer space of graphite oxide and layered aluminosilicate nanoclays. Different characterization techniques demonstrated the successful intercalation of adamantylamine and showed that the final pillared materials have an increased specific surface area. In addition these hybrids were found to be capable of adsorbing significant quantities of organic pollutants, which entails a great potential for environmental remediation applications. Moreover they were found to present improved cytotoxic activity on A549 cancer cells, whilst the cytotoxicity towards MRC-5 cells (normal) was minimal, a fact that renders them suitable as antiproliferative agents in biomedical applications.

Chapter 4 describes the chemical oxidation of carbon nanodiscs, industrially prepared via the so-called pyrolytic Kværner Carbon Black & H_2 process, towards the formation of a hydrophilic analogue. The detailed characterization of the pristine and the oxidized material is described and the study of the cytotoxic properties of the oxidized nanodiscs is reported. Besides resulting in the separation of carbon nanodiscs from the mixed nanodiscs/nanocones/soot starting material, the oxidation treatment causes the attachment of oxygen-containing functional groups (epoxy, hydroxyl and carboxyl groups) on the nanodisc surface, improving the solubility in polar solvents and thereby the use in various applications. The study of the cytotoxicity properties showed that the oxidized nanodiscs can act as cytotoxic agent and promises well for their future use in nanobiocatalytic systems.

Chapter 5 presents a review of various experimental studies of the synthesis and properties of carbon nanostructures containing organic-inorganic cage-like polyhedral oligomeric silsesquioxane (POSS) nanoparticles The aim is to illustrate the improvements of chemical and physical properties that can be achieved by the combination of POSS with different carbon nanostructures focusing on the potential impact of these hybrid nanostructures on various technological applications.

Chapter 6 reports the intercalation of iron substituted (Fe^{+3}) cubic silsesquioxanes in a sodium and an acid-activated montmorillonite to form novel catalytic pillared structures. A variety of characterization techniques was applied to prove the successful intercalation of the cubic silsesquioxanes into the clay matrices as well as the formation of pillared structures after calcination. The final pillared hybrids possess high specific area and contain α-Fe_2O_3 (hematite) nanoparticles as verified by Mössbauer spectroscopy. Catalytic measurements showed that the final hybrid pillared materials catalyse the conversion of isopropanol to diisopropylether and propene due to high specific area and presence of acid sites on the surface; the selectivity is affected by stereochemical parameters.

Chapter 7 presents the fabrication of metal (Cu^{2+} and Fe^{+3}) decorated POSS thin films via the Langmuir –Schaefer method or via a combination of this method with self-assembly, using a simple surfactant such as arachidic acid (AA). Characterization with different techniques proofed the successful deposition of the layers, leading to a periodically repeated AA-Metal (Cu^{2+} and Fe^{+3})-POSS-AA unit. Moreover the interlayer distance between the units was found to be affected by the coordination of the metal ions. Additionally, comparison of the two fabrication protocols showed that the hybrid films deposited following synthetic route involving self-assembly process lead to better ordered structures.

ΠΡΑΚΤΙΚΟ

της Επταμελούς Εξεταστικής Επιτροπής για την αναγόρευση σε διδάκτορα του Τμήματος Μηχανικών Επιστήμης Υλικών του Πανεπιστημίου Ιωαννίνων την κ. **Γεωργία Πότση.**

Η Γενική Συνέλευση Ειδικής Σύνθεσης (Γ.Σ.Ε.Σ) του Τμήματος Μηχανικών Επιστήμης Υλικών (ΤΜΕΥ) του Πανεπιστημίου Ιωαννίνων στη συνεδρίαση της αριθμ. **290/28.11.2016** ύστερα από την κρίση της Τριμελούς Συμβουλευτικής Επιτροπής ότι η ερευνητική εργασία της υποψηφίας διδάκτορος κ. **Γεωργίας Πότση** έχει ολοκληρωθεί και έχει κατατεθεί στο Τμήμα, όρισε σύμφωνα με το άρθρο 12 παρ.5 εδ. Β του Ν.2083/92, και το άρθ. 9 παρ.4 εδ. α του Ν. 3685/2008 Επταμελή Εξεταστική Επιτροπή που αποτελείται από τους κ.κ. **Δημήτριο Γουρνή** Καθηγητή του ΤΜΕΥ του Πανεπιστημίου Ιωαννίνων, **Μιχαήλ Καρακασίδη** Καθηγητή και Πρόεδρο του ΤΜΕΥ του Πανεπιστημίου Ιωαννίνων, **Petra Rudolf** Καθηγήτρια στο Zernike Institute for Advanced Materials του University of Groningen (Ολλανδίας), **Αλκιβιάδη Παϊπέτη** Καθηγητή του ΤΜΕΥ του Πανεπιστημίου Ιωαννίνων, **Χαράλαμπο Σταμάτη,** Καθηγητή του Τμήματος Βιολογικών Εφαρμογών και Τεχνολογιών του Πανεπιστημίου Ιωαννίνων, **Αλέξιο Δούβαλη** Αναπληρωτή Καθηγητή του Τμήματος Φυσικής του Πανεπιστημίου Ιωαννίνων, και **Αθανάσιο Μπουρλίνο** Επίκουρο Καθηγητή του Τμήματος Φυσικής του Πανεπιστημίου Ιωαννίνων, για να αναπτύξει ενώπιον της η υποψήφια διδάκτορας κ. **Γεωργία Πότση** τη διατριβή της με θέμα: **«Ανάπτυξη και μελέτη καινοτόμων υβριδικών και σύνθετων υλικών με ανόργανες φυλλόμορφες νανοδομές».**

Η Επταμελής Εξεταστική Επιτροπή, συνήλθε **σήμερα 21 Δεκεμβρίου 2016 ημέρα Τετάρτη και ώρα 15:00 μ.μ. στο χώρο του Νέου Κτιρίου του ΤΜΕΥ του Πανεπιστημίου Ιωαννίνων** για να εξετάσει την διδακτορική διατριβή της υποψηφίας διδάκτορος κ. **Γεωργίας Πότση**. Η Καθηγήτρια κ. Petra Rudolf συμμετείχε στην διαδικασία μέσω τηλεδιάσκεψης όπως είχε ενημερώσει με έγγραφό της (στον Πρόεδρο της Εξεταστικής Επιτροπής κ. Δ. Γουρνή).

Χρέη προέδρου της Εξεταστικής Επιτροπής ανέθεσαν τα μέλη της στον κ. **Δημήτριο Γουρνή,** Καθηγητή του Τμήματος Μηχανικών Επιστήμης Υλικών του Πανεπιστημίου Ιωαννίνων.

Στο σημείο αυτό, τίθεται υπόψη της 7μελούς Εξεταστικής Επιτροπής το αρθ. 36 του Ν.1268/82, τα άρθ. 12 και 13 του Ν. 2083/92 και το άρθ. 9 παρ.4 εδ. α του Ν. 3685/2008 και τα αρθ. 40 και 41 του Εσωτερικού Κανονισμού Λειτουργίας του

Πανεπιστημίου Ιωαννίνων (ΦΕΚ 310/10.03.05 τ. 2^{o}). Τα μέλη της Επιτροπής έλαβαν εγκαίρως (15 Δεκεμβρίου 2016) και μελέτησαν τη διατριβή της υποψήφιας.

Η υποψήφια κ. **Γεωργία Πότση** ανέπτυξε ενώπιον της Επιτροπής τη διατριβή της με θέμα: **«Ανάπτυξη και μελέτη καινοτόμων υβριδικών και σύνθετων υλικών με ανόργανες φυλλόμορφες νανοδομές»** τονίζοντας τα σημεία, στα οποία κατά τη γνώμη της η διατριβή είναι πρωτότυπη και αποτελεί συμβολή στην επιστήμη.

Τα μέλη της Εξεταστικής Επιτροπής απηύθυναν ερωτήσεις στην υποψήφια, μετά την προφορική ανάπτυξη απ' αυτήν του θέματος. Η ανάπτυξη και οι ερωτήσεις έγιναν σε δημόσια συνεδρίαση.

Στη συνέχεια το ακροατήριο και η υποψήφια αποχώρησαν και τα μέλη της Εξεταστικής Επιτροπής συσκέφθηκαν και ψήφισαν, υπέρ της παραδοχής της διατριβής, **με ψήφους επτά (7) και κατά μηδέν (0).**

Πρότειναν, δε, με ψήφους έξι (7) έναντι μηδενός (0) το βαθμό **Άριστα** εφαρμόζοντας την παρ. 6 του αρθ. 40 του Εσωτερικού Κανονισμού Λειτουργίας του Πανεπιστημίου Ιωαννίνων (ΦΕΚ 310/10.03.05 τ. 2^{o}).

Το παρόν πρακτικό μετά την υπογραφή του από τα υπόλοιπα μέλη της Επταμελούς Εξεταστικής Επιτροπής αποσταλεί ταχυδρομικώς στην Καθηγήτρια Petra Rudolf για την έγκριση και τη σύμφωνη γνώμη της.

Ιωάννινα, 21 Δεκεμβρίου 2016

Η Εξεταστική Επιτροπή

1. **Δημήτριος Γουρνής**, Καθ. του ΤΜΕΥ του Παν/μίου Ιωαννίνων
2. **Μιχαήλ Καρακασίδης**, Καθ. του ΤΜΕΥ του Παν/μίου Ιωαννίνων
3. **Petra Rudolf**, Καθ. στο Zernike Inst. for Adv. Mater. του University of Groningen Petra Rudolf
4. **Χαράλαμπος Σταμάτης**, Καθ. του Τμ. Βιολ. Εφ. Τεχν. του Παν/μίου Ιωαννίνων
5. **Αλκιβιάδης Παϊπέτης**, Καθ. του ΤΜΕΥ του Παν/μίου Ιωαννίνων
6. **Αλέξιος Δούβαλης**, Αναπλ. Καθ. του Τμ. Φυσικής του Παν/μίου Ιωαννίνων
7. **Αθανάσιος Μπουρλίνος**, Επικ. Καθ. του Τμ. Φυσικής του Παν/μίου Ιωαννίνων

UNIVERSITY OF IOANNINA

university of groningen

Contract double Ph.D. degree *(dubbelpromotie)*

Between

The University of Groningen (*Rijksuniversiteit Groningen*),
Broerstraat 5, 9712 CP Groningen, the Netherlands,
Hereinafter referred to as **UoG**
represented by Prof. Dr. S. Poppema, President

and

the University of Ioannina,
Department of Materials Science and Engineering (DMSE), University Campus, 45110 Ioannina, Greece.
represented by Prof. Dr. M. A. Karakassides, President/Department Chair of DMSE

jointly referred to as **'the partner institutions'**

In conformity with the rules and regulations for PhD degrees at both institutions.
For the University of Groningen:

- The Dutch Higher Education and Research Act (*Wet op het hoger onderwijs en wetenschappelijk onderzoek*)
- The Ph.D. Regulations of the University of Groningen (*Promotiereglement*)

For the University of Ioannina:

- The Internal Regulation of the University of Ioannina (FEK 310/10.03.2005)
- The Ph.D. Regulations of the Department of Materials Science and Engineering of University of Ioannina.

PART I: Administrative matters

Article 1

The Ph.D. candidate to whom this contract pertains is

Georgia Potsi
born **11/4/1982**
Nationality: **Greek**

The University of Groningen and the University of Ioannina agree to register Ms **Georgia Potsi** as a Ph.D. candidate, under joint supervision of the University of Groningen and the University of Ioannina.

Article 2
The Ph.D. candidate is supervised by

1. Prof. Dr. Petra Rudolf
University of Groningen
Zernike Institute for Advanced Materials
Faculty of Mathematics and Natural Sciences

2. Prof. Dr. Dimitrios Gournis
University of Ioannina
Department of Materials Science and Engineering (DMSE)

Article 3
The enrolment of the Ph.D. candidate is effective from **1/10/2012.** The expected period of research is set to 4 years; therefore, the Ph.D. thesis is expected to be submitted to the manuscript committee by **30/9/2016.** This period can only be extended in exceptional cases, after a favourable opinion given by the partner institutions and on proposition by the Ph.D. supervisors. This proposition must be introduced 3 months before the expected date of the Ph.D. thesis submission set above.

Article 4
The University of Groningen and the University of Ioannina will instruct the Ph.D. candidate to register at both institutions.

Article 5
The University of Groningen and the University of Ioannina will instruct the Ph.D. candidate to arrange insurance coverage, which is valid in both the Netherlands and in Greece. The candidate is responsible for insuring herself for all foreseen and unforeseen healthcare expenses, as well as arranging personal liability insurance.

PART II: Research supervision and thesis preparation

Article 6
Both universities recognize the validity of the research project undertaken by the Ph.D. candidate. All rules of the University of Groningen pertaining to scientific publications are in force.

Article 7
1. The theme of the dissertation is: **Design and Development of Novel Layered Nanostructured Hybrid Materials for Environmental, Medical, Energy and Catalytic Applications**

2. The dissertation will be written in English. A summary of the dissertation will be written in English and Dutch.

3. Both partner institutions will instruct the doctoral candidate to follow the rules of both institutions concerning the registering, the description and the reproduction of the thesis.

Article 8

1. Prof. Dr. Petra Rudolf is designated as Ph.D. supervisor. She is appointed as a Professor at the University of Groningen. Prof. Dr. Dimitrios Gournis, appointed as a Professor at the University of Ioannina, is designated as Ph.D. supervisor.
2. The supervisors will consult regularly on the research progress of the doctoral candidate. The supervision is equally divided between both institutions. Each institute will invest 50% of the allotted time for supervision. The daily supervision and scientific mentoring resides with the supervisor located where the research work is being undertaken at that particular moment.

Article 9

The research project will be carried out at both institutions following a plan, which can be found in the attached appendix; the plan is jointly approved by the two Ph.D. supervisors. Any modification of this plan must be submitted to the two institutions by the two Ph.D. supervisors at least one month in advance.

Article 10

1. The intellectual property rights of the thesis, the publication, the use and protection of the research results shall be safeguarded in accordance with the specific regulations of both institutions.

2. Foreground intellectual property rights shall be the property of both institutions. The institutions shall jointly apply to obtain and/or maintain the relevant intellectual property rights and shall strive to set up appropriate agreements in order to do so.

PART III: Evaluation and conferral of degree

Article 11

The authorisation of the thesis submission is given by the University of Groningen, in accordance with Dutch regulations. The Assessment Committee and the Examining Committee are designated by the legal authorities of the University of Groningen.

Article 12

1. After the positive assessment of the Ph.D. supervisors, the thesis can be submitted to the Assessment Committee.

2. The Assessment Committee consists of four persons. Only full professors employed by a university who have not co-authored with the doctoral candidate may be members of the Assessment Committee.

3. The Assessment Committee consists at least of one professor from the University of Groningen and at least one professor from the University of Ioannina.

4. The Assessment Committee shall be composed by mutual consent between the partner institutions, in accordance with the regulations in force at the partner institutions.

Article 13

1. After the positive assessment of the Assessment Committee, the thesis can be submitted to the Examining Committee.

2. The Examining Committee shall consist of at least five persons;
   - full professors, from the University of Groningen, the University of Ioannina and from other universities;
   - a maximum of 2 University Readers/Associate Professors or Lecturers/Assistant Professors with Ph.D.;
   - the members of the Assessment Committee;
   - the chair.

   The supervisors are not members of the PhD Examining Committee.

3. The Examining Committee shall be composed by mutual consent between the partner institutions, in accordance with the regulations in force at the partner institutions.

Article 14

1. The Examining Committee allows the doctoral candidate to publically defend her thesis after a positive assessment by the Assessment Committee.

2. The thesis will be defended, in English, during a public ceremony at the University of Groningen. After the Examining Committee has given a favourable recommendation, the University of Groningen will confer upon the candidate the doctorate degree of the University of Groningen and the doctoral certificate affixed with the Great Seal of the University.

3. A short seminar on the thesis, presented in English, will be given by the candidate at the University of Ioannina. This seminar will allow the Ph.D. candidate to demonstrate mastery of her research subject to the faculty of the University of Ioannina. The University of Ioannina will then confer upon the candidate the doctorate degree of the University of Ioannina.

4. The conferral of the doctoral doctorate degree of the University of Ioannina shall occur subsequent to, and in a separate ceremony from, the conferral of the doctorate degree of the University of Groningen.

5. The University of Groningen will award the degree Doctor *(translated into English as: Doctor of Philosophy (PhD))*. The University of Ioannina will award the degree of Doctor in Materials Science and Engineering.

6. Each University will issue its own degree certificate, which will mention the joint nature of the supervision by the partner institutions, leading to the award of a double doctorate.

Article 15

The present agreement holds as long as necessary for the completion of the doctorate-/Ph.D. degree. The agreement may be reviewed on an annual basis by each institution and may be terminated if good reason is found to do so. In addition, the agreement may be termination the initiative of the Ph.D. candidate or following collegial advice from the Ph.D. supervisors. As long as the agreement is in force the institutions commit themselves to supporting the Ph.D. candidate in continuing the project.

Groningen, 14-9-2015

Prof. Dr. Sibrand Poppema
The President of
the University of Groningen

Ioannina,

Prof. Dr. Michael Karakassides.
Department Chair of DMSE
University of **Ioannina**

Petra Rudolf

Prof. Dr. Petra Rudolf
First thesis supervisor
University of Groningen

Prof. Dr. Dimitrios Gournis
Second thesis supervisor
University of **Ioannina**

Visa:
Ms Georgia Potsi
The Ph.D. candidate

Keep Ithaka always in your mind.

Arriving there is what you’re destined for.

But don’t hurry the journey at all.

Better if it lasts for years,

so you’re old by the time you reach the island,

wealthy with all you’ve gained on the way,

not expecting Ithaka to make you rich.

Ithaka gave you the marvelous journey.

Without her you wouldn't have set out.

She has nothing left to give you now.

And if you find her poor, Ithaka won’t have fooled you.

Wise as you will have become, so full of experience,

you’ll have understood by then what these Ithakas mean..

By C. P. CAVAFY

Translation by E.Keele

Contents

CHAPTER 1

Introduction

1.1. Motivation

This thesis represents part of my research efforts aiming at the generation of new knowledge on the functionalization of carbon nanodiscs as well as the intercalation of graphene oxide and clays using a simple diamondoid derivative or polyhedral oligomeric silsesquioxanes (POSS).

The thesis also contains a study on fabrication of new complex materials by the Langmuir-Schaefer method based on metal decorated POSS.

The target of this work was the design and development of novel layered nanostructured hybrid materials for environmental, medical, energy and catalytic applications.

1.2. Graphene, Graphite oxide and carbon nanodiscs

1.2.1. Graphene

Graphene is a one-atom-thick sp^2-bonded carbon 2D sheet consisting of carbon atoms tightly packed into a planar two-dimensional hexagonal lattice. It possesses exceptional properties, which differ from those of all the other carbon allotropes discovered so far. Its extraordinary electron mobility, combined with its high thermal and mechanical stability, chemical inertness, large surface area, elasticity and the possibility to modify electrochemically its electronic structure,[1][2][3] place graphene at the top of the list of candidates for the development of new nanomaterials for a plethora of applications including molecular electronics, biosensors, environmental sensors and energy storage nanodevices.[4][5][6][7][8] Graphene can be produced by five basic methods; reduction of graphene oxide, liquid exfoliation of graphite, chemical vapor deposition using a carbon source, growth by heating silicon carbide and mechanical cleavage of graphite.[9]

1.2.2. Graphene oxide

Graphite oxide (GO) is an oxygen rich derivative of graphite decorated with hydroxyl, epoxy, and carboxyl groups (sp^3-oxo moieties).[10][11][12] These functional groups are created by strong oxidation and distributed randomly on the basal planes and edges of the GO sheets, generating aliphatic regions (sp^3 - carbon atoms) within the sp^2-hybrized matrix, as illustrated in Figure 1.1. Due to the existence of such hydrophilic moieties, GO can swell and can be intercalated with various moieties. Both GO and intercalated GO are being considered for numerous applications such as supercapacitors,[13] high mobility transistors,[14] lithium batteries,[15] hydrogen storage, adsorption of organic moieties[16] removal of pollutants from aqueous solutions and in biomedical applications.[8] In our experiments, we chose to use a chemical preparation approach since allows the production of product in comparatively large scale and low cost. As oxidation method we decided to use Staudenmaier method because it is a milder oxidative procedure comparing to Brodie or Hummers-Offeman methods. Moreover, Staudenmaier method leads to the formation of higher amount of distributed epoxy than carboxyl and hydroxyl groups on the surface of the graphene oxide nanosheets. The presence of these epoxy groups favor the reactions with amine ending moieties that are used for the synthesis of the hybrid materials presented in this thesis at ambient conditions.[17][18]

1.2.3. Carbon nanodiscs

Carbon nanodiscs (CNDs) are a new bottom-up prepared carbon nanomaterial with well-defined size on the micron scale. They are ultra-thin quasi two-dimensional particles with diameter 1-4 μm and thickness, typically in the range 10–30 nm.[19] They are produced through the so-called pyrolytic Kværner Carbon Black & H_2 (CB&H) Process,[20] where hydrocarbons (typically heavy oil) are decomposed to carbon and H_2 based on the use of an industrial-scale carbon-arc plasma torch generator operating at a temperature around 2000 ^oC. CNDs are considered a promising material in various engineering aspects due to their exceptional electrochemical properties.[21]

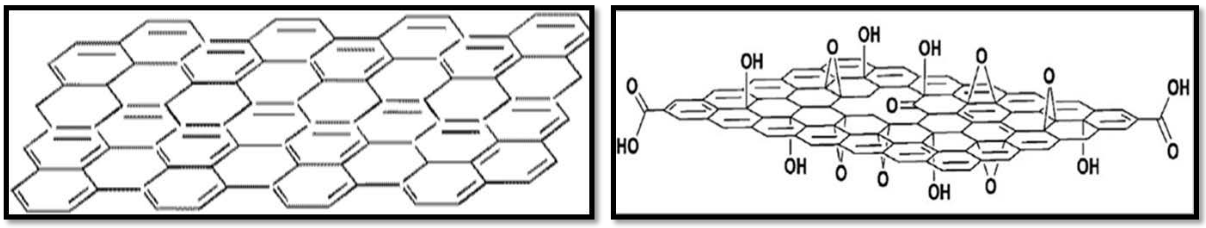

Figure 1.1. Schematic representation of graphene and graphene oxide structure

1.3. Clays

Natural clays are the product of weathering of rocks, which make up 40 % of the earth crust. They are phyllosilicates and consist of silicon oxygen tetrahedra and aluminum oxygen octhaedra[22] as sketched in Figure 1.2. Clays are used in a variety of industrial applications[23] as absorbents,[23] pharmaceutical additives,[24][25] in fertilizers,[26] as drilling fluids in oil drilling,[27] in cosmetics[28] *etc*. The most important properties of clays are

isomorphic substitution, *i.e*. the possibility for ions of smaller valence to substitute ions of the clay platelets;

cation exchange capacity, which is the total capacity of a soil to hold exchangeable cations;

ability to swell when dispersed in polar solvents, a reversible process, which is determined by their charge density;

porosity which is affected by the drying process after dispersion;

and finally the Brønsted and Lewis acidity, present due to the active acid sites on the clay platelets.[29]

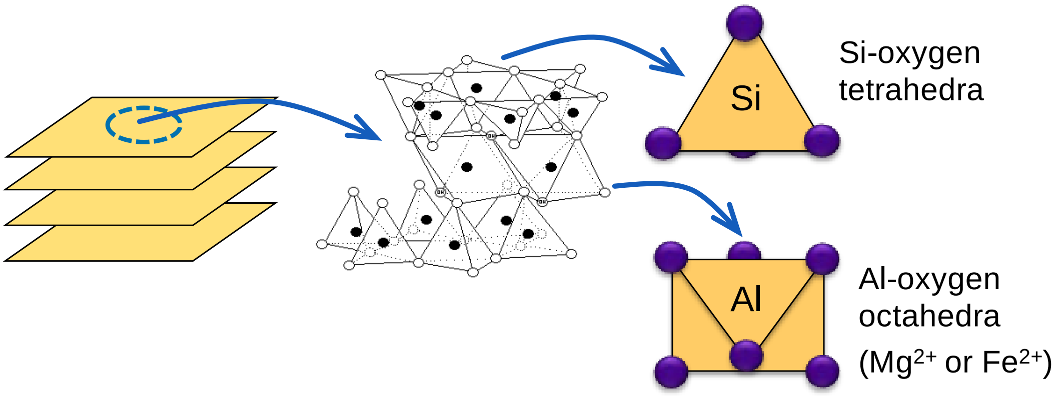

Figure 1.2. Schematic representation of the clay structure

1.3.1. Pillared Clays

The main disadvantage of clays is their lack of permanent porosity. A normal clay swells upon hydration but its interlayer shrinks again after dehydration. To create a structure in which the platelets are kept permanently at a certain distance, clays can be pillared with a variety of pillaring species such as organic cations (organo-clays), organometallic pillars, metal oxide sols (*e.g.* imogolite), metal complexes, polyoxocations and mixed pillaring species[30][31] as schematically shown in Figure 1.3. The produced pillared structures can be used in numerous applications such as in catalysis,[32] in biomedicine,[8] in environmental remediation[33] *etc*.

1.4. Polyhedral oligosilsesquioxanes (POSS)

Silsesquioxanes belong to the family of silicone resins.[34] They are described with the general formula $RSiO_{3/2}$ tend to form three dimensional (3D) cage-like highly symmetric frameworks known as polyhedral oligosilsesquioxanes (POSS). Several structures are known for silsesquioxanes, including random, ladder, partially condensed and cage (*e.g*. T8, T10 and T12) types.[35] These cubic, hexagonal,

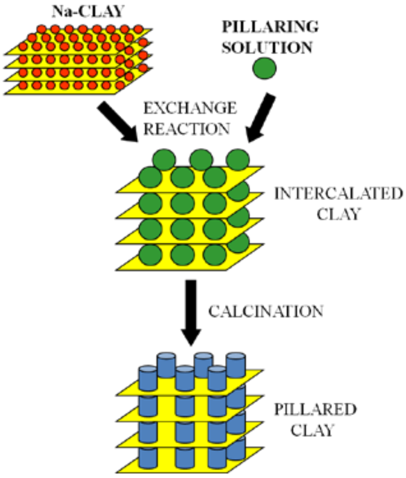

Figure 1.3. Schematic representation of pillaring procedure.

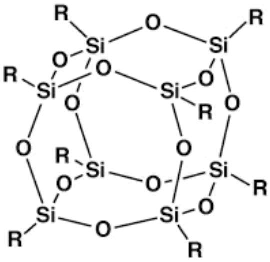

Figure 1.4. Molecular structure of a cubic polyhedral oligomeric silsesquioxane (POSS).

octagonal, decagonal, dodecagonal or even open cage like structure are derived from hydrolytic condensation reactions of trifunctional organosilicon monomers.[36] The example of a cubic POSS is shown in Figure 1.4.

Polyhedral oligomeric silsesquioxanes appear as highly promising candidates for the synthesis of hybrid nanomaterials suitable for a wide range of applications such as for polymer nanocomposites;[37] in catalysis;[38] energy storage;[39][40] environmental applications[41] and biomedicine.[42][43][44]

1.5. Langmuir Blodgett/Langmuir Schaefer techniques

The Langmuir–Blodgett (LB) technique that was introduced by Langmuir and Blodgett (yielding Irving Langmuir the Nobel prize in Chemistry in 1932), is a useful tool to prepare thin molecular films, ranging from one to several tens or even hundreds of molecular layers.[45] In general, it is applied to amphiphilic molecules where a polar (hydrophilic) and a non-polar (hydrophobic) part is present.[46] These molecules can form stable Langmuir films at the air/water interface, which can subsequently be transferred onto chosen substrates.[47][48] The deposition of the LB films takes place in a water trough equipped with moving barriers. The amphiphilic molecules (surfactants) are spread on the water surface, whereupon the hydrophilic part stays in contact with the water surface while the hydrophobic part points away from the water surface, thus preventing the molecules from dissolving. Then the barriers of the trough are closed, forcing the molecules to change from a 2D gas state at the air/water interface first to the liquid and finally the solid phase. During this compression the surface pressure is increased while the area per molecule is decreasing, as shown in Figure 1.5. When the solid phase is reached and stabilized, a substrate is dipped onto the surface vertically and the molecules are deposited on both sides of the substrate. In 1938 Schaefer introduced a variation of the technique where the dipping of the substrate is horizontal, known as Langmuir Schaefer method (LS). LB and LS techniques enable the fabrication of single molecule films with control over the packing density of molecules. They also enable the creation of multilayer structures with varying layer composition.

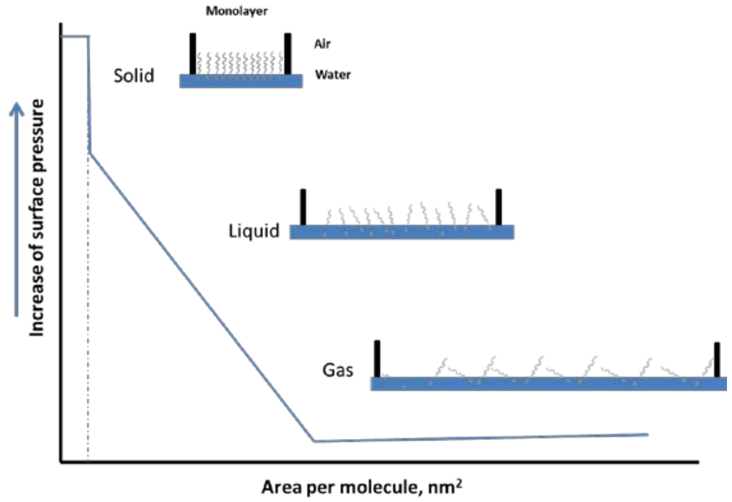

Figure 1.5. Surface pressure versus area isotherm (schematic curve).

1.6. Outline of the thesis

The research work described in this thesis is organized in seven chapters as follows:

Chapter 2 describes the experimental techniques that were used to prepare and to characterize the studied materials; the methods employed to determine possible future applications for the produced materials are also illustrated.

Chapter 3 reports the synthesis of multi-functional pillared layered materials synthesized by intercalation of cage-shaped adamantylamine molecules into the interlayer space of graphite oxide and layered aluminosilicate nanoclays. The produced hybrid materials were characterized for what concerns their structure and composition; they were found to exhibit an antiproliferative activity for cells, as well as a high adsorption power for small organic pollutants from aqueous solutions.

Chapter 4 presents the oxidation of carbon nanodiscs towards the formation of a hydrophilic analogue, the detailed characterization of the pristine and produced material as well as a study of the cytotoxicity properties of the final product.

Chapter 5 is dedicated on our review article ‘’Carbon Nanostructures Containing Polyhedral Oligomeric Silsesquioxanes (POSS)’’ giving an overview of the synthesis and properties of carbon nanostructures containing organic-inorganic cage-like polyhedral oligomeric silsesquioxane (POSS) nanoparticles.

Chapter 6 describes the intercalation of iron-decorated POSS in natural and in acid activated clays, the characterization of the pristine and produced pillared materials as well as a study of their catalytic properties in the decomposition of isopropanol.

Finally, Chapter 7 reports the fabrication of metal (iron and copper) decorated POSS thin films. The LS films were produced using either the Langmuir –Schaefer method or a combination of this method with self-assembly.

References

[1] H. Seo, S. Ahn, J. Kim, Y.-A. Lee, K.-H. Chung, K.-J. Jeon, *Scientific Reports* **2014**, *4*, 5642.

[2] J. Ye, M. F. Craciun, M. Koshino, S. Russo, S. Inoue, H. Yuan, H. Shimotani, A. F. Morpurgo, Y. Iwasa, *Proceedings of the National Academy of Sciences of the United States of America* **2011**, *108*, 13002–13006.

[3] P. Zygouri, G. Potsi, E. Mouzourakis, K. Spyrou, D. G. and P. Rudolf, *Current Organic Chemistry* **2015**, *19*, 1791–1799.

[4] C.-H. Lu, H.-H. Yang, C.-L. Zhu, X. Chen, G.-N. Chen, *Angewandte Chemie International Edition* **2009**, *48*, 4785–4787.

[5] K. Chen, Z.-L. Zhang, Y.-M. Liang, W. Liu, *Sensors (Basel, Switzerland)* **2013**, *13*, 6204–6216.

[6] Q. Wu, Y. Xu, Z. Yao, A. Liu, G. Shi, *ACS Nano* **2010**, *4*, 1963–1970.

[7] Y. Wang, Z. Shi, Y. Huang, Y. Ma, C. Wang, M. Chen, Y. Chen, *The Journal of Physical Chemistry C* **2009**, *113*, 13103–13107.

[8] K. Spyrou, G. Potsi, E. K. Diamanti, X. Ke, E. Serestatidou, I. I. Verginadis, A. P. Velalopoulou, A. M. Evangelou, Y. Deligiannakis, G. Van Tendeloo, et al., *Advanced Functional Materials* **2014**, *24*, 5841–5850.

[9] T. Zhang, J. Liu, C. Wang, X. Leng, Y. Xiao, L. Fu, *Biosensors and Bioelectronics* **2017**, *89*, 28–42.

[10] A. Lerf, H. He, M. Forster, J. Klinowski, *The Journal of Physical Chemistry B* **1998**, *102*, 4477–4482.

[11] N. I. Kovtyukhova, P. J. Ollivier, B. R. Martin, T. E. Mallouk, S. A. Chizhik, E. V Buzaneva, A. D. Gorchinskiy, *Chemistry of Materials* **1999**, *11*, 771–778.

[12] N. I. Kovtyukhova, B. R. Martin, J. K. N. Mbindyo, P. A. Smith, B. Razavi, T. S.

Mayer, T. E. Mallouk, *The Journal of Physical Chemistry B* **2001**, *105*, 8762–8769.

[13] H.-K. Jeong, M. Jin, E. J. Ra, K. Y. Sheem, G. H. Han, S. Arepalli, Y. H. Lee, *ACS Nano* **2010**, *4*, 1162–1166.

[14] P. K. Ang, S. Wang, Q. Bao, J. T. L. Thong, K. P. Loh, *ACS Nano* **2009**, *3*, 3587–3594.

[15] A. Kumar, A. L. M. Reddy, A. Mukherjee, M. Dubey, X. Zhan, N. Singh, L. Ci, W. E. Billups, J. Nagurny, G. Mital, et al., *ACS Nano* **2011**, *5*, 4345–4349.

[16] W. Lv, D.-M. Tang, Y.-B. He, C.-H. You, Z.-Q. Shi, X.-C. Chen, C.-M. Chen, P.-X. Hou, C. Liu, Q.-H. Yang, *ACS Nano* **2009**, *3*, 3730–3736.

[17] H. L. Poh, F. Sanek, A. Ambrosi, G. Zhao, Z. Sofer, M. Pumera, *Nanoscale* **2012**, *4*, 3515–3522.

[18] M. Ciszewski, A. Mianowski, *CHEMIK* **2013**, *67*, 267–274.

[19] T. Garberg, S. N. Naess, G. Helgesen, K. D. Knudsen, G. Kopstad, A. Elgsaeter, *Carbon* **2008**, *46*, 1535–1543.

[20] S. Lynum, J. Hugdahl, K. Hox, R. Hildrum, M. Nordvik, **2008 (patent).**

[21] J. G. S. Moo, M. Pumera, *RSC Advances* **2012**, *2*, 1565–1568.

[22] S. B. Hendricks, *The Journal of Geology* **1942**, *50*, 276–290.

[23] H. H. Murray, *Applied Clay Science* **2000**, *17*, 207–221.

[24] M. I. Carretero, M. Pozo, *Applied Clay Science* **2009**, *46*, 73–80.

[25] A. López-Galindo, C. Viseras, P. Cerezo, *Applied Clay Science* **2007**, *36*, 51–63.

[26] S. Komarneni, B. L. Newalkar, D. Li, T. Gheyi, C. L. Lopano, P. J. Heaney, J. E. Post, *Journal of Porous Materials* **2003**, *10*, 243–248.

[27] P. W. Fischer, J. F. Cook, **1951** (**book**).

[28] M. I. Carretero, M. Pozo, *Applied Clay Science* **2010**, *47*, 171–181.

[29] F. Bergaya, G. Lagaly, in *Handbook of Clay Science* (Ed.: B.K.G.T. and G.L.B.T.-D. in C.S. Faïza Bergaya), Elsevier, **2006**, pp. 1–18*18* **(book section).**

[30] W. Jones, *Catalysis Today* **1988**, *2*, 357–367.

[31] F. Figueras, *Catalysis Reviews* **1988**, *30*, 457–499.

[32] A. K. Ladavos, P. N. Trikalitis, P. J. Pomonis, *Journal of Molecular Catalysis A: Chemical* **1996**, *106*, 241–254.

[33] A. Gil, L. M. Gandia, M. A. Vicente, Catalysis Reviews **2000**, 42, 145–212.

[34] Y. Kaneko, E. B. Coughlin, T. Gunji, M. Itoh, K. Matsukawa, K. Naka, *International Journal of Polymer Science*, ***2012*****,** (***book section 2pages).***

[35] D. B. Cordes, P. D. Lickiss, F. Rataboul, *Chemical Reviews* **2010**, *110*, 2081–2173.

[36] R. H. Baney, M. Itoh, A. Sakakibara, T. Suzuki, *Chemical Reviews* **1995**, *95*, 1409–1430.

[37] K. S. Meenakshi, E. P. J. Sudhan, S. A. Kumar, M. J. Umapathy, *Silicon* **2011**, *3*, 45–52.

[38] A. Maiti, R. H. Gee, R. Maxwell, A. P. Saab, *Chemical Physics Letters* **2007**, *440*, 244–248.

[39] H.-J. Sun, Y. Tu, C.-L. Wang, R. M. Van Horn, C.-C. Tsai, M. J. Graham, B. Sun, B. Lotz, W.-B. Zhang, S. Z. D. Cheng, *Journal of Materials Chemistry* **2011**, *21*, 14240–14247.

[40] A. Gomathi, K. Gopalakrishnan, C. N. R. Rao, *Materials Research Bulletin* **2010**, *45*, 1894–1898.

[41] W.-B. Zhang, Y. Tu, H.-J. Sun, K. Yue, X. Gong, S. Z. D. Cheng, *Science China Chemistry* **2012**, *55*, 749–754.

[42] D. J. Clarke, J. G. Matisons, G. R. Simon, M. Samoc, A. Samoc, *Applied Organometallic Chemistry* **2008**, *22*, 460–465.

[43] A. Tan, S. Y. Madani, J. Rajadas, G. Pastorin, A. M. Seifalian, *Journal of Nanobiotechnology* **2012**, *10*, 1–8.

[44] X. Shen, Y. Cui, Y. Pang, H. Qian, *Electrochimica Acta* **2012**, *59*, 91–99.

[45] C. P. L. Rubinger, R. L. Moreira, B. R. A. Neves, L. A. Cury, C. A. Ferreira, A. Meneguzzi, *Synthetic Metals* **2004**, *145*, 147–151.

[46] S. A. Hussain, *Journal of Science Forum* **2010**, *Vol 1 No.*, 23–34.

[47] G. G.Roberts, *Langmuir- Blodgett Films*, Springer Science+Business Media New York, **1990**.

[48] R. Y. N. Gengler, D. Gournis, A. H. Aimon, L. M. Toma, P. Rudolf, *Chemistry – A European Journal* **2012**, *18*, 7594–7600.

CHAPTER 2

Experimental Techniques

2.1. Preparation of host layered materials

2.1.1. Graphene oxide (Chapter 3)

Graphene oxide was produced from graphite powder using a modified Staudenmaier's method.[1][2] In a typical synthesis, 10 g of powdered graphite (purum, powder ≤ 0.2 mm; Fluka) were added to a mixture of concentrated sulphuric acid (400 mL, 95–97 wt%) and nitric acid (200 mL, 65 wt%) while cooling in an ice-water bath. Potassium chlorate powder (200 g, purum, >98.0%; Fluka) was added to the mixture in small portions while stirring and cooling. The reactions were quenched after 18 hs by pouring the mixture into distilled water and the oxidation product washed until a pH 6. The sample was then dried at room temperature.

2.1.2. Natural and Synthetic Clays (Chapters 3 and 6)

The clay used in the study reported in Chapter 3 was a natural Wyoming montmorillonite **(SWy-2)** obtained from the Source Clay Minerals Repository, University of Missouri, Columbia, with a cation exchange capacity (CEC) of 78 meq/100 g clay. The clay was fractionated to < 2 μm by gravity sedimentation and purified by standard methods in clay science.[3]A sodium-exchanged sample (Na^+-SWy-2) was prepared by immersing the clay in an aqueous solution of sodium chloride (1N). The cation exchange was completed by washing and centrifuging three times with the NaCl solution. The sample was finally washed with distilled deionized water and transferred into dialysis tubes in order to obtain chloride-free clay and then dried at room temperature. A synthetic trioctahedral hectorite, Laponite RD (Lap), produced by Laporte Industries Ltd., with structural formula $Na_{0.8}[Mg_{5.4}Li_{0.4}]Si_8O_{20}(OH)_4$, a CEC of 48.1 meq/100 g clay and average particle size of 20 nm was used for the cytotoxic measurements. The clay used in Chapter 6 was a natural Texas montmorillonite **(STx-1),** with a cation exchange capacity (CEC) equal to

80 mequiv/100g clay and particle size ≤ 2 μm, obtained from the Source Clay Minerals Repository at the University of Missouri, Columbia and purified applying the same method as described above.

2.1.3. Acid activation of clay (Chapter 6)

For the preparation of acid-activated-clay **(HT)** object of the study reported in Chapter 6, natural Texas montmorillonite STx-1 (50.0 g) was ground and magnetically stirred with 250 mL of 2 M H_2SO_4 (from Riedel-deHaen) at 80 °C for 2 hs in a round-bottom flask. The slurry was cooled in air, centrifuged and washed with distilled water; the operation was repeated twice. The sample contained in a dialysis membrane was placed in deionized water and the water was renewed until the pH was neutral and the conductivity was stable.[4][5] The sample was finally dried at room temperature.

2.1.4. Carbon nanodiscs CNDs (Chapter 4)

The nanodiscs sample (also containing a small fraction of conical structures and amorphous carbon), produced by the CB&H process[6][7] and further annealed at 2500 - 2700 °C, was purchased from Strem Chemicals, Inc. (France). The cones and soot components were removed in the oxidation procedure described below.

2.1.5. Preparation of Clay/Adamantylamine hybrid (Chapter 3)

The Clay/Adamantylamine hybrid object of the study reported in Chapter 3 was synthesized by the following procedure: 300 mg of Na^+-SWy-2 dispersed in 100 mL distilled deionized water were reacted with 50 mg of 1-adamantylamine (97%, Aldrich) dissolved in 20/1 (v/v) ethanol/water. This amount corresponds to 1.5 times the CEC of SWy-2 montmorillonite. 5 drops of HCl 1M were then added and the mixture was stirred at room temperature for 24 hs. The residue was separated by centrifugation, washed three times with distilled deionized water and air-dried by spreading over a glass plate (product: **SWy-2/ADMA**). A similar procedure was used for the intercalation of ADMA (30 mg) in synthetic Laponite (sample: **Lap/ADMA**).

2.1.6. Preparation of graphene oxide/adamantylamine hybrid (Chapter 3)

The GO/Adamantylamine hybrid object of the study reported in Chapter 3 was synthesized by the following procedure: 300 mg 1-adamantylamine were dissolved in ethanol (50 mL) and added dropwise to a dispersion of GO in distilled deionized water (100 mg GO in 50 mL) under vigorous stirring (pH=8). Upon addition of adamantylamine the GO solid swelled instantly. The reaction continued for 24 hs at room temperature. The GO derivative was isolated by centrifugation and washed three times with 1:1 (v/v) ethanol/water and dried in air (sample denoted as **GO/ADMA**).

2.1.7. Oxidation of carbon nanodiscs (Chapter 4)

The oxidization of carbon nanodiscs was achieved using a modified Staudenmaier's method.[1] In a spherical flask, 500 mg of CNDs were dispersed in a mixture of 20 mL H_2SO_4 (95-97 %) and 10 mL HNO_3 (65 %) while placed in an ice-water bath (0 ^oC) and the system was stirred for 20 minutes. 10 g of $KClO_3$ were then added in small portions to the mixture under vigorous stirring and the reaction was completed after 18 hs. The oxidation product **(oxCNDs**) was separated by centrifugation (3500 rpm, 10 min) and washed several times with distilled water until a pH of 6 was reached. The remaining solid was spread on a glass plate and was air-dried.

2.1.8. Organosilane solutions (Chapters 6 and 7)

The organosilane used in the study described in Chapters 6 and 7 was 3-(2-aminoethylamino)-propyltrimethoxysilane,(EDAPTMOS),$H_2N(CH_3)_2NH(CH_2)_3Si(OCH_3)_3$, from Fluka Chemicals. The formation of the octameric oligosiloxane from the hydrolytic polycondensation of the monomer occurs after dilution of EDAPTMOS in ethanol-water (v/v = 14/1) to give a solution of concentration 0.45 M.[8][9][10] 30 mL of an aqueous 0.1 M $FeCl_2$ solution (3 mmol) was reacted with 20 mL of the above solution (9 mmol) upon stirring. The colour of the ferrous chloride solution changed from pale orange to dark green, indicative of the complexation of ferrous cations with the amino functional group of the corresponding siloxane molecules. The produced Fe-EDAPTMOS complex discussed in Chapter 6 was used immediately after its formation in order to avoid oxidation of the ferrous cations before the intercalation between clay platelets.

The Fe-EDAPTMOS-clay complexes were prepared by reacting, under stirring, a 0.5 wt% clay suspension with aliquots of the above siloxane complex solution such that the ratio R=[Fe-EDAPTMOS]/[clay] = 3. Within 1 h from the addition of iron-complex the colour of the slurry changed gradually from green to orange, indicating the oxidation of Fe(II) to Fe(III). After stirring for 6 hs the clay-organosilane aggregates were washed with water five times, separated by centrifugation and air-dried by spreading on glass plates. In order to prepare the pillared clays, the intercalated with the Fe-EDAPTMOS clay samples were calcined in air at 500 ^oC for 3 hs.

For the fabrication of the highly ordered Cu^{2+}/Fe^{3+} substituted POSS thin films with the LS method (Chapter 7) an additional metal organosilane solution was prepared. 30 mL of an aqueous 0.1 M $CuCl_2$ solution (3 mmol) was reacted with 13.5 mL of the above described oligosiloxane solution (6 mmol) upon stirring. The colour of the copper chloride solution changed from light blue to dark purple after mixing. The produced Cu-EDAPTMOS complex was used 24 hs after its formation. Arachidic acid (AA) was used dissolved in chloroform (concentration of 0.2 mg/mL). LS films were prepared on a Nima Technology thermostated 612D LB trough at temperature of 23±0.5 ^oC. Ultra-pure water with resistivity of greater than 18 MΩ-cm was used to prepare the subphase.

2.2. Characterization Techniques

2.2.1. X-ray Diffraction (XRD) (Chapters 3, 4, 6 and 7)

The XRD patterns for Chapters 3, 4 and 6 were collected on a D8 Advance Bruker diffractometer by using Cu K_α (40 kV, 40 mA) radiation and a secondary beam graphite monochromator. The patterns were recorded in the 2-theta (2θ) range from 2 to 80°, in steps of 0.02° and a counting time of 2 s per step. Samples were in the form of films supported on glass substrates. For the preparation of the films, aqueous suspensions of the hybrids were deposited on glass plates and the solvent was allowed to evaporate slowly at ambient temperature. For the LS Cu^{2+}/Fe^{3+} substituted POSS thin films reported in Chapter 7, diffraction measurements were performed on (15-20)-layer-thick films. Arachidic Acid-Metal POSS hybrid films, deposited on hydrophobic silicon wafers. The out-of-plane X-ray reflectivity data for the hybrid films were collected under ambient conditions with a Philips PANanalytical X'Pert MRD diffractometer. A Cu Kα (λ=1.5418 Å) radiation source was used (operated at 40 keV, 40 meV), while a 0.25° divergence slit and a 0.125° antiscattering slit were employed. The 2θ scans were performed from 0.6° to 15° with 0.02° steps and a counting time of 15 s per step.

2.2.2. FTIR spectroscopy (Chapters 3, 4 and 6)

Infrared spectra reported in Chapters 3 and 4 were measured with a SHIMADZU 8400 infrared spectrometer, in the region of 400-4000 cm^{-1}, equipped with a deuterated triglycine sulphate (DTGS) detector. Each spectrum was the average of 200 scans collected at 2 cm^{-1} resolution by means a SPECAC variable-angle attachment. Samples were in the form of KBr pellets containing ca. 2 wt % sample. A different set up was used for the data discussed in Chapter 6 namely a Perkin–Elmer Spectrum GX infrared spectrometer,equipped with a (DTGS) detector. Each spectrum spanning the region of 400–4000 cm^{-1} was the average of 64 scans, collected with 2 cm^{-1} resolution. Also in this case samples were in the form of KBr pellets containing *ca*. 2 wt% sample.

2.2.3. Raman spectroscopy (Chapters 3 and 4)

Raman spectra were recorded with a Micro – Raman system RM 1000 RENISHAW, with excitation at 532 nm (Nd – YAG). A power of 1 mW was used with a 1 μm focus spot in order to avoid photodecomposition of the samples. The range of measurement for samples measured was 1000–2400 cm^{-1}.

2.2.4. Thermal analysis (Chapters 3, 4 and 6)

Thermogravimetric (TGA) and differential thermal (DTA) analyses were performed using a Perkin Elmer Pyris Diamond TG/DTA. Samples of approximately 5 mg were heated in air from 25 °C to 850 °C, at a rate of 5 °C/min (Chapters 3 and 4). The measurements discussed in Chapter 4 were performed using a Shimadzu DTG 60 Thermal Analyzer. Samples of approximately 15 mg were heated in air from 25 to 600 °C, at a rate of 10 °C/min.

2.2.5. X-ray Photoelectron Spectroscopy (XPS) (Chapters 3, 4, 6 and 7)

For the XPS measurements discussed in Chapter 3, 150 nm thick gold films supported on mica were used as substrates. All samples were dispersed in distilled deionized water and after stirring and sonication for 30 min, a small drop of the suspension was left to dry in air on the substrate. Samples were introduced via a load-lock system into a SSX-100 (Surface Science Instruments) photoelectron spectrometer, equipped with a monochromatic Al Kα X-ray source (hν = 1486.6 eV). The base pressure in the spectrometer was 1×10^{-10} Torr during all measurements. The energy resolution was set to 1.16 eV in order to minimize the measuring time. The photoelectron take off angle was 37° with respect to the surface normal. An electron flood gun providing 0.3 eV kinetic energy electrons in combination with a gold grid mounted about 1 mm above the sample was used in the case of clays and clay hybrids to compensate for sample charging. All binding energies of GO hybrids were referenced to the C1s core level of the C-C bond set to the nominal value of 285.0 eV, while in the case of montmorillonite clays, all binding energies were referenced to the Si2p core level of smectite clay at 102.8 eV.[11] Spectral analysis was performed by means of a least squares curve-fitting program (WinSpec) developed at the LISE, University of Namur, Belgium; the fit included a Shirley background subtraction and peak deconvolution employing mixed Gaussian−Lorentzian functions. For the N1s line, however, a linear background subtraction was employed since the low peak intensity did not allow for a Shirley background subtraction. The same protocol was followed for the spectra presented in Chapter 4 with the difference that the electron flood gun provided 0.2 eV kinetic energy electrons and that no gold grid was used. Similarly for the data reported in Chapter 6 an electron flood gun provided 0.1 eV kinetic energy electrons; no gold grid was used for these measurements either.

For the XPS measurements discussed in Chapter 7 (Arachidic Acid - Metal POSS hybrid films) silicon wafers (Prime Wafer) were used as substrates. The surface of substrates was made hydrophobic by modification with octadecyltrichlorosilane (purchased from Sigma Aldrich) prior to the LS film deposition.

2.2.6. Atomic force microscopy (Chapter 4)

Atomic force microscopy images were obtained in tapping mode with a 3D Multimode Nanoscope, using Tap-300G silicon cantilevers with a tip radius <10 nm and a force constant of ≈20–75 N m^{-1}. Samples were dispersed in ethanol and deposited onto silicon wafers (P/Bor, single side polished, purchased from Si-Mat) by drop casting. Measurements were performed by Antonios Kouloumpis (University of Ioannina, Greece).

2.2.7. Mössbauer spectra (Chapter 6)

^{57}Fe Mössbauer spectra (MS) for powder samples were collected at room temperature 300K (26.85 ^{o}C) and 10K (-263.15 ^{o}C), using constant acceleration spectrometers, equipped with a ^{57}Co(Rh) sources kept at RT and a closed loop He (ARS) Mössbauer cryostat. Calibration of the spectrometers was done using metallic α-Fe at RT and all isomer shift (IS) values are reported relative to this standard. The fitting of the recorded MS was done using the IMSG code. Measurements were performed by Prof. Alexios Douvalis (University of Ioannina, Greece).

2.2.8. High-resolution transmission electron microscopy (Chapter 3)

High-resolution transmission electron microscopy (HRTEM) data were collected using a FEI Tecnai G^2 microscope operated at 200 keV. Sample was prepared by dispersing the powder form of SWy-2/ADMA hybrid in ethanol before depositing onto a honeycomb carbon film supported by a copper grid. Measurements were performed by Prof. Ke Xiaoxing (University of Antwerp, Belgium).

2.2.9. Surface area and porosity measurements (Chapter 3 and 6)

The surface areas and the pore volumes of the samples in Chapter 3 were determined by a SORPTOMATIC 1900 Thermo Finnigan porosimeter, using nitrogen as adsorbent at 77K (-196.15 ^{o}C). Prior to the determination of the adsorption-desorption isotherms the samples were degassed at 200 ^{o}C in vacuum of 5x10^{-2} mbar for 20 hs. The specific surface area of the samples was calculated by applying the BET equation using the linear part ($0.05 < P/P_o < 0.15$) of the adsorption isotherm and assuming a closely packed BET monolayer, with $\alpha_m(N_2)=0.162$ nm^2 at 77 K. In Chapter 6 the same protocol was used but with the relative pressure range $0.01 < P/P_0 < 0.30$.

2.2.10. Catalytic measurements (Chapter 6)

The catalytic decomposition of isopropanol took place in a bench-scale flow reactor. The reactor consisted of a silica tube (1 cm in diameter) with a sealed-in quartz bed onto which 0.20 g of the catalyst was placed. The system was heated in a tubular furnace with a temperature control system accurate to within ±1 ^{o}C. Analysis of reactants and products was carried out by sampling 1 cm^3 of the gases in a Fisons GC-9130 gas chromatograph equipped with a flame ionization detector. The column used for analysis was a DB-WAX, 30 m x 0.32 mm, and with film thickness 0.5 μm, supplied by J&W scientific. Helium used as carrier gas in the gas chromatograph. Another line drove Helium through a saturator bottle (40±1 cm^3 min^{-1}) containing the isopropanol (at constant temperature), whose vapour was then driven to the reactor. Under the experimental conditions the partial pressure of isopropanol was 33 mmHg. Measurements were taken in the range of 90 to 200 ^{o}C in 5 or 10 ^{o}C intervals. Before the catalytic experiments were started, the catalyst was heated at 500 ^{o}C for 2 hs under Helium flow to remove adsorbed water from the pores. No signs of catalyst ‘die off’ were observed on the time scale of our experiments. The products detected were propene, diisopropyl ether and water. From the percentage degree of total conversion of isopropanol we calculated the reaction rate at each reaction temperature. Moreover the selectivity for each of the two main products, propene and diisopropyl ether, at various degrees of total conversion of isopropanol was also determined. Measurements were performed by Prof. Athanasios Ladavos (University of Patra, Greece) and Prof. Dimitrios Petrakis (University of Ioannina, Greece).

2.2.11. Study of cytotoxicity in vitro (Chapters 3 and 4)

For the cytotoxicity study reported in Chapter 3: (a) Cell lines and cell culture used with **GO**, **GO/ADMA**, **LAP** and **LAP/ADMA** were Human lung cancer cells (A549) and normal human fetal lung fibroblasts (MRC-5), provided by Dr. Evangelos Kolettas, Laboratory of Physiology, Faculty of Medicine, University of Ioannina. All different cell lines were cultured in Dulbecco's Modified Eagles Medium (DMEM) enriched with 10% fetal bovine serum (FBS), 100 IU/mL penicillin, 100 μg/mL streptomycin and 1.4 mM L-Gloutamin, at 37^{o}C, with 5% CO_2. All materials were provided by Costar and PAA. (b) MTT assay: Cell growth inhibitory ability of the substances, expressed by the average IC_{50} value (substance's concentration required for 50% inhibition of cell growth), was analyzed using the MTT assay (3-(4,5-Dimethylthiazol-2-yl)-2,5-diphenyltetrazolium bromide). Briefly, 3×10^3 A549 cells and 5×10^3 MRC-5 cells were cultured overnight on 96-well plates and culture media containing different concentrations (ranging from 1 to 850 μg/mL) of **ADMA**, **Lap**, **Lap/ADMA**, **GO** and **GO/ADMA** were added. All substances were dissolved in sterilized water (solvent). The 96-well plates with culture media containing different volumes of sterilized water (solvent), equal to volumes of solutions added to the test wells, were considered as control. After incubation for 48 hs, 50 μL of MTT were added in each well from a stock solution (3 mg/mL), and incubated for additional 3 hs. The yielded purple formazans were re-suspended in 200 μL of DMSO, using a multi-channel pipette. The solution was spectrophotometrically measured (540 nm, background absorbance measured at 690 nm subtracted) using a microplate spectrophotometer (Multiskan Spectrum, Thermo Fisher Scientific, Waltham, USA). All the experiments were performed at least in triplicate. IC_{50} values were determined by the curve of percentage of inhibition versus dose. Measurements were performed by Dr. Ioannis Verginadis and Dr. Anastasia Velalopoulou (University of Ioannina, Greece).

For the cytotoxicity study reported in chapter 4: (c) Cell lines and cell culture used with **oxCNDs** were the human embryonic kidney cell line Hek293T and the human adenocarcinoma HeLa cell line, which were obtained by Dr. E. Mastrobattista

(Utrecht University). The cells were cultured in high glucose D-MEM medium with 10% fetal bovine serum and 1% Penicllin/ Streptomycin. The cells were maintained at 37 °C in a humidified 5% CO_2 incubator for 24 hs. After that stage the sterilized and diluted compound was added in different concentration. (d) XTT toxicity tests: In vitro cytotoxicity studies were performed using the XTT (2,3-Bis(2-methoxy-4-nitro-5-sulfophenyl)-2H-tetrazolium-5-carboxanilide inner salt) colorimetric method [12] according to the literature.[13] Briefly, cells were seeded into flat bottomed 96-well plates at a concentration of 20.000 for Hek and 10.000 for HeLa cells per well. After 24 hs of incubation the medium was replaced and dispersed **oxCNDs** in D-MEM at concentrations of 2-1000 μg mL^{-1} were added. Cell-seeded wells with only D-MEM growth medium were used as controls. The mitochondrial redox function, translated as cell viability of all cell groups was assessed by the XTT assay at selected time point of 48 hs post-incubation. The absorbance was measured for each well by a spectrophotometric [SpectraMax M3] at 490 nm plate reader. The experiment was repeated in triplicate. Measurements were performed by Karolin Romhild (University of Groningen, The Netherlands).

2.2.12. Adsorption of chlorophenols (Chapter 3)

a) Swelling of materials: 10 mg of **GO** or **GO/ADMA** were swelled for 20 hs in methanol under stirring in glass vials. Then, distilled deionized water was added to a final MeOH/H_2O = 70/30 (v/v). 10 mg of **SWy-2** or **SWy-2/ADMA** were swelled for 20 hs in distilled deionized water (pH=4.5) under stirring in glass vials. After 20 hs methanol was added so the final volume ratio MeOH/H_2O = 70:30 (v/v). This methanol/H_2O mixture was chosen for both materials, since the goal of this experiment was to compare the performance of the clay and GO-based materials. (b) Adsorption: The solutes used were 2,4,6-trichlorophenol (2,4,6-TCP) pentachlorophenol (PCP) and 2,4-dichlorophenol (2,4-DCP) purchased from Aldrich (purity 97%). Stock solutions of 0.8 mM 2,4-DCP, 2,4,6-TCP and PCP were prepared in MeOH/H_2O [70:30 v/v]. Adsorption experiments were performed in batch. 2,4-DCP, 2,4,6-TCP or PCP were added, at concentrations ranging between 7 μM and 70 μM, in

10 mg of swelled dispersions of the pristine and hybrid materials. The pH of the reaction mixture was adjusted using NaOH to pH=5.3 for both 2,4-DCP and 2,4,6-TCP and pH=4.5 for PCP to ensure the presence of protonated form of the phenols since the pK_a of 2,4-DCP is 6.79, the pK_a of 2,4,6-TCP is 6.23 and the pK_a of PCP is 4.7.[14] Screening experiments showed that the adsorption was completed in 90 min. Thus measurements were performed after 2 hs of incubation to ensure adsorption equilibrium. Then the samples were centrifuged and UV-Vis spectra of supernatants were measured in quartz cuvettes 6Q, 1x1cm. Controls were run for chlorophenol solutions every 2 hs with no solid material in the reaction mixture. The UV-Vis spectra were recorded using a Perkin-Elmer Lambda-35 double beam spectrometer. Quantification of the chlorophenols was done using the peaks at 280 nm for 2,4-DCP, at 290 nm for 2,4,6-TCP and at 210 nm for PCP. By comparing the UV-vis spectra for solutions with known phenol concentrations with the corresponding spectra recorded on our materials we calculate the concentration of chloroplenols adsorbed. Measurements were performed by Eleni Seristratidou (University of Ioannina, Greece).

References

[1] *L. Staudenmaier, Berichte der deutschen chemischen Gesellschaft **1898**, 31, 1481–1487.*

[2] *D. V Stergiou, E. K. Diamanti, D. Gournis, M. I. Prodromidis, Electrochemistry Communications **2010**, 12, 1307–1309.*

[3] *D. Gournis, E. A. Mantaka-Marketou, A. M. Karakassides, D. Petridis, Physics and Chemistry of Minerals **2001**, 28, 285–290.*

[4] *P. Falaras, F. Lezou, Journal of Electroanalytical Chemistry **1998**, 455, 169–179.*

[5] *C. N. Rhodes, D. R. Brown, Journal of the Chemical Society, Faraday Transactions **1995**, 91, 1031–1035.*

[6] *A. Krishnan, E. Dujardin, M. M. J. Treacy, J. Hugdahl, S. Lynum, T. W. Ebbesen, Nature **1997**, 388, 451–454.*

[7] *S. Lynum, J. Hugdahl, K. Hox, R. Hildrum, M. Nordvik, **2008 (patent)**.*

[8] *D. Petridis, D. Gournis, M. A. Karakassides, Molecular Crystals and Liquid Crystals Science and Technology. Section A. Molecular Crystals and Liquid Crystals **1998**, 311, 345–350.*

[9] *T. Cassagneau, D. J. Jones, J. Roziere, The Journal of Physical Chemistry **1993**, 97, 8678–8680.*

[10] .P. Olivera-Pastor, P. Maireles-Torres, E. E. Rodríguez-Castellón, A. Jiménez-López,, T. Cassagneau, D. J. Jones, J. Rozière, *Chemistry of Materials* **1996**, *8*, 1758–1769.

[11] *D. Briggs, M. P. Seah, Practical Surface Analysis by Auger and X-Ray Photoemission Spectroscopy, John Wiley & Sons Ltd., Chichester, **1983**.*

[12] *T.LRiss, R.A.Moravec,A.L. Niles et al. "Cell Viability Assays," can be found under http://www.ncbi.nlm.nih.gov/books/NBK144065/**(Internet page)***

*[13] D. M. Kuhn, M. Balkis, J. Chandra, P. K. Mukherjee, M. A. Ghannoum, Journal of Clinical Microbiology **2003**, 41, 506–508.*

*[14] T. Ebina, T. Iwasaki, A. Chatterjee, M. Katagiri, G. D. Stucky, The Journal of Physical Chemistry B **1997**, 101, 1125–1129.*

CHAPTER 3

Towards novel multi-functional pillared nanostructures: effective intercalation of adamantylamine in graphene oxide and smectite clays

Multi-functional pillared materials were synthesized by intercalation of cage-shaped adamantylamine (ADMA) molecules into the interlayer space of graphite oxide (GO) and aluminosilicate clays. The physicochemical and structural properties of these hybrids, determined by XRD, FTIR, Raman, XPS and TEM show that they can serve as tunable hydrophobic/hydrophilic and stereospecific nanotemplates. Thus in the ADMA-pillared clay hybrid the phyllomorphous clay provides a hydrophilic nanoenvironment where local hydrophobicity is modulated by the presence of ADMA moieties. On the other hand, in ADMA-pillared GO hybrid, both aromatic rings of GO sheets and ADMA molecules define a hydrophobic nanoenvironment where sp^3-oxo moieties (epoxy, hydroxyl and carboxyl groups) present on GO modulate hydrophilicity. As test applications we demonstrate that these pillared nanostructures are capable of selective/stereospecific trapping of small chlorophenols or can act as cytotoxic agents.

This chapter is based on the article: Towards novel multi-functional pillared nanostructures: effective intercalation of adamantylamine in graphene oxide and smectite clays by K. Spyrou, G. Potsi*, E .K. Diamanti* et al., Advanced Functional Materials 37, (24) 5841-5850, 2014.*

*K. Spyrou, G. Potsi and E. K. Diamanti have contributed to this work in equal manner.

3.1. Introduction

Diamondoids have been extensively studied in recent years due to their successful application in diverse fields of nano- and biotechnology[1] which rely on the physical and chemical properties[2, 3, 4] imparted by their unique (cage-like) structure of tricyclic saturated hydrocarbons. Applications reported in the literature for these "molecular diamonds" include their use as templates in nanotechnology, or as molecular building blocks for the synthesis of novel catalysts,[5] high temperature polymers,[6] or hybrid nanostructures.[7] In the pharmaceutical industry diamondoids are employed in drug delivery and as drug targeting agents,[8] as well as in antiviral drugs (influenza A)[9] and in the treatment of Parkinson and Alzheimer.[10] To further extend the use of diamandoids, host/guest chemistry can help to tune or protect the properties of these molecules. In this context, adamantylamine (ADMA), an adamantane derivative with a covalently attached amino group, is expected to be an ideal pillaring block to be incorporated in layered host materials such as aluminosilicate clays or graphene oxide (GO), giving rise to new hybrid multifunctional nanostructures.

Layered materials represent a diverse and largely untapped source of two-dimensional (2D) nanosystems with high specific surface area and exceptional physicochemical properties that are important for applications such as catalysis, sensing, environmental remediation, biotechnology, and energy storage.[11, 12, 13, 14, 15, 16] The nature of the environment between the 2D nanometer-sized sheets regulates the topology of the intercalated molecules and affects possible supramolecular rearrangements or reactions, such as self-assembling processes that are usually not easily controlled in solution.[17, 18, 19, 20] Smectite clays and graphene oxide are two archetypical layered materials; smectite clays are minerals consisting of aluminosilicate nanoplatelets, with a unique combination of swelling, intercalation and ion exchange properties that make them valuable nanostructures[21, 22, 23] for use as catalysts,[24, 25] templates in organic synthesis,[26, 27] building blocks for composite materials,[17, 28, 29, 30, 31] adsorbents of inorganic and/or organic pollutants,[32, 33] as active agents or excipients of medicinal products[34, 35] and as constituents of modified drug delivery systems (MDDS)[36] in pharmaceutical industry. In most cases, the intercalation process is a simple ion-exchange procedure between hydrated cations present in the galleries of the clay and organic/or inorganic cation moieties. Unlike the intercalation of graphite, that of smectite clays does not necessarily involve charge transfer between the host and the guest species. On the other hand, graphite oxide (GO) is an oxygen rich derivative of graphite decorated with hydroxyl, epoxy, and carboxyl groups (sp^3-oxo moieties).[37, 38, 39] These functional groups are created by strong oxidation and distributed randomly on the basal planes and edges of the GO sheets, generating aliphatic regions (sp^3-carbon atoms). Due to the existence of such hydrophilic moieties, GO presents similar properties as smectite clays in that it is prone to swelling and intercalation. Both GO and intercalated GO are being considered for numerous applications such as supercapacitors,[40] high mobility transistors,[41] lithium batteries,[42] hydrogen storage, adsorption of organic moieties[43] or the removal of pollutants (*e.g*. chlorophenols) from aqueous solutions; recently they have also attracted interest regarding their potential use in biomedical applications. GO has already been studied in drug delivery formulation and bioanalysis[44, 45, 46, 47, 48, 49] as well as for its potential cytotoxic action.[50, 51] In contrast to clays, the intercalation process of GO involves covalent bonding of guest molecules to the oxygen-containing groups on the GO surfaces (nucleophilic substitution reactions). It has been demonstrated that, under proper conditions, GO can be exfoliated in water forming colloidal suspensions of single graphene oxide sheets.[52, 53]

In this study, we report on the intercalation of adamantylamine (ADMA) into two types of layered matrices, graphene oxide and smectite clay. Apart from the different structural and geometrical characteristics (*e.g.* interlayer space) that might occur using different matrices, and which in turn define stereospecific properties to the final pillared structures, the choice of these two 2D-nanotemplates was also motivated by their ability to provide, in conjunction with the adamantane moieties, diverse tunable hydrophobic or hydrophilic character (environment) in the final hybrids. Thus, in ADMA-pillared clay hybrid, smectite clay provides a hydrophilic nanoenvironment where local hydrophobicity is modulated by the presence of ADMA moieties while in ADMA-pillared GO hybrid, both aromatic rings of GO sheets and ADMA molecules define a hydrophobic nanoenvironment where oxygen-containing groups present on GO modulate hydrophilicity. Since the incorporation of ADMA into these layered materials opens the way to diverse applications in the chemical, pharmaceutical and electronic (sensor) industry, we decided to perform also two representative case studies of great importance in biomedicine and environmental remediation, namely the use of these hybrid nanostructures as antiproliferative agents in cells and effective adsorbents for the removal of organic pollutants from aqueous solution.

3.2. Results and discussion

The smectite clay consists of octahedral alumina layers, each fused between two tetrahedral silica layers. In the tetrahedral sheet Al^{+3} can replace Si^{+4} creating a negative charge. Occasionally Fe^{+3} cations are also present in the tetrahedral lattice. In the octahedral sheets negative charging may occur by substitution of Mg^{+2} for Al^{+3}. Fe^{+2} and Fe^{+3} may also part of the octahedral sheets. The negative charge of the isomorphous substituents is compensated by hydrated cations (usually sodium) present in the interlayer space. These charge balancing cations can be replaced with water soluble organic or inorganic cationic species;[21, 22, 23] this approach was followed to intercalate ADMA in two different clay minerals, namely SWy-2 montmorillonite (product called SWy-2/ADMA) in the following) and a synthetic trioctahedral hectorite, Laponite RD (product called Lap/ADMA). Initially the terminal amine groups of adamantylamine had to be protonated to form a cationic adamantane species. The intercalation of the positively charged adamantylamine,

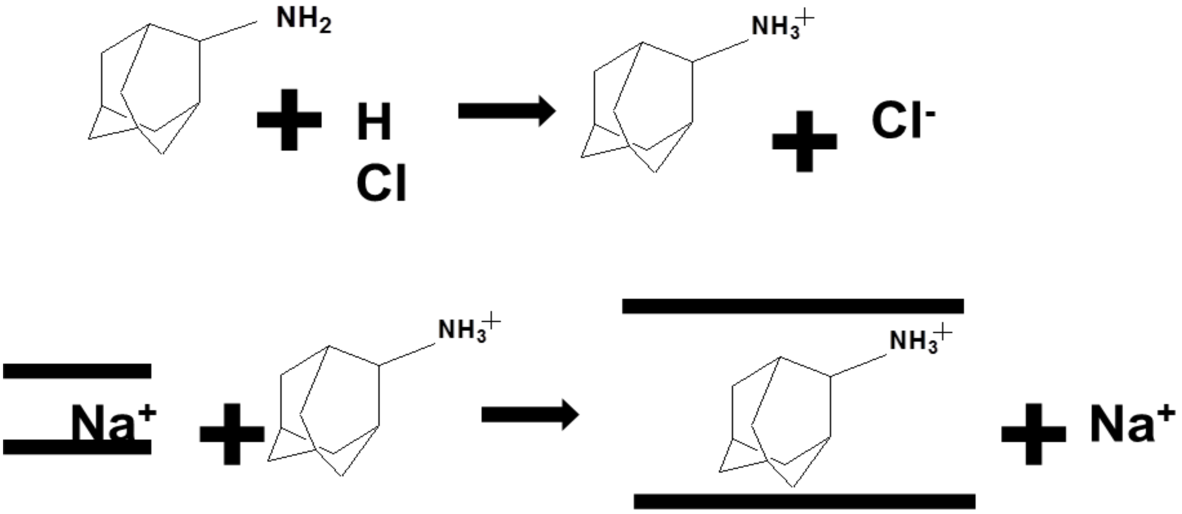

Scheme 3.1. Schematic representation of the intercalation process of adamantylamine, after the protonation of the amine end groups, into the interlayer space of clay. The bold lines represent the negatively charged clay platelets.

dispersed in aqueous solution, is achieved by ion-exchange according to the reaction. The process is illustrated in Scheme 3.1:

Contrary to clay minerals, GO does not contain charge balancing cations, thus intercalation is obtained by grafting to functional groups on the GO surface and/or adsorption of molecules held between the basal planes by van der Waals interactions. ADMA was intercalated in oxidized graphite as sketched in Scheme 3.2; the product is called GO/ADMA in the following. When ADMA, dissolved in distilled deionized water, was added to a water dispersion of GO an immediate flocculation of GO particles was observed. This phenomenon is induced by the insertion of adamantylamine in the GO galleries through covalent bonding via the amine functionality of the adamantane derivative (see XPS data below). The amine end groups interact via a ring opening reaction of the epoxide groups of GO.[52, 53, 54]

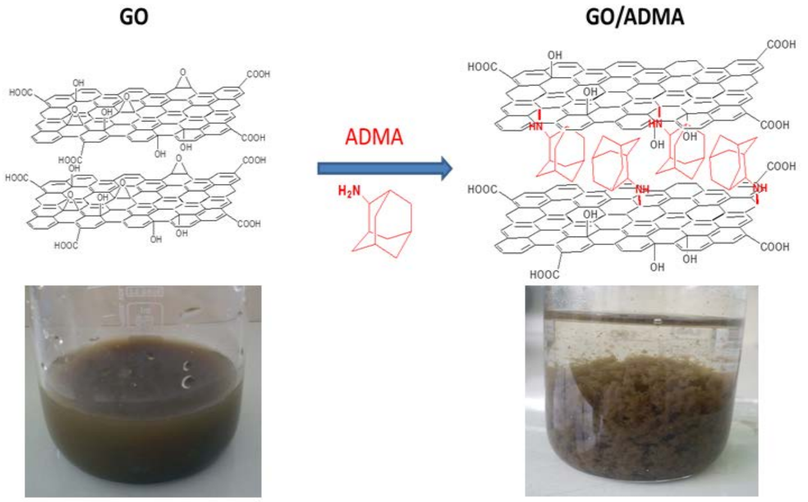

Scheme 3.2. Schematic representation of the synthetic procedure of GO/ADMA.

The success of the intercalation reaction can be proven by X-ray diffraction, which allows estimating the interlayer spacing between GO or clay sheets. The XRD patterns of GO/ADMA and SWy-2/ADMA are displayed in Figure 3.1. The insertion of adamantylamine between the aluminosilicate and graphene oxide layers increases the interlayer distance. More specifically, for intercalation in SWy-2 clay, the basal d_{001}-spacing, which is 12.4±0.3 Å in the initial montmorillonite clay, becomes 15.6±0.4 Å after the modification; this corresponds to an interlayer separation $\Delta = 15.6-9.6 = 6$ Å, where 9.6 Å represents the thickness of a clay layer.[20] This value is in accordance with the size of the adamantylamine molecule if we assume an orientation perpendicular to the aluminosilicate platelets.[55] In the case of GO/ADMA, the 001 diffraction peak, centred at ~12° in pristine GO, shifts to lower angles corresponding to a d_{001}-spacing of 10.4±0.3 Å. Taking into account the thickness of a graphene oxide layer (6.1 Å),[56] this corresponds to an interlayer separation $\Delta = 10.4 - 6.1 = 4.3$ Å occupied by the ADMA pillaring moieties. This value implies that the adamantane derivative must adopt an inclined orientation in the GO interlayer space.[57, 58, 59]

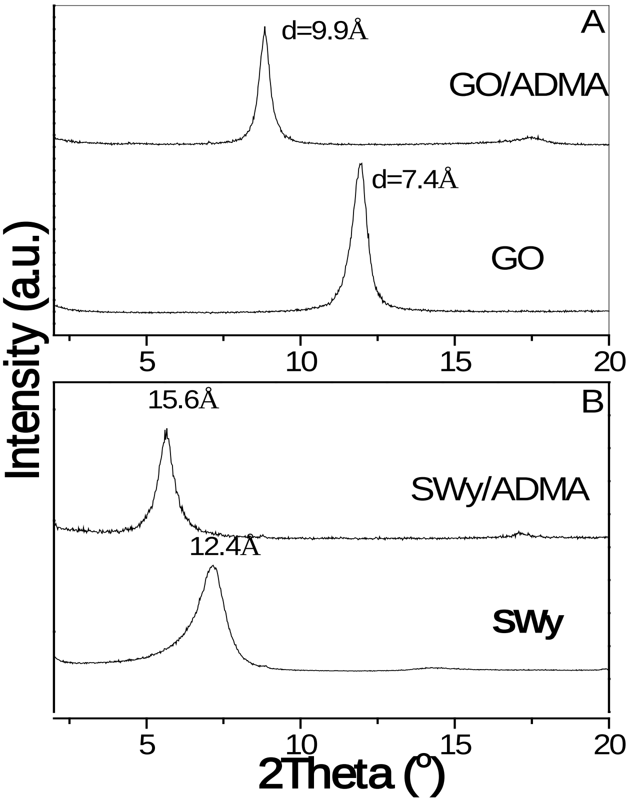

Figure 3.1. Comparison of the X-ray diffraction patterns of the hybrid pillared systems (A) SWy-2/ADMA and (B) GO/ADMA with those of the pristine layered matrices (SWy-2 and GO).

The results for laponite (Figure 3.2) are similar to those for montmorillonite: the basal d_{001}-spacing, which is 12.0±0.3 Å in the initial laponite clay, becomes 15.5±0.4 Å after the intercalation of adamantylamine; this corresponds to an interlayer separation of 15.5 Å - 9.6 Å = 5.9 Å. This value is in agreement with the size of the adamantylamine molecule if we assume an orientation perpendicular to that of the aluminosilicate platelets as sketched in Scheme 3.1.

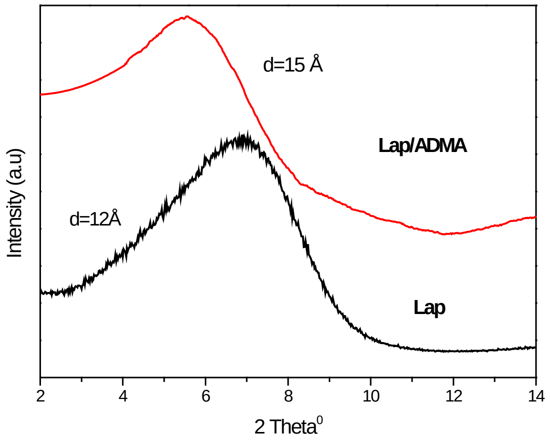

Figure 3.2. XRD patterns of the hybrid Lap/ADMA in comparison with pristine Laponite

An additional tool for the characterization of hybrid pillared materials is FTIR spectroscopy, which can confirm the successful incorporation of the adamantane derivative in the layered matrices. Figure 3.3 displays the FTIR spectra of SWy-2 and GO before and after the intercalation process. In the case of SWy-2/ADMA, the spectrum displays all the characteristic bands arising from aluminosilicate clay at 465 cm^{-1} (Si-O-Si and Si-O bending vibrations), 524 cm^{-1} (Si-O-Si bending), 778 cm^{-1} (Si-O deformation), 797 cm^{-1} (Si-O and Si-O-Al stretching), 884 cm^{-1} (Al-Fe-OH deformation), 918 cm^{-1} (Al-OH-Al bending), 1047 cm^{-1} (Si-O-Si stretching) and 1639 cm^{-1} (H_2O bending).[60, 61] In addition, the presence of adamantylamine in the hybrid material is revealed by the bands centred at 2863 cm^{-1} and 2921 cm^{-1} corresponding to stretching vibrations of C-H, as well as by the peak at 1520 cm^{-1}, due to N-H vibrations.[19, 62] In the case of GO/ADMA the same peaks originating from the ADMA molecules are also present in the spectrum, together with characteristic bands arising from GO at 3410 cm^{-1} (hydroxyl stretching vibration of C-OH groups), 1621 cm^{-1} (C=O stretching vibrations of the -COOH groups), 1396 cm^{-1} (O-H deformations of the C-OH groups) and 1062 cm^{-1} (C-O stretching vibrations).[63]

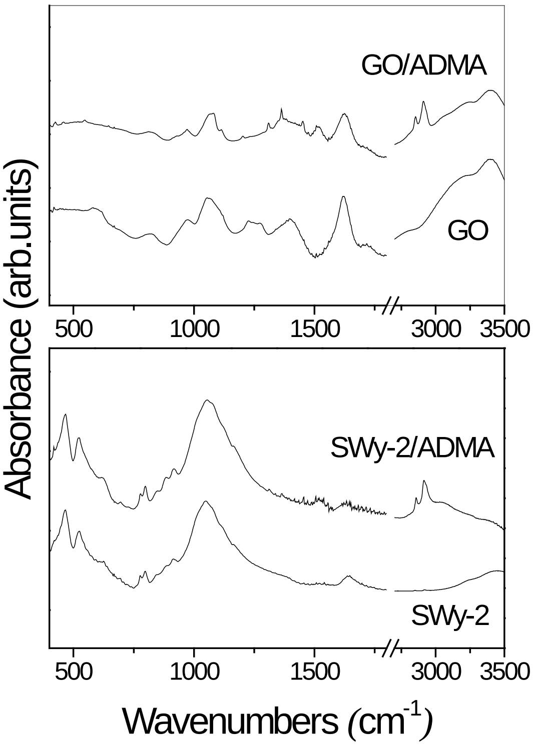

Figure 3.3. FTIR spectra of the hybrid pillared systems SWy-2/ADMA and GO/ADMA; the FTIR spectra of pristine SWy-2 and GO are plotted for comparison.

The FTIR spectrum of Lap/ADMA shown in Figure 3.4 displays in addition to the characteristic bands arising from the aluminosilicate clay a peak at approximately 1515 cm^{-1}, due to N-H vibrations as well as the bands centred at 2863 cm^{-1} and 2921 cm^{-1} corresponding to stretching vibrations of C-H; this testifies to the intercalation of the adamantylamine moieties in between the clay sheets.

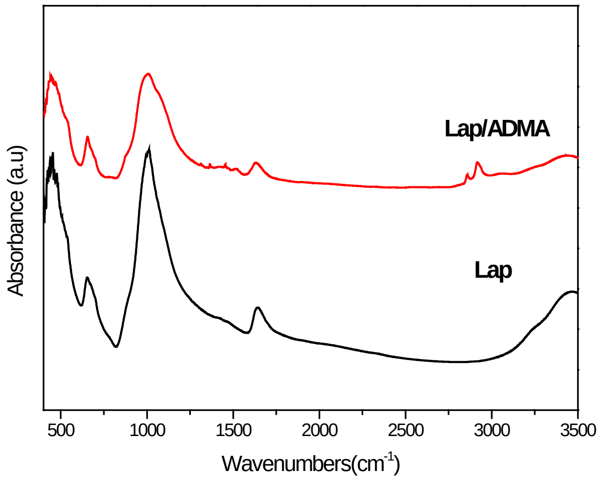

Figure 3.4. FTIR spectra of Lap/ADMA and pristine Laponite

In the case of GO/ADMA Raman measurements were performed as well and are presented in Figure 3.5. Raman spectroscopy is widely used in the characterization of carbon systems because it provides information about their structure. The Raman spectrum of the graphite used as starting material includes the G peak at approximately ~1580 cm^{-1}, as well a very weak 2D band located at ~ 1353 cm^{-1}, caused by the tangential E_{2g} in-plane vibration mode of the graphite lattice and second order boundary phonons (A_{1g} breathing mode) respectively.[64] The 2D band is associated with defects leading to sp^3 carbon atoms.[65] The GO sample exhibits strong fluorescence and therefore its weak Raman spectrum could not be observed when exciting at 532 nm. To overcome this problem, a sample obtained by deposition of GO sheets on a gold substrate, as described elsewhere,[53] was used. After the chemical oxidation of graphite the G band is broadened and shifted slightly to 1594 cm^{-1}, while the D band at 1363 cm^{-1} becomes prominent due to defects created by the attachment of oxygen-containing groups (sp^3-oxo moieties) to the carbon basal planes.[66] The degree of disorder in the carbon flakes can be expressed by the ratio between intensities of the G and D bands. In the case of GO, the I_D/I_G ratio is 1.06

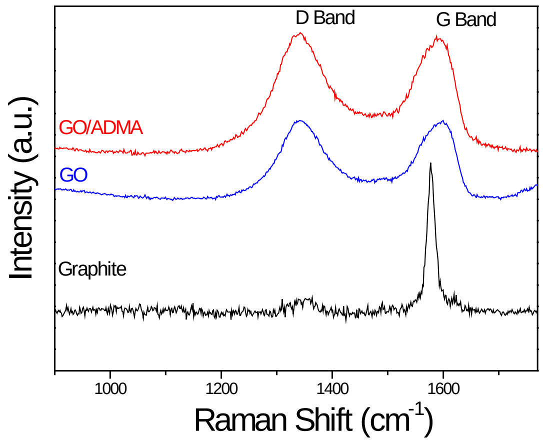

Figure 3.5. Raman spectra of pristine graphite, GO and GO/ADMA excited at 532 nm.

pointing to the creation of sp^3 domains in the oxidation treatment. After the intercalation of the organic moieties that ratio remains almost the same. This gives further support to the covalent bonding of the adamantane derivatives to the epoxy groups on the GO surface since such a bonding does not decrease the number of aromatic carbon-carbon bonds.

To verify the presence and integrity of the adamantylamine cycloalkanes within the layered nanostructures, as well as to analyse the chemical environment of ADMA, we employed X-ray photoelectron spectroscopy (XPS). The XPS spectrum of GO/ADMA reveals in C1*s* core level region (Figure 3.6 left) the characteristic contribution of C-C/C-H bonds of the GO lattice and of the adamantane cyclohexane ring centred at a binding energy of 285.0 eV; these bonds contribute 54.3 % of the total carbon 1*s* intensity. The peak at 286.3 eV is due to C-O/C-N bonds and represents 23.8 % of the total carbon 1*s* intensity. Finally two components at 287.9 eV and 289.6 eV are

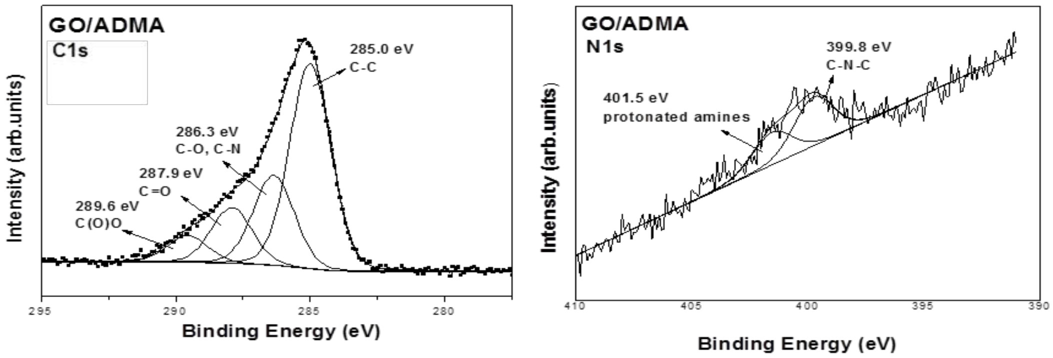

Figure 3.6. XPS spectra of the C1*s* (left) and N1*s* (right) core level regions of the GO/ADMA hybrid.

attributed to carbonyl (C=O) and carboxyl (O-C=O) groups respectively, which are created on the basal planes and at the boarders of the carbon sheets by the acid treatment. The N1*s* core level region of the XPS spectrum of GO/ADMA, plotted in Figure 3.6 (right) exhibits two main peaks, located at 399.8 eV and 401.5 eV.

These peaks arise from the amine end groups of ADMA chemically grafted to the epoxy groups of GO,[67, 68] and from protonated amines ionically bonded to the carboxylic acid anionic groups of GO,[69] respectively as is shown in Figure 3.7 where the N1*s* XPS spectra of pristine GO and GO/ADMA, are compared. The spectrum of GO/ADMA exhibits two main peaks, located at 399.8 eV and 401.5 eV in binding energy. They arise from the amine end groups of ADMA chemically grafted to the epoxy groups of GO[36] and from protonated amines ionically bonded to the carboxylic acid anionic groups of GO, respectively. In fact, the corresponding spectrum of pristine ADMA is deconvoluted into two photoelectron peaks, one at 400.1 eV, which is attributed to the amine groups of the organic molecule and a second one at 401.5 eV due to protonated amines. After intercalation no amine peak is found but a contribution typical of C-N-C bonds appears at 399.8 eV, indicating the successful functionalization of ADMA in the GO galleries, while the protonated groups remain at the same binding energy value.

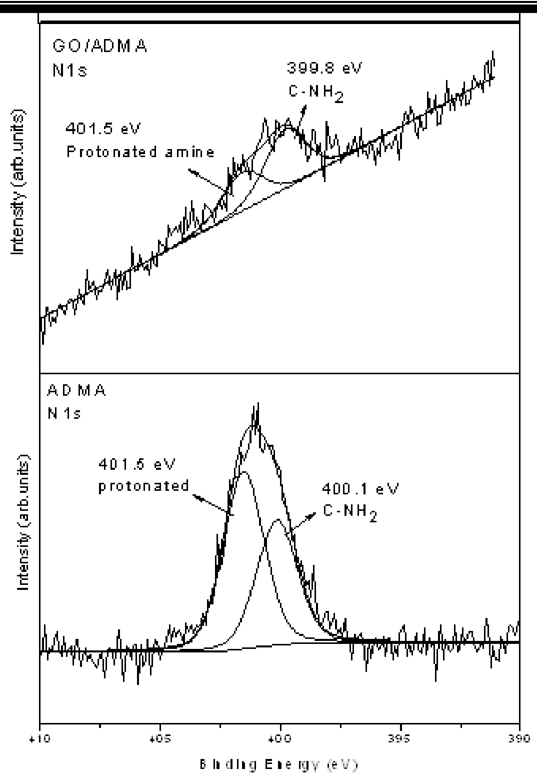

Figure 3.7. Comparison between the N1*s* core level photoemission spectra of adamantylamine and GO/ADMA hybrid (on gold substrates)

XPS measurements were also performed for the SWy-2/ADMA hybrid system. The survey spectra of SWy-2 and SWy-2/ADMA are shown in Figure 3.8. Characteristic photoelectron and Auger peaks of O, Si, Al, and Mg are clearly distinguishable in the spectrum of pristine montmorillonite clay. A small carbon peak appears, mainly due to adventitious carbon always present on the outer surface of air-exposed[70, 71] materials but also due to soil organic matter present in natural clay minerals.[70, 72] After the insertion of ADMA a pronounced increase in the intensity of the carbon signal points to the presence of adamantylamine inside the clay galleries. Quantitatively, the incorporation of ADMA in the clay is determined by measuring the

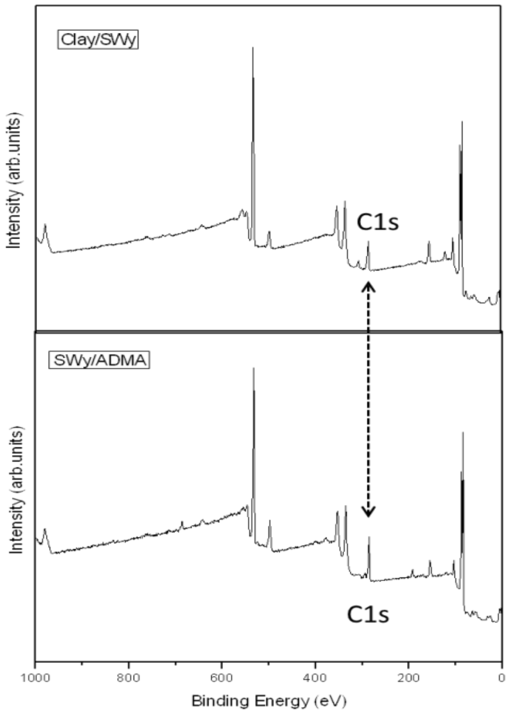

Figure 3.8. XPS survey spectra of the pristine montmorillonite clay, SWy-2, and the hybrid obtained after intercalation of adamantylamine, SWy-2/ADMA.

ratio between the carbon 1*s* and the silicon 2*p* core level photoemission intensities before and after the intercalation process. The C1*s* / Si2*p* intensity ratio increased from 1.42±0.06 before the incorporation of adamantylamine to 2.79±0.11 after the introduction of ADMA, as shown in Figure 3.9.

The presence of the amine terminal groups on adamantane is deduced from the N1*s* photoelectron spectrum shown in Figure 3.10. More specifically the N1*s* core level spectrum is deconvoluted into two peaks, one located at 401.5 eV due to the protonated amines of adamantine molecules intercalated into the SWy-2 galleries (64.3 % of the total N1s intensity) and one centred at 399.5 eV attributed to non-protonated amine groups (35.7 % of the total N1s intensity) of adamantane that interacts through hydrogen and van der Waals bonding with the aluminosilicate surfaces and/or other intercalated adamantane molecules.

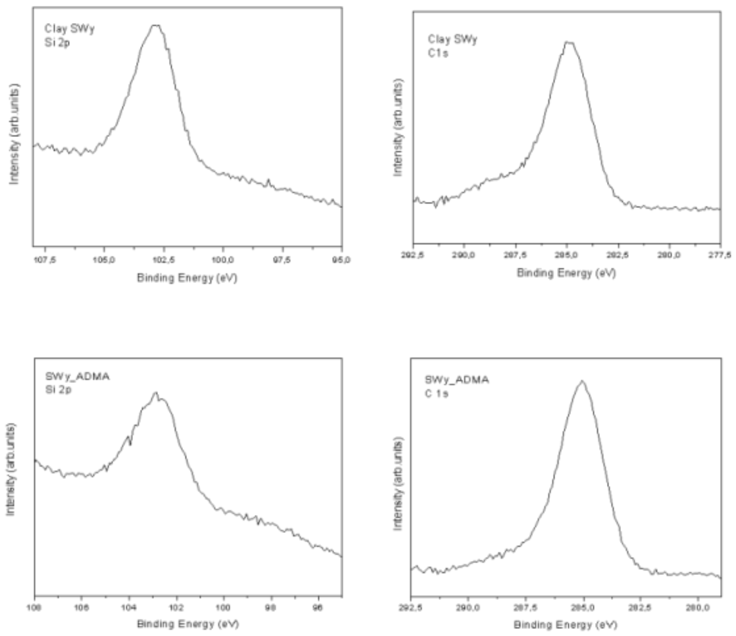

Ratio C/Si 1.42 ±0.06

Ratio C/Si 2.79 ±0.11

Figure 3.9. Comparison between the C1*s* and Si2*p* core level regions of the XPS spectra of pristine montmorillonite clay, SWy-2, and of the hybrid obtained after intercalation of adamantylamine, SWy-2/ADMA. The ratios between the C1*s* and the Si2*p* spectral intensities are indicated.

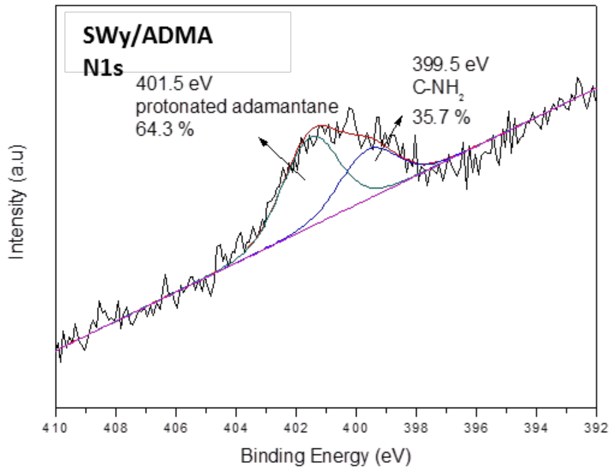

Figure 3.10. XPS spectrum of the N1*s* core level region of SWy-2/ADMA.

To estimate the amount of adamantylamine introduced in GO and in clay, thermogravimetric (TGA) and differential thermal analysis (DTA) measurements were performed on the two pillared hybrids as well as on the pristine materials. Based on these data, the weight loss observed in the temperature range 280–400 °C, which originates from the combustion of the amino groups of adamantylamine,[73, 74] was calculated to be equal to 8 and 4 wt% for GO/ADMA and SWy-2/ADMA, respectively. Moreover, in the case of SWy-2/ADMA, between 400 °C and 700 °C another weight loss of 8.5 wt%, due to combustion of the cycloalkane of adamantylamine, is observed. Based on these weight losses, we estimate that the amount of intercalated adamantylamine in the SWy-2/ADMA hybrid corresponds to ~12.5 wt%. In the case of GO/ADMA the second weight loss cannot be distinguished from the combustion of the graphene oxide layers, which takes place in this same temperature range.

In more detail the thermogravimetric (TGA) and differential thermal analysis (DTA) of pure graphite, graphene oxide, and the two composite nanostructures are displayed in Figures 3.11 a, b and c. The DTA curve of graphite (top left) exhibits an exothermic peak at 700 ^{o}C due to the combustion of carbon layers, while in the case of graphene oxide we have the presence of two exothermic peaks centred at 250 °C and 500 °C, which correspond to a 30 wt% and a 50 wt% weight loss, respectively. These peaks are attributed to the removal of oxygen-containing functional groups, created after the acid treatment of graphite (first peak), and to carbon combustion (second peak).[52] In the case of GO/ADMA, the DTA curve exhibits one exothermic peak at ~201 °C with 30 wt% weight loss, ascribed to the removal of oxygen-containing functional groups, while the combustion of the carbon layers appears at 540 °C. The weight loss observed in the temperature range 280–400 °C originates from the combustion of the amino groups of adamantylamine and represents ~8 wt% of the total mass of the material.

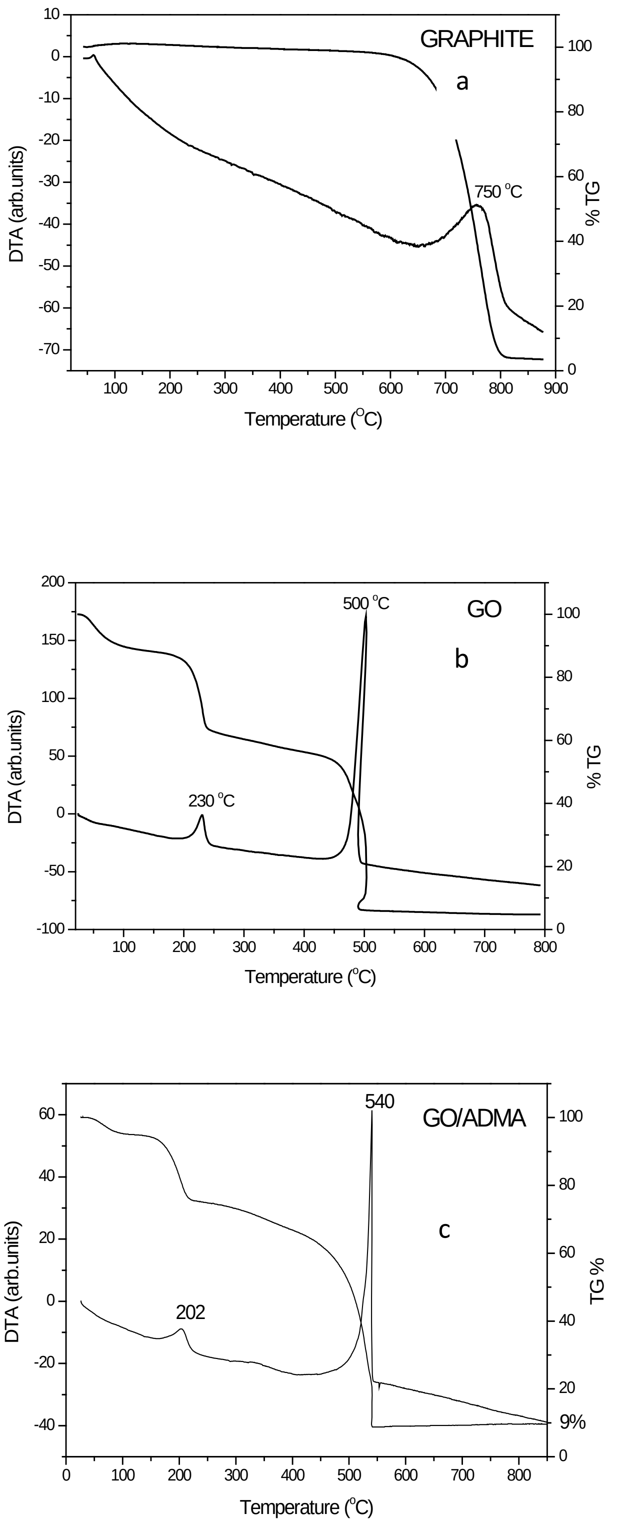

Figure 3.11. DTA and TGA curves of pristine graphite (a), GO (b) and of the GO/ADMA hybrid (c)

Thermogravimetric (TGA) and differential thermal analysis (DTA) of Lap/ADMA are displayed in Figure 3.12b. In the thermogravimetric analysis of this hybrid system we observe at 100 °C a weight loss of about 6.5 wt%, corresponding to the removal of physisorbed water. Above 100 °C and up to 400 °C a weight loss of 12 wt% due to the calcination of the amino groups of adamantylamine can be seen. Finally, between 400 °C and 750 °C another weight loss of 8 wt% is observed, which is due to combustion of the cycloalkane of adamantylamine. The two thermogravimetric weight losses between that range (400 °C and 750 °C) are probably due to adamantylamine molecules which reside with different orientation in the interlayer space of the laponite clay.

Undeniable proof for the successful intercalation of ADMA in the interlayer space of the montmorillonite clay mineral comes from the High-Resolution Transmission Electron Microscopy images. **Figure 3.13** shows HRTEM images of the SWy-2/ADMA hybrid system. From the TEM image of ADMA-intercalated SWy-2 at low magnification (Figure 3.13a) the inter sheet separation can be estimated, while the high degree of stacking of the clay platelets is also confirmed. The basal spacing is measured to be approximately 1.5 nm in agreement with the XRD findings. Moreover, in the TEM image at higher magnification shown at Figure 3.13 b, as well as in the zoomed-in image shown in Figure 3.13 d, intercalated ADMA layers (indicated by yellow arrows) can be recognized between clay layers, which are composed of an octahedral layer (pink arrow) sandwiched between two tetrahedral layers (blue arrows), as expected for a 2:1 layered silicate like montmorillonite (an octahedral alumina layer fused between two tetrahedral silica layers).

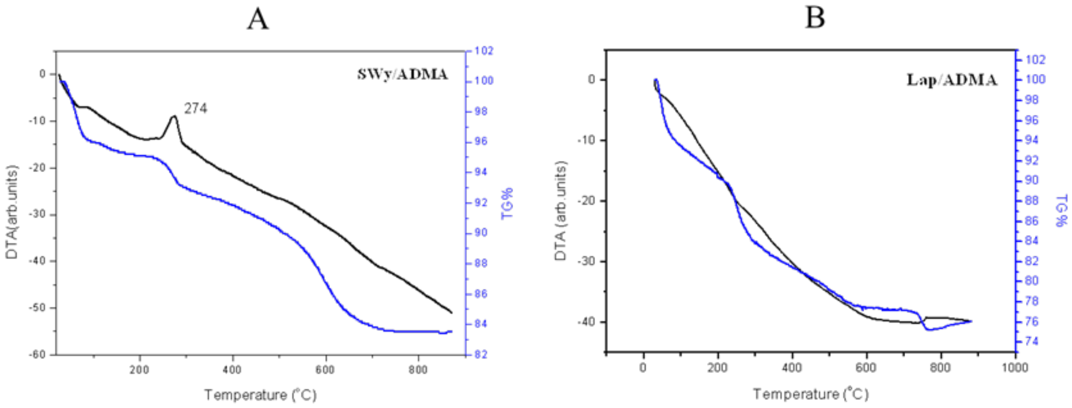

Figure 3.12. DTA and TGA curves of (a) SWy-2/ADMA and (b) DTA and TGA curves of Lap/ADMA.

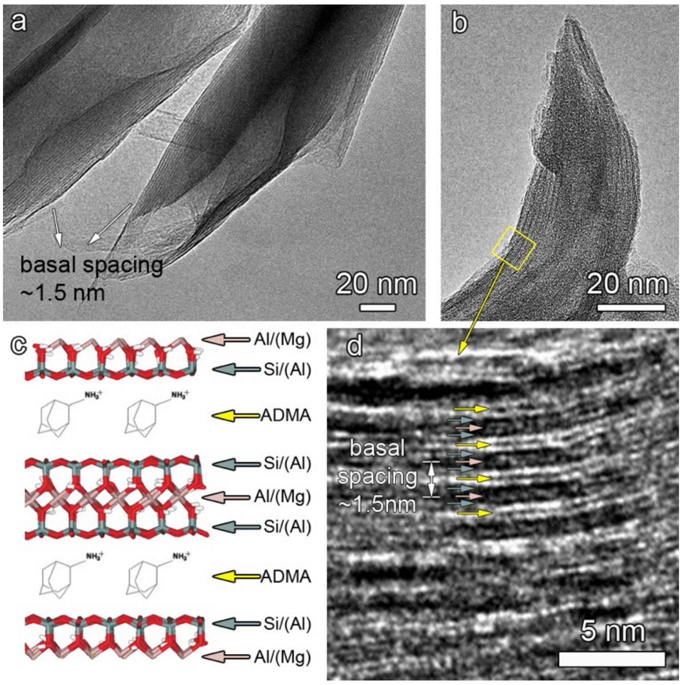

Figure 3.13. (a) TEM image of ADMA-intercalated SWy-2 at low magnification. Basal spacing is measured to be approximately 1.5 nm, consistent with the XRD measurement. (b) TEM image at higher magnification, with a zoomed-in image shown in (d). Intercalated ADMA layer (indicated by yellow arrows) can be recognized between clay layers which are composed (c) of tetrahedral layer (blue arrow) plus octahedral layer (pink arrow) plus tetrahedral layer (blue arrow).

Nitrogen adsorption-desorption measurements at 77K (-196.14 °C) were performed on both GO/ADMA and SWy-2/ADMA in order to reveal the creation of pillared structures. **Table 3.1** reports the specific-surface-areas obtained through BET analysis (S_{BET}) for the pristine layered matrices, GO and SWy-2, and for the corresponding pillared hybrid nanostructures. The specific surface area of pure GO (~ 9 m^2 g^{-1}) is small, indicating that N_2 can only adsorb on the external surfaces of GO and reduced GO while the interlayer space of GO is inaccessible. However, for the GO/ADMA hybrid the specific surface area is four times larger (37 m^2 g^{-1}) than for GO, supporting the hypothesis that adamantylamine acts as pillaring species. In fact, this result implies that nitrogen adsorbs not only on the external surface but also in the pores created by the ADMA pillars. The results were more pronounced in the case of the montmorillonite hybrid, which showed a significantly increased BET surface area (135 m^2 g^{-1}) compared to pristine montmorillonite clay.

Table 3.1. Specific surface area values for GO and SWy-2 and final hybrids GO/ADMA and SWy-2/ADMA.

	Specific Surface Area (S_{BET}) (m^2g^{-1})
GO	9
GO/ADMA	37
SWy-2	65
SWy-2/ADMA	135

In view of possible applications for these new pillared hybrids, we tested whether SWy-2/ADMA and GO/ADMA are capable of adsorbing organic pollutants (phenol derivatives) from solution. In Figure 3.14 the adsorption isotherms of 2.4.6-trichlorophenol (TCP), 2.4-dichlorophenol (DCP) and pentachlorophenol (PCP), in the starting material (SWy-2) and in the SWY-2/ADMA hybrid are shown. The adsorption isotherms present a plateau at increased chlorophenol:clay ratios which defines the maximum adsorption capacity of the material, listed in Table 3.2. As evident from the isotherms, TCP and DCP phenols adsorb in the interlayer space of the pristine clay as well as in the pores of SWy-2/ADMA, while the adsorption of PCP remained zero in all cases.

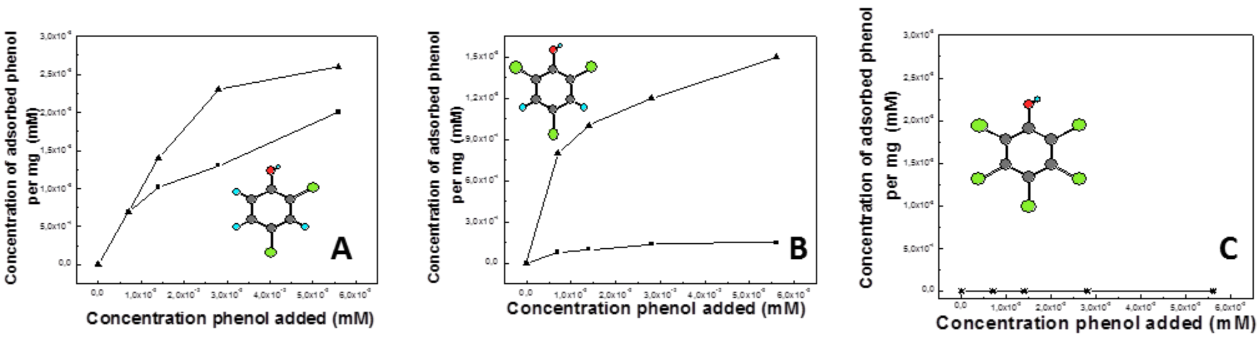

Figure 3.14. (A) Langmuir adsorption isotherms of 2,4-DCP on pristine SWy-2 clay (■) and SWy-2/ADMA (▲), (B) Adsorption isotherms of 2,4,6-TCP on pristine SWy-2 clay (☐) and SWy-2/ADMA (△), (C) Adsorption isotherms of PCP on pristine SWy-2 clay (☒) and SWy-2/ADMA (⨳).

Table 3.2. Maximum adsorption capacity for chlorophenol [mM per mg] by SWy-2 montmorillonite clay, GO and their derivatives SWy-2/ADMA and GO/ADMA.

Chlorophenol	SWy-2	SWy-2/ADMA	GO	GO/ADMA
2,4-DCP	$20×10^{-4}$	$27×10^{-4}$	0	$32×10^{-4}$
2,4,6-TCP	$2×10^{-4}$	$15×10^{-4}$	0	$1.3×10^{-4}$
PCP	0	0	0	0

From **Table 3.2** one notices the adsorption of the various phenols followed a consistent trend for all materials.

The uptake of DCP was significantly higher than for TCP. Strikingly the adsorption of PCP remained zero in all cases; the adamantylamine-intercalated clay showed an improved adsorption capacity with respect to that of the pristine clay. Indeed, SWy-2/ADMA adsorbed significantly higher amounts of DCP for all concentrations of added phenol and showed a 40 % enhanced uptake compared to the pristine clay at the highest phenol concentrations, see Table 3.2. SWy-2/ADMA also adsorbed almost eight times more TCP than the SWy-2. Comparing the three types of chlorophenol we conclude that the higher adsorption of DCP than of TCP as well as the negligible adsorption of PCP could be explained by the molecular size of the three phenols (stereospecific trapping): TCP and PCP are larger so they might block the pores of the pillared hybrid and thereby hamper the adsorption of further molecules (see physical model below).

Figure 3.15 presents the adsorption isotherms for TCP, DCP and PCP by GO/ADMA and by pristine GO. GO appears to adsorb none of the chlorophenols, whereas GO/ADMA adsorbs selectively only DCP while the adsorption of TCP and of PCP was minimal.

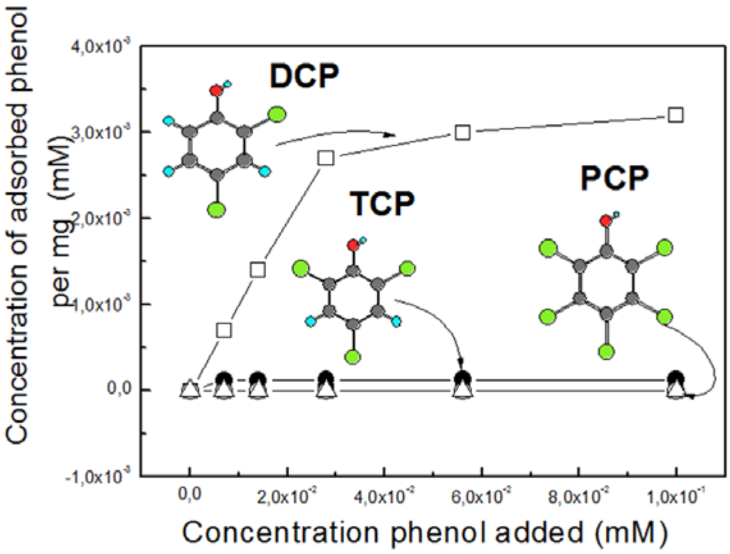

Figure 3.15. Adsorption isotherms of 2,4-DCP on pristine GO (■) and on GO/ADMA (☐); of 2,4,6-TCP on pristine GO (○) and on GO/ADMA (●); of PCP on pristine GO (△) and on GO/ADMA(▲).

Table 3.3. Molecular volume (Å^3) chemical structure and space filling surface of different phenols and of ADMA (calculated with ChemDraw7.0)

	Molecular volume (Å^3)	Chemical structure	Space filling surface
Pentachlorophenol	83.21	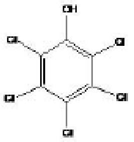	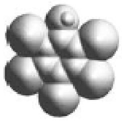
2,4,6-Trichlorophenol	67.92	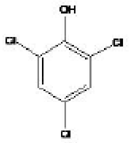	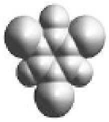
2,4-Dichlorophenol	60.25	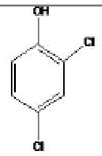	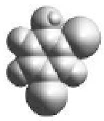
Adamantane	79.54	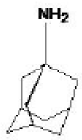	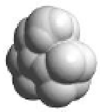

The observed differences in the uptake of PCP, 2,4,6-TCP and 2,4-DCP can be attributed to the difference in the molecular size of the phenols. As illustrated in Table 3.3, the molecular volumes are 60.3 Å^3 for DCP, 67.9 Å^3 for TCP and 83.2 Å^3 for PCP. Thus, the more bulky PCP is adsorbed less by the pillared clay and not at all by GO/ADMA, while DCP seems to be able to penetrate (stereospecific trapping) in the interlayer space of both SWy-2/ADMA and GO/ADMA. This can be explained if we take into account the change in the interlayer space as deduced from XRD (Figure 3.1). The interlayer distance of the pristine SWy-2 clay is 2.8 Å and becomes 6.0 Å in SWy-2/ADMA. On the other hand, the interlayer distance in pristine GO is 1.3 Å, which is much smaller than that of the pristine SWy-2 clay, and becomes 4.3 Å after modification with adamantylamine. Despite this increase, only DCP can be accommodated GO/ADMA and this results in the observed significant adsorption of DCP in contrast to TCP and PCP (selective/stereospecific adsorption).

Another possible future application of the pillared layered nanostructures is their use as cytotoxic agents. We chose laponite and intercalated laponite for these tests because this synthetic clay with small platelet size is used in pharmaceutical industry as drug carrier.[75] Nevertheless, there is a gap in knowledge concerning Laponite's *in vitro* antiproliferative activity. Thus, the present study evaluated the *in vitro* cytotoxic activity of adamantylamine, laponite and of the intercalated laponite, Lap/ADMA, against a cancer cell line (A549) and a normal one (MRC-5). Parallel to Lap/ADMA we also tested the cytotoxic behaviour of GO and GO/ADMA. The IC_{50} (μg/mL) values for cell proliferation (MTT assay) after 48 hs of treatment with adamantane hybrids and pristine materials are shown in Table 3.4 for A549 and MRC-5 cells and schematically presented in Figure 3.16. The IC_{50} values of ADMA, Lap and Lap/ADMA for A549 cells were 122±13.7 μg/mL, 205±20.7 μg/mL and 91±5.0 μg/mL. It is noteworthy that Lap and Lap/ADMA exhibited cytotoxic activity on MRC-5 cells (normal cells) in concentration higher than 250 μg/mL (288±41.8 μg/mL and 307±32.2 μg/mL for Lap and Lap/ADMA, respectively). The IC_{50} (μg/mL) values for cell proliferation (MTT assay) after 48 hs of treatment with GO and GO/ADMA for A549 cells were 259±48 μg/mL and 192±27.6 μg/mL, respectively, whereas GO and GO/ADMA exhibit cytotoxic action on normal cells (MRC-5) in concentration higher than 400 μg/mL (IC_{50} values for MRC-5 cells were 1480±39.6 μg/mL and 425±52.6 μg/mL for GO and GO/ADMA, respectively). What we observe is that Lap, Lap/ADMA, GO, GO/ADMA and ADMA exhibited antiproliferative activity against A549 cells. The control wells, containing different volumes of sterilized water (solvent) equal to volumes of the solutions added to the test wells, did not present any cytotoxicity against both cell lines (data not presented here). All substances, except ADMA, exhibited a mild cytotoxic activity on MRC-5 cells, with IC_{50} values being higher than 250 μg/mL and among all, Lap/ADMA is the most cytotoxic agent against the cancer cell line. In addition, Lap/ADMA showed a significantly higher cytotoxicity ($p<0.05$) compared to that of laponite (starting material) and adamantylamine against A459 cells. Similarly there is a statistically significant difference between cell lines treated with GO and GO/ADMA ($p<0.05$). Also GO/ADMA showed a lower cytotoxicity ($p<0.05$) compared with GO.

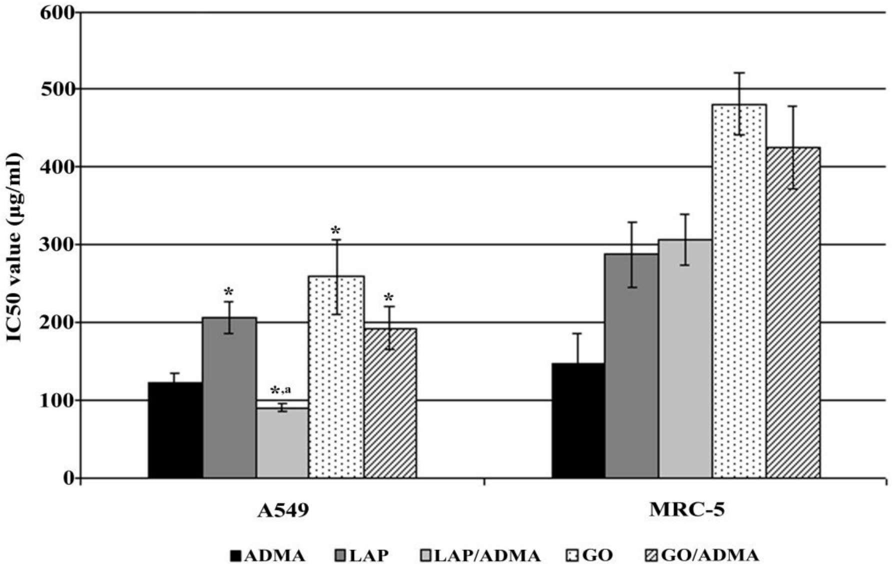

Figure 3.16. IC_{50} (μg/mL) values of ADMA, Lap/ADMA and GO/ADMA on A549 and MRC-5 cells, compared with pristine laponite clay (Lap) and GO.

Table 3.4. IC_{50} values (μg/mL) of ADMA, Lap, Lap/ADMA, GO and GO/ADMA on A459 and MRC-5 cells.

IC_{50} (μg/mL)	*A549*	*MRC-5*
ADMA	122 ± 13.7	149 ± 38.6
Lap	205 ± 20.7*	288 ± 41.8
Lap/ADMA	91 ± 5.0*,a	307 ± 32.2
GO	259 ± 48*	480 ± 39.6
GO/ADMA	192 ± 27.6*	425 ± 52.6

*Significant difference between cell lines; [a]Significant difference between Lap and Lap/ADMA; $p < 0.05$. Data are presented as mean ± σ (where σ is the standard deviation).

3.3. Conclusions

We successfully achieved the intercalation of adamantylamine into the interlayer space of layered host materials, namely graphite oxide, montmorillonite and laponite clay. X-ray diffraction measurements demonstrated the successful intercalation of adamantylamine into all three host matrixes. In the case of montmorillonite an undeniable proof for the successful intercalation comes from TEM images. X-ray photoelectron spectroscopy, FTIR spectroscopy as well as thermogravimetric and differential thermal analysis illustrated the type of interactions between the host materials and the intercalated molecules as well as informing on the intercalation yield. Porosimetry measurements revealed that pillared structures were created and gave the specific surface area of the hybrid nanostructures. The hybrid nanomaterial obtained by intercalation of adamantylamine into montmorillonite clay is capable of adsorbing significant quantities of organic pollutants, which entails a significant potential for environmental remediation. GO/ADMA showed a stereospecificity-determined, selective DCP uptake. Finally the hybrid nanostructures obtained by intercalation of adamantylamine into laponite clay and graphene oxide were investigated for their cytotoxicity against one cancer cell line and one normal cell line. The findings revealed that Lap/ADMA and GO/ADMA presented improved cytotoxic activity on A549 cells, whilst the cytotoxicity towards MRC-5 cells (normal cells) is maintained or only slightly increased as compared to Lap and GO, respectively. Possibly, these combinations act synergistically by combining two different molecular pathways, leading to higher cytotoxicity. Further biological investigation is needed to elucidate the roles of Lap, GO, ADMA and their combinations on cancer and normal cell lines. We established a controllable and reproducible method for the synthesis of multi-functional materials with potential for exploitation in the fields of environmental remediation and biomedical applications.

References

*[1] G. Ali Mansoori, in Advances in Chemical Physics, John Wiley & Sons, Inc., **2008**, pp. 207-258.*

*[2] G. C. McIntosh, M. Yoon, S. Berber, D. Tománek, Physical Review B - Condensed Matter and Materials Physics **2004**, 70, 045401-045408.*

*[3] R. C. Merkle, Nanotechnology **2000**, 11, 89-99.*

*[4] R. Rawls, Chemical and Engineering News **2002**, 80, 13.*

*[5] S. I. Zones, Y. Nakagawa, G. S. Lee, C. Y. Chen, L. T. Yuen, Microporous and Mesoporous Materials **1998**, 21, 199-211.*

*[6] M. A. Meador, Annual Review of Materials Science **1998**, 28, 599-630.*

*[7] G. A. Mansoori, T. F. George, G. Zhang, L. Assoufid, Molecular Building Blocks for Nanotechnology: From Diamondoids to Nanoscale Materials and Applications: Preface, Vol. 109, Springer, **2007**.*

*[8] H. Ramezani, G. A. Mansoori, Topics in Applied Physics **2007**, 109, 44-71.*

*[9] A. Orzeszko, R. Gralewska, B. J. Starościak, Z. Kazimierczuk, Acta Biochimica Polonica **2000**, 47, 87-94.*

*[10] J. G. Hardman, L. E. Limbird, The pharmacological basis of therapeutics, 10th ed., McGraw-Hill Book Co, New York, **2001(book)**.*

*[11] M. S. Whittingham, A. J. Jacobson, Intercalation Chemistry, Academic, New York, **1982(book)**.*

*[12] A. Vaccari, Appl. Clay Sci. **1999**, 14, 161-198.*

*[13] M. Darder, M. Lopez-Blanco, P. Aranda, F. Leroux, E. Ruiz-Hitzky, Chemistry of Materials **2005**, 17, 1969-1977.*

*[14] J. D. Choi, G. M. Choi, Sens. Actuator B-Chem. **2000**, 69, 120-126.*

[15] *L. L. Zhang, S. Y. Zhao, X. N. Tian, X. S. Zhao, Langmuir **2010**, 26, 17624-17628.*

[16] *J. N. Coleman, M. Lotya, A. O'Neill, S. D. Bergin, P. J. King, U. Khan, K. Young, A. Gaucher, S. De, R. J. Smith, I. V. Shvets, S. K. Arora, G. Stanton, H.-Y. Kim, K. Lee, G. T. Kim, G. S. Duesberg, T. Hallam, J. J. Boland, J. J. Wang, J. F. et al., Science **2011**, 331, 568-571.*

[17] *T. Shichi, K. Takagi, Journal of Photochemistry and Photobiology C: Photochemistry Reviews **2000**, 1, 113-130.*

[18] *D. Gournis, V. Georgakilas, M. A. Karakassides, T. Bakas, K. Kordatos, M. Prato, M. Fanti, F. Zerbetto, Journal of the American Chemical Society **2004**, 126, 8561-8568.*

[19] *D. Gournis, L. Jankovic, E. Maccallini, D. Benne, P. Rudolf, J. F. Colomer, C. Sooambar, V. Georgakilas, M. Prato, M. Fanti, F. Zerbetto, G. H. Sarova, D. M. Guldi, Journal of the American Chemical Society **2006**, 128, 6154-6163.*

[20] *B. K. G. Theng, The Chemistry of Clay Organic Reactions, Adam Hilger, London, **1974(book)**.*

[21] *T. J. Pinnavaia, Science **1983**, 220, 365-371.*

[22] *J. Konta, Appl. Clay Sci. **1995**, 10, 275-335.*

[23] *G. Lagaly, Solid State Ionics **1986**, 22, 43-51.*

[24] *A. Cornelis, P. Lazlo, (Ed.: NATO-ASI), **1986**, pp. 165, 213-228 **(goverment document)**.*

[25] *J. A. Ballantine, (Ed.: NATO-ASI), **1986**, pp. 165, 197-212 **(goverment document)**.*

[26] *V. Georgakilas, D. Gournis, D. Petridis, Angewandte Chemie - International Edition **2001**, 40, 4286-4288.*

[27] V. Georgakilas, D. Gournis, A. B. Bourlinos, M. A. Karakassides, D. Petridis, Chemistry - A European Journal ***2003****, 9, 3904-3908.*

[28] J. T. Kloprogge, Journal of Porous Materials ***1998****, 5, 5-41.*

[29] A. Gil, L. M. Gandía, M. A. Vicente, Catalysis Reviews - Science and Engineering ***2000****, 42, 145-212.*

[30] Y. Ma, W. Tong, H. Zhou, S. L. Suib, Microporous and Mesoporous Materials ***2000****, 37, 243-252.*

[31] K. Ohtsuka, Chemistry of Materials ***1997****, 9, 2039-2050.*

[32] M. Boufatit, H. Ait-Amar, W. R. Mc Whinnie, Desalination ***2008****, 223, 366-374.*

[33] T. A. Wolfe, T. Demirel, E. R. Baumann, Clay Clay Min. ***1985****, 33, 301-311.*

[34] C. Viseras, P. Cerezo, R. Sanchez, I. Salcedo, C. Aguzzi, Appl. Clay Sci. ***2010****, 48, 291-295.*

[35] M. I. Carretero, Appl. Clay Sci. ***2002****, 21, 155-163.*

[36] C. Aguzzi, P. Cerezo, C. Viseras, C. Caramella, Appl. Clay Sci. ***2007****, 36, 22-36.*

[37] A. Lerf, H. He, M. Forster, J. Klinowski, Journal of Physical Chemistry B ***1998****, 102, 4477-4482.*

[38] N. I. Kovtyukhova, Chemistry of Materials ***1999****, 11, 771-778.*

[39] N. I. Kovtyukhova, B. R. Martin, J. K. N. Mbindyo, P. A. Smith, B. Razavi, T. S. Mayer, T. E. Mallouk, Journal of Physical Chemistry B ***2001****, 105, 8762-8769.*

[40] H. K. Jeong, M. Jin, E. J. Ra, K. Y. Sheem, G. H. Han, S. Arepalli, Y. H. Lee, ACS Nano ***2010****, 4, 1162-1166.*

[41] P. K. Ang, S. Wang, Q. L. Bao, J. T. L. Thong, K. P. Loh, Acs Nano ***2009****, 3, 3587-3594.*

[42] A. Kumar, A. L. M. Reddy, A. Mukherjee, M. Dubey, X. B. Zhan, N. Singh, L. Ci, W. E. Billups, J. Nagurny, G. Mital, P. M. Ajayan, Acs Nano, 5, 4345-4349.

[43] W. Lv, D. M. Tang, Y. B. He, C. H. You, Z. Q. Shi, X. C. Chen, C. M. Chen, P. X. Hou, C. Liu, Q. H. Yang, Acs Nano ***2009****, 3, 3730-3736.*

[44] Z. Liu, J. T. Robinson, X. Sun, H. Dai, J. Am. Chem. Soc. ***2008****, 130, 10876-10877.*

[45] C.-H. Lu, C.-L. Zhu, J. Li, J.-J. Liu, X. Chen, H.-H. Yang, Chemical Communications ***2010****, 46, 3116-3118.*

[46] X. Sun, Z. Liu, K. Welsher, J. Robinson, A. Goodwin, S. Zaric, H. Dai, Nano Research ***2008****, 1, 203-212.*

[47] X. Yang, X. Zhang, Y. Ma, Y. Huang, Y. Wang, Y. Chen, Journal of Materials Chemistry ***2009****, 19, 2710-2714.*

[48] W. Yang, K. R. Ratinac, S. P. Ringer, P. Thordarson, J. J. Gooding, F. Braet, Angewandte Chemie International Edition ***2010****, 49, 2114-2138.*

[49] L. Zhang, J. Xia, Q. Zhao, L. Liu, Z. Zhang, Small ***2010****, 6, 537-544.*

[50] Y. Chang, S.-T. Yang, J.-H. Liu, E. Dong, Y. Wang, A. Cao, Y. Liu, H. Wang, Toxicology Letters ***2011****, 200, 201-210.*

[51] K. Wang, J. Ruan, H. Song, J. Zhang, Y. Wo, S. Guo, D. Cui, Nanoscale Res Lett ***2010****, 6, 8.*

[52] A. B. Bourlinos, D. Gournis, D. Petridis, T. Szabo, A. Szeri, I. Dekany, Langmuir ***2003****, 19, 6050-6055.*

[53] R. Y. N. Gengler, A. Veligura, A. Enotiadis, E. K. Diamanti, D. Gournis, C. Jozsa, B. J. van Wees, P. Rudolf, Small ***2010****, 6, 35-39.*

[54] D. R. Dreyer, S. Park, C. W. Bielawski, R. S. Ruoff, Chemical Society Reviews ***2010****, 39, 228-240.*

[55] R. N. Tiwari, L. Chang, Journal of Applied Physics ***2010****,* 3 *,*4*, 45501. .*

[56] I. Dekany, R. Kruger-Grasser, A. Weiss, Colloid and Polymer Science ***1998****, 276, 570-576.*

[57] A. G. Johnston, D. A. Leigh, A. Murphy, J. P. Smart, M. D. Deegan, Journal of the American Chemical Society ***1996****, 118, 10662-10663.*

[58] D. A. Leigh, A. Murphy, J. P. Smart, A. M. Z. Slawin, Angewandte Chemie (International Edition in English) ***1997****, 36, 728-732.*

[59] C. Seel, F. Vögtle, Chemistry - A European Journal ***2000****, 6, 21-24.*

[60] M. A. Karakassides, D. Gournis, D. Petridis, Clay Minerals ***1999****, 34, 429-438.*

[61] M. A. Karakassides, D. Petridis, D. Gournis, Clay Clay Min. ***1997****, 45, 649-658.*

[62] P. Stathi, K. Litina, D. Gournis, T. S. Giannopoulos, Y. Deligiannakis, Journal of Colloid and Interface Science ***2007****, 316, 298-309.*

[63] D. W. Lee, L. De Los Santos V, J. W. Seo, L. L. Felix, A. Bustamante D, J. M. Cole, C. H. W. Barnes, Journal of Physical Chemistry B ***2010****, 114, 5723-5728.*

[64] F. Tuinstra, J. L. Koenig, Journal of Chemical Physics ***1970****, 53, 1126..*

[65] M. A. Pimenta, G. Dresselhaus, M. S. Dresselhaus, L. G. Cançado, A. Jorio, R. Saito, Physical Chemistry Chemical Physics ***2007****, 9, 1276-1291.*

[66] K. N. Kudin, B. Ozbas, H. C. Schniepp, R. K. Prud'homme, I. A. Aksay, R. Car, Nano Letters ***2008****, 8, 36-41.*

[67] M. Herrera-Alonso, A. A. Abdala, M. J. McAllister, I. A. Aksay, R. K. Prud'homme, Langmuir ***2007****, 23, 10644-10649.*

[68] Y. Lin, A. M. Rao, B. Sadanadan, E. A. Kenik, Y. P. Sun, Journal of Physical Chemistry B ***2002****, 106, 1294-1298.*

[69] *E. Metwalli, D. Haines, O. Becker, S. Conzone, C. G. Pantano, Journal of Colloid and Interface Science* ***2006****, 298, 825-831.*

[70] *D. Gournis, L. Jankovic, E. Maccallini, D. Benne, P. Rudolf, J.-F. Colomer, C. Sooambar, V. Georgakilas, M. Prato, M. Fanti, F. Zerbetto, G. H. Sarova, D. M. Guldi, Journal of the American Chemical Society* ***2006****, 128, 6154-6163.*

[71] *T. L. Barr, in Practical Surface Analysis, 2nd ed. (Eds.: D. Briggs, M. P. Seah), John Wiley, Chinchester, U.K.,* ***1990****, p. Chapt. 8.*

[72] *D. Gournis, A. E. Mantaka-Marketou, M. A. Karakassides, D. Petridis, Physics and Chemistry of Minerals* ***2001****, 28, 285-290.*

[73] *S. P. Economopoulos, G. Rotas, Y. Miyata, H. Shinohara, N. Tagmatarchis, ACS Nano* ***2010****, 4, 7499-7507.*

[74] *A. Enotiadis, K. Angjeli, N. Baldino, I. Nicotera, D. Gournis, Small* ***2012****, 8, 3338-3349.*

[75] *J. K. Park, Y. B. Choy, J.-M. Oh, J. Y. Kim, S.-J. Hwang, J.-H. Choy, International Journal of Pharmaceutics* ***2008****, 359, 198-204.*

Appendix

Adsorption of chlorophenols

The left panel of Figure S9 presents UV-Vis spectra for 2,4,6-TCP and 2,4-DCP and PCP. Quantification of the chlorophenols was done using the peak at 280 nm for 2,4-DCP, the peak at 290 nm for 2,4,6-TCP and the one at 210 nm for PCP, as marked by arrows. By comparing these UV-Vis spectra for solutions with known phenol concentrations with the corresponding spectra recorded after adsorption on pristine SWy-2 and on the two types of SWy-2/ADMA hybrids – see examples in the right panel of Figure S1 - we could calculate the concentration of chlorophenol adsorbed in each case and compile the adsorption isotherms.

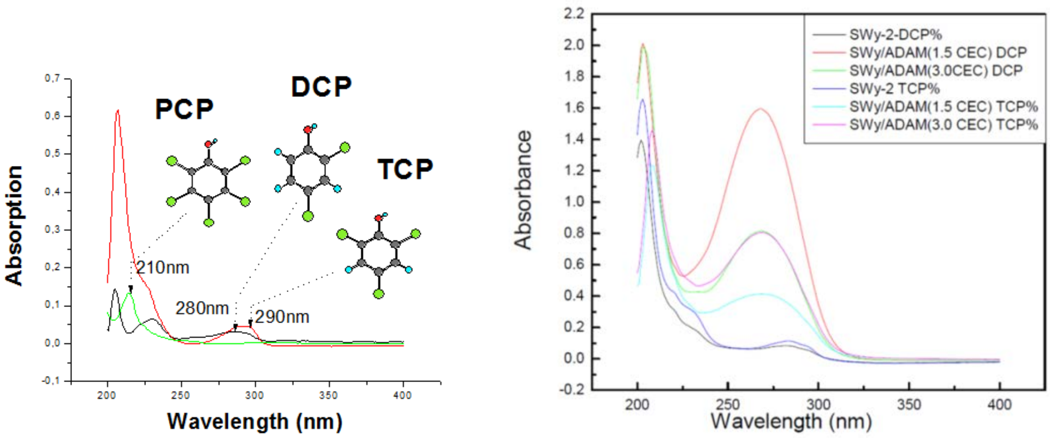

Figure S1. Left panel: UV-Vis spectra of 20 μM 2.4.6-trichlorophenol (TCP, red curve), 2.4-dichlorophenol (DCP, black curve) and pentachlorophenol (PCP, green curve) in MetOH:H_2O 70:30 v/v. The arrows mark the peaks used for quantitative analysis of adsorption. **Right panel:** UV-vis spectra of 2.4.6-trichlorophenol (TCP) and 2.4-dichlorophenol (DCP) adsorbed on SWy-2/ ADMA prepared with 1.5 and 3.0 CEC).

Table S1. Molecular volume (Å^3) Chemical structure and space filling surface of different phenols (calculated with ChemDraw7.0)

	Molecular volume (Å^3)	Chemical structure	Space filling surface
Pentachlorophenol	83.21	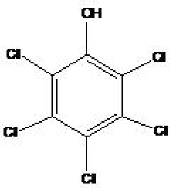	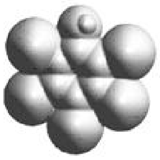
2,4,6-Trichlorophenol	67.92	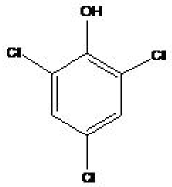	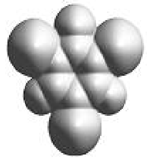
2,4-Dichlorophenol	60.23	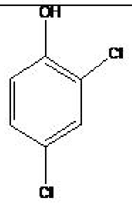	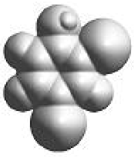
Adamantane	79.34	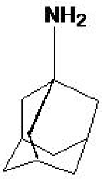	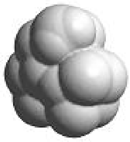

CHAPTER 4

Oxidized carbon nanodiscs as cytotoxic agents

In this work we report the fabrication of soluble hydrophilic carbon nanodiscs by the chemical oxidation of insoluble pristine carbon nanodiscs (CNDs) using the method that is commonly used for the graphite oxidation. The pristine CNDs were prepared through the pyrolytic Kvaerner Carbon Black & H_2 process using an industrial-scale carbon-arc plasma torch generator. The oxidized product is decorated with various oxygen-containing functional polar groups, converting the insoluble CNDs to a hydrophilic derivative that can be easily disperse in polar solvents including water. These hydrophilic derivatives are expected to find application a wide range of fields including biomedicine. In this work they were tested as antiproliferative agents for two cell lines, a healthy and a cancer one, in order to investigate their cytotoxic properties.

This Chapter is partially based on the article by P. Zygouri, T.Tsoufis, A. Kouloumpis, M. Patila, G.Potsi, Z. Sideratou, F. Katsaros, G. Charalambopoulou, H. Stamatis, P. Rudolf, T. A. Steriotis and D. Gournis, Hydrophilic oxidized carbon nanodiscs: A promising multifunctional nanocarbon for bioapplications, to be submitted.

4.1. Introduction

Among the many nanomaterials synthesized the last decades carbon nanostructured materials occupy the most prominent position. This is due to the unusual potential of carbon to form many allotropes thanks to its sp^3, sp^2 and sp hybridization. Carbon low-dimensional nanostructures include the 0D fullerenes, the 1D carbon nanotubes and the 2D graphene. Their discovery and investigation[1][2]lead to two Nobel prizes awarded to Kroto, Smalley, Curl in 1996 for the discovery of fullerenes and to Novoselov and Geim in 2010 for the discovery of graphene. Carbon nanostructures distinguish themselves for low density, high specific surface, tunable pore structure, chemical stability as well as the excellent electronic, thermal and mechanical properties and hence are promising candidates for a wide range of applications including organic electronic[3]photovoltaics,[4]biological and medical applications,[5][6] catalyst supports,[7] field emission devices,[8] nanoprobes,[9] sensors,[8] semiconductor devices,[10] composite materials (polymeric or ceramic),[11][12][13][14] nanoelectronics,[15] gas separations,[7] supercapacitors,[16] and energy storage materials[17].

Carbon nanodiscs (CNDs), are synthesized through the so-called pyrolytic Kvaerner Carbon Black & H_2 (CB&H) Process, [18][19] where hydrocarbons (typically heavy oil) are decomposed to carbon and H_2 based on the use of an industrial-scale carbon-arc plasma torch generator operating at a temperature around 2000 °C. The carbon product consists of three different turbostratic graphitic microstructures, namely flat CNDs (no pentagons), conical carbon structures (1-5 pentagons) and amorphous carbon (soot), with volume fractions around 82 %, 5 % and 13 %, respectively[19]. CNDs are micron sized, ultrathin quasi two-dimensional particles with diameter 1-4 μm, while the co-existing carbon cones are of similar size. Garberg *et al.*[20] showed that CNDs are multilayer structures with a graphitic core and outer non-crystalline layers. CNDs are considered to have homogeneous thickness, typically in the range 10–30 nm. The degree of graphitization can be greatly promoted by post heat-treatment at 2700 °C under argon[21]. Annealed CNDs and cones are almost single crystalline in the c-direction and may thus be considered as stacks of a limited number of graphene layers (usually < 100)[21].

The size of these disc-like carbon nanostructures is large enough to maintain important graphite properties such as electrical conductivity and on the other hand, small enough and even ideal in some cases, for applications in biotechnology, nanomedicine and drug delivery. The main disadvantage of CNDs is that - like all other carbon structures - they are insoluble in polar solvents, which renders them difficult to process.

Chemical modification of their surface is a solution to this problem since it improves their ability to disperse in organic solvents and water. It is thus through functionalization that they become more compatible with other materials and more easily included in the preparation of composites. The aim of this project is to apply a simple and reproducible approach for the chemical oxidation of CNDs, similar to the well-known Staudenmaier's method[22]that has been applied for the chemical oxidation of graphite[23][24]. As we shall show in the following, strong acid treatment results the CND surface decoration with various oxygen-containing functional polar groups such as hydroxyl, carboxyl and epoxy groups. These functional groups convert the CNDs into a hydrophilic derivative, which is completely soluble in polar solvents including water. A beneficial side effect of the acid treatment is that it also separates the CNDs from the nanocones and soot in the mixed starting material. A number of characterization techniques was applied to characterize the functionalized nanodiscs, namely Fourier transform infrared (FTIR), μ-Raman and X-ray photoelectron spectroscopies, X-ray diffraction, thermogravimetric analysis (DTA/TGA) and atomic force microscopy (AFM). Oxidized carbon nanodiscs are expected to have a wide range of diverse applications in the chemical and pharmaceutical industry, as well as in electronics. In this project we tested the cytotoxic properties of oxCNDs on two different cell lines in order to investigate potential future applications in biomedicine and bio-catalysis.

4.2. Results and discussion

To verify that the oxidation of CNDs results in the creation of oxygen containing groups covalently attached on the surface of the discs similarly to graphene oxide, we employed FTIR and XPS spectroscopies. The FTIR spectra of pristine and oxidized carbon nanodiscs are shown in Figure 4.1. Contrary to the pristine CNDs oxidized carbon nanodiscs exhibit intensive vibrational bands in the region of 1000-1700 cm^{-1}. More specifically, the band at 1058 cm^{-1} is assigned to stretching vibrations of C–O groups, while the weak peak at 1405 cm^{-1} is due to bending vibrations (deformation) of hydroxyl groups C-OH groups [25][26]. The band at 1620 cm^{-1} is attributed to the C=O stretching vibrations of the –COOH groups[26], while the the band at 1230cm^{-1} is assigned to asymmetric stretching of C-O-C bridges in epoxy groups and to deformation vibrations of O-H in the carboxylic acid groups. The presence of all these characteristic vibrational bands testifies to the successful oxidation of the carbon nanodiscs.

The XPS spectrum of the C1s core level region of oxCNDs shown in Figure 4.2 can be deconvoluted in three main contributions: the first peak at a binding energy of 284.8 eV is assigned to the C-C bonds of the graphitic framework[27] and accounts for 82.4 %

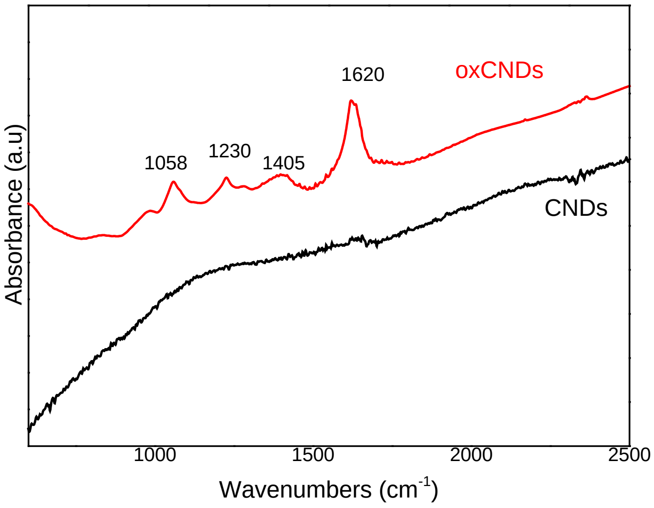

Figure 4.1. FT-IR spectra of pristine (black) and oxidized carbon nanodiscs (red).

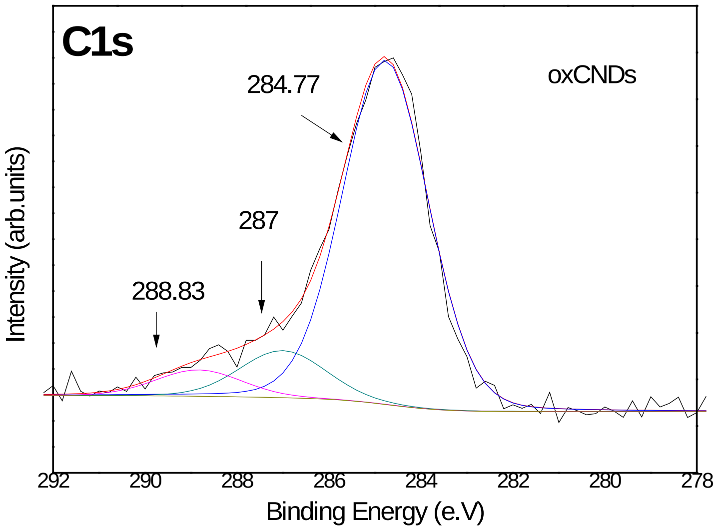

Figure 4.2. XPS spectrum of the C 1s core level region of oxidized carbon nanodiscs (oxCNDs).

of the overall carbon 1s intensity; a second peak attributed to C-O bonds at 287.0 eV makes up 11.2 % of the total C1s intensity, while a third contribution at 288.8 e.V (6.2% of the overall C1s intensity) is assigned to O-C=O bonds.[28][29] These contributions from C-O, C=O and O-C=O bonds do not appear in the corresponding XPS spectrum of the starting material[30] and hence the oxygen-containing groups must have formed during the strong acidic treatment of the CNDs. The oxidation process is therefore similar to that of graphene oxide produced from graphite with the Staudenmaier's method.[29][31][32][33][34]

An additional technique that confirmed the successful oxidation of CNDs was Raman spectroscopy. The Raman spectra of pristine and oxidized carbon nanodiscs are presented in **Figure 4.3.** Both show the characteristic first-ordered G- and D- bands at around 1600 and 1350 cm^{-1}, respectively. The G-band originates from the doubly degenerate *E2g* mode around the Brillouin zone centre and is associated with sp^2-hybridized carbon atoms. The D-band is related to sp^3 hybridized carbon atoms as it

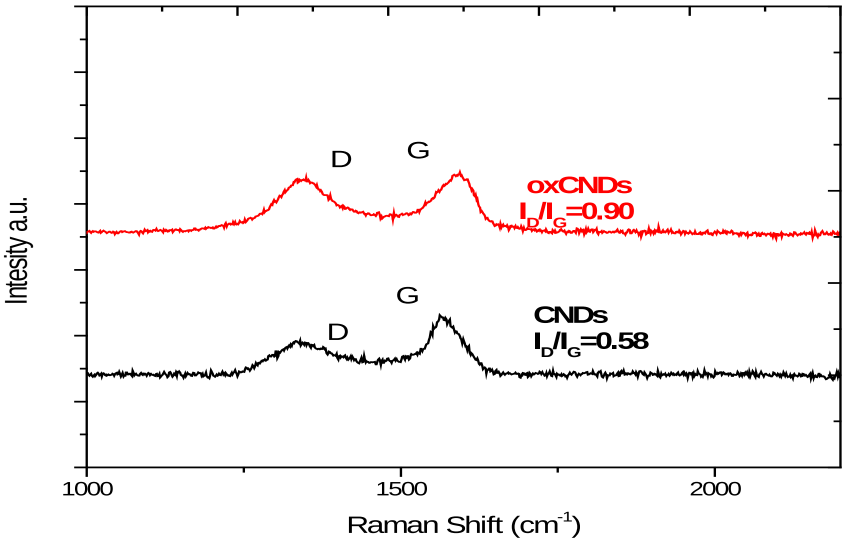

Figure 4.3. Raman spectra of pristine CNDs (black) and oxCNDs (red)

requires a defect or an edge for its activation by double resonance, thus indicating the presence of lattice defects and distortions.[35][36][37][38]The ratio of the D- to G-band intensities (I_D/I_G) is indicative of the quality of the graphitic lattice and was found to be 0.57 for the pristine CNDs. The important increase of the I_D/I_G ratio in oxCND sheets which is at least 0.90 as can be postulated via the relative increase of the D′ band (1620 cm^{-1}) which exceeds the intensity of the G band[39] confirms the change in the hybridization of the carbon atoms from sp^2 to sp^3, due to the creation of oxygenated groups (hydroxyl, carboxyl or epoxide) that are covalently attached to the double bonds of aromatic groups.

The results from the thermogravimetric analysis (TGA) of pristine and oxidized carbon nanodiscs are shown in Figure 4.4. In the pristine CNDs, the major drop in the mass is observed around 630 °C, followed by complete decomposition of the material, indicating the thermal destruction of the graphitic network of the carbons nanodiscs. In the case of oxCNDs a continuous weight loss is observed at the temperature range between 140 and 320 °C; we attribute this loss to the removal of the oxygen containing groups (hydroxyl, carboxyl, epoxy) covalently attached to the graphitic layers of CNDs. The drop in the mass is estimated to be 25 wt% indicating the degree

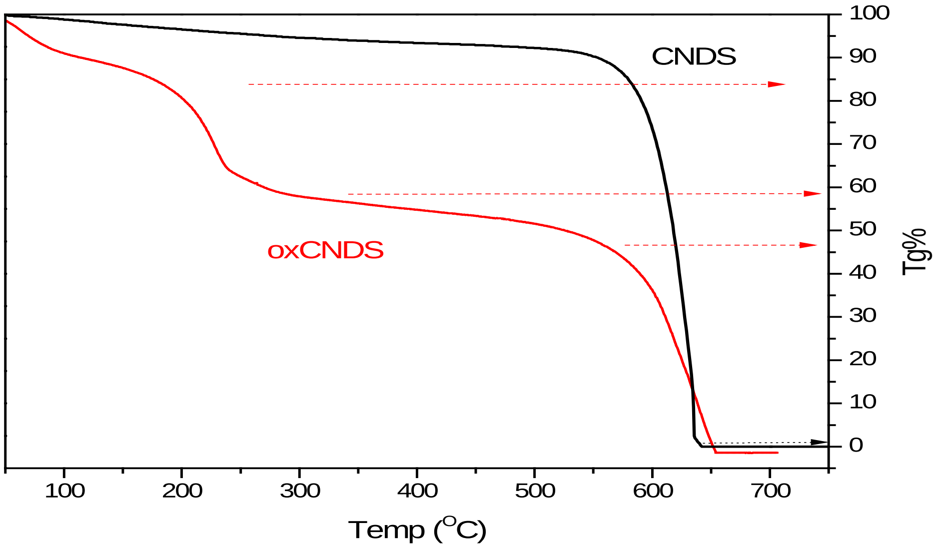

Figure 4.4. Weight loss curves collected during the thermogravimetric analysis of pristine (black) and oxidized carbon nanodiscs (red).

of functionalization that has occurred upon oxidation of the pristine CNDs. Moreover, carbon combustion (decomposition of graphitic lattice) occurs at lower temperatures compared to pristine CNDs, namely around 440 °C, since the presence of oxygenated species facilitates an accelerated graphitic network combustion.

The X-ray diffraction patterns of pristine and oxidized carbon nanodiscs are presented in Figure 4.5a. Pristine CNDs display a well-defined peak at 26.6°, which is attributed to the 002 reflection of the graphite lattice and mirrors a basal spacing d_{002}=3.4 Å. In the case of oxCNDs this diffraction peak disappears and a new sharp one is present at lower angles (~11.4 °). The latter is due to the principal 001 reflection and corresponds to a basal spacing of d_{001}= 7.7 Å, indicative of the successful oxidation of graphitic layers of the CNDs with the creation of oxygen-containing groups that are randomly distributed on the basal planes and edges of the graphenic nanodiscs.

The morphology of the oxidized nanodiscs was examined thoroughly with AFM microscopy. Figure 4.5b shows a representative micrograph of isolated nanodiscs

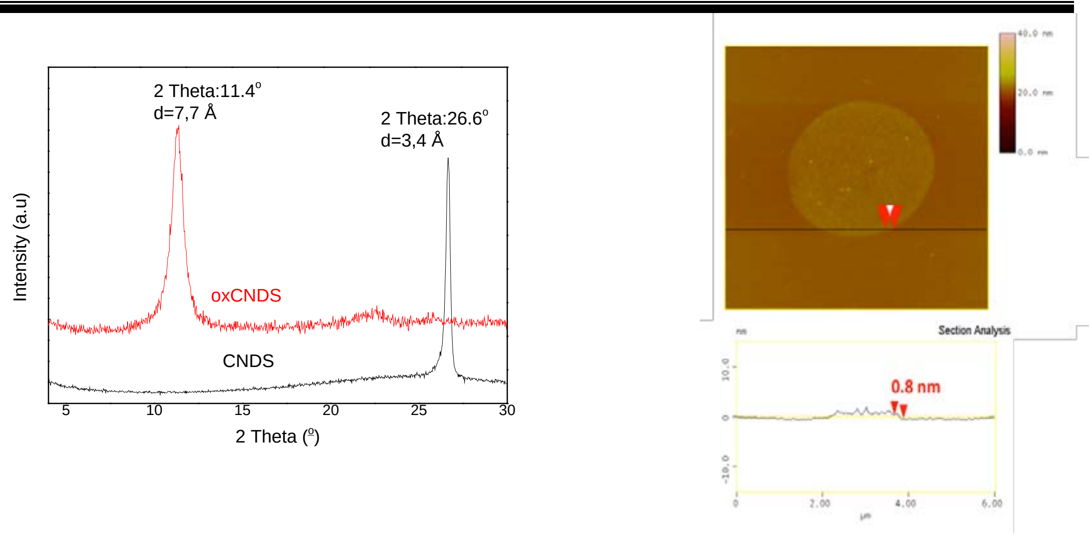

Figure 4. 5. X-ray diffraction patterns (a) pristine (black|) and oxidized carbon nanodisks (red), (b) AFM image of oxCNDs.

with a thickness of 0.8 Å, as calculated from topographical height profile These monoatomic graphitic nanodiscs are the majority of the scanned area. However, nanodiscs with thickness between 2 and 5 nm are also present, indicating the occurrence of larger discs consisted of several graphitic layers.

In view of possible applications for these new oxidized nanocarbons we tested whether oxCNDs can be used as cytotoxic agent on human embryonic kidney Hek293T and human adenocarcinoma HeLa cell lines. The results of the cell viability assays shown in Figures 4.6 and 4.7. Figure 4.6 shows the absorbance related to mitochondrial redox function, indicative of cell viability of the cell lines. When oxCNDs in the range of 0 μg/ml- 1mg/ml are added, we can observe that comparing the effect of oxCNDs on both Hek293T (healthy) and HeLa (cancer) cells, HeLa cells are effected more by the presence of oxCNDs. A way to quantify this effect is to determine the half maximal inhibitory concentration or IC_{50} values for both cell lines, *i.e.* the concentration oxCNDs required for 50 % inhibition of cell growth. As we see in Figure 4.7, in the case of Hek293T cell line IC_{50} amounts to 82 μg/ml. In other words, for this concentration half of the cells (50%) are still alive after adding the oxCNDs. On the other hand, in the case of HeLa cancer cells, only 33 μg/ml are needed to achieve the same effect. Therefore oxCNDs are a very promising hybrid material suitable not only as an effective support for enzyme immobilization for the development of nanobiocatalytic systems as reported previously[40]but also antiproliferative agent on a specific cancer line.

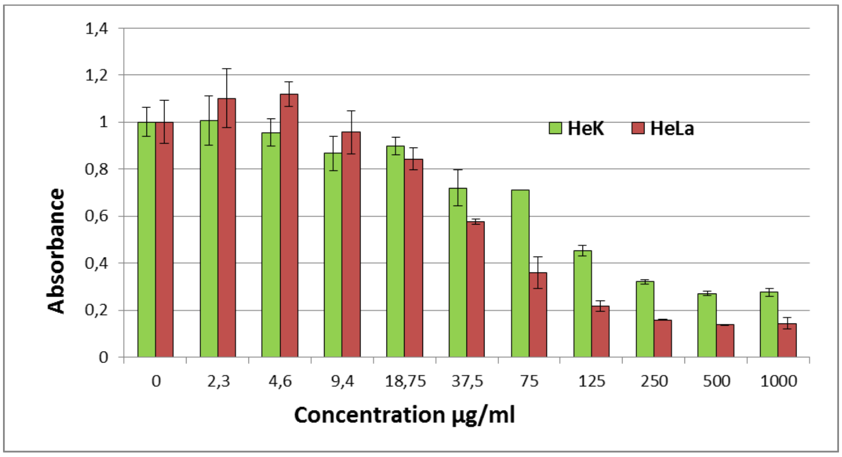

Figure 4.6. Absorbance % graph of oxCNDs for Hek293T (green) and HeLa(red) cell lines for concentration 0 μg-1000 μg.

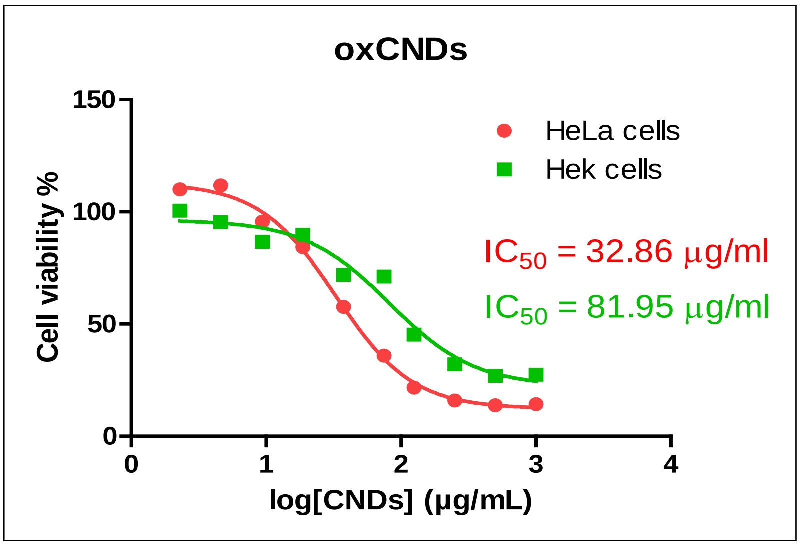

Figure 4.7. IC_{50} graph of oxCNDs for Hek293T (green) and HeLa (red) cell lines.

4.3. Conclusions

Insoluble carbon nanodiscs produced by the CB&H_2 process were successfully oxidized using a simple approach based on the well-known Staudenmaier's method. After strong acid treatment the surface of the CNDs is decorated with various oxygen-containing functional polar groups such as hydroxyl, carboxyl and epoxy groups, converting the completely insoluble CNDs into a hydrophilic derivative that is dispersible in many polar solvents, including water. X-ray diffraction, FTIR, XPS and Raman spectroscopies confirm the successful chemical functionalization and the presence of oxygen-containing functional groups covalently attached on the oxCNDs. Thermogravimetric and differential thermal analysis showed the high degree of functionalization of the pristine CNDs. Morphology studies by AFM microscopy show that the material is composed mainly of isolated monoatomic graphenic nanodiscs with a mean diameter in the range of 1 and 2 μm and a thickness of 0.8 Å; a small minority of few layer flakes is also observed. These hydrophilic nanostructures were tested as cytotoxic agents. Cell viability assays revealed that oxCNDs exhibited significant higher cytoxic activity on adenocarcinoma HeLa cell lines than on human embryonic kidney Hek293T cells, indicating that oxidized carbon nanodiscs is a very promising hybrid material for future biomedical applications.

References

[1] J. Ginsberg, *American Chemical Society* **2010**, **(*Commemorativ*e Booklet).**

[2] A. K. Geim, K. S. Novoselov, *Nat Mater* **2007**, *6*, 183–191.

[3] J. Wu, W. Pisula, K. Müllen, *Chemical Reviews* **2007**, *107*, 718–747.

[4] F. Wang, D. Kozawa, Y. Miyauchi, K. Hiraoka, S. Mouri, Y. Ohno, K. Matsuda, *Nat Commun* **2015**, *6* **(*Article number: 6305,open access).***

[5] M. Patila, I. V Pavlidis, E. K. Diamanti, P. Katapodis, D. Gournis, H. Stamatis, *Process Biochemistry* **2013**, *48*, 1010–1017.

[6] A. Galano, *Nanoscale* **2010**, *2*, 373–380.

[7] P. Serp, M. Corrias, P. Kalck, *Applied Catalysis A: General* **2003**, *253*, 337–358.

[8] M. Inagaki, L. R. Radovic, *Carbon* **2002**, *40*, 2279–2282.

[9] S. Subramoney, *Advanced Materials* **1998**, *10*, 1157–1171.

[10] V. Georgakilas, D. Gournis, V. Tzitzios, L. Pasquato, D. M. Guldi, M. Prato, *Journal of Materials Chemistry* **2007**, *17*, 2679–2694.

[11] D. Tasis, N. Tagmatarchis, A. Bianco, M. Prato, *Chemical Reviews* **2006**, *106*, 1105–1136.

[12] R. Andrews, D. Jacques, D. Qian, T. Rantell, *Accounts of Chemical Research* **2002**, *35*, 1008–1017.

[13] H. He, C. Gao, *Chemistry of Materials* **2010**, *22*, 5054–5064.

[14] M. Moniruzzaman, K. I. Winey, *Macromolecules* **2006**, *39*, 5194–5205.

[15] P. K. Ang, S. Wang, Q. Bao, J. T. L. Thong, K. P. Loh, *ACS Nano* **2009**, *3*, 3587–3594.

[16] E. Frackowiak, F. Béguin, *Carbon* **2001**, *39*, 937–950.

[17] A. Kumar, A. L. M. Reddy, A. Mukherjee, M. Dubey, X. Zhan, N. Singh, L. Ci, W. E. Billups, J. Nagurny, G. Mital, et al., *ACS Nano* **2011**, *5*, 4345–4349.

[18] S. Lynum, J. Hugdahl, K. Hox, R. Hildrum, M. Nordvik, **2008 (patent)**.

[19] A. Krishnan, E. Dujardin, M. M. J. Treacy, J. Hugdahl, S. Lynum, T. W. Ebbesen, *Nature* **1997**, *388*, 451–454.

[20] T. Garberg, S. N. Naess, G. Helgesen, K. D. Knudsen, G. Kopstad, A. Elgsaeter, *Carbon* **2008**, *46*, 1535–1543.

[21] W. Zhang, M. Dubois, K. Guérin, P. Bonnet, E. Petit, N. Delpuech, D. Albertini, F. Masin, A. Hamwi, *Carbon* **2009**, *47*, 2763–2775.

[22] H. L. Poh, F. Sanek, A. Ambrosi, G. Zhao, Z. Sofer, M. Pumera, *Nanoscale* **2012**, *4*, 3515–3522.

[23] R. Y. N. Gengler, A. Veligura, A. Enotiadis, E. K. Diamanti, D. Gournis, C. Józsa, B. J. van Wees, P. Rudolf, *Small* **2010**, *6*, 35–39.

[24] D. V Stergiou, E. K. Diamanti, D. Gournis, M. I. Prodromidis, *Electrochemistry Communications* **2010**, *12*, 1307–1309.

[25] D. W. Lee, L. De Los Santos V., J. W. Seo, L. L. Felix, A. Bustamante D., J. M. Cole, C. H. W. Barnes, *The Journal of Physical Chemistry B* **2010**, *114*, 5723–5728.

[26] K. Spyrou, G. Potsi, E. K. Diamanti, X. Ke, E. Serestatidou, I. I. Verginadis, A. P. Velalopoulou, A. M. Evangelou, Y. Deligiannakis, G. Van Tendeloo, et al., *Advanced Functional Materials* **2014**, *24*, 5841–5850.

[27] D. Yang, A. Velamakanni, G. Bozoklu, S. Park, M. Stoller, R. D. Piner, S. Stankovich, I. Jung, D. A. Field, C. A. Ventrice Jr., et al., *Carbon* **2009**, *47*, 145–152.

[28] T. Tsoufis, F. Katsaros, Z. Sideratou, G. Romanos, O. Ivashenko, P. Rudolf, B. J. Kooi, S. Papageorgiou, M. A. Karakassides, *Chemical Communications* **2014**, *50*,

10967–10970.

[29] J. W. Chiou, S. C. Ray, S. I. Peng, C. H. Chuang, B. Y. Wang, H. M. Tsai, C. W. Pao, H.-J. Lin, Y. C. Shao, Y. F. Wang, et al., *The Journal of Physical Chemistry C* **2012**, *116*, 16251–16258.

[30] N. Mahato, N. Parveen, M. H. Cho, *Materials Express* **.**, *5*, 471–479.

[31] M. Acik, C. Mattevi, C. Gong, G. Lee, K. Cho, M. Chhowalla, Y. J. Chabal, *ACS Nano* **2010**, *4*, 5861–5868.

[32] D. Long, W. Li, L. Ling, J. Miyawaki, I. Mochida, S.-H. Yoon, *Langmuir* **2010**, *26*, 16096–16102.

[33] D. C. Marcano, D. V Kosynkin, J. M. Berlin, A. Sinitskii, Z. Sun, A. Slesarev, L. B. Alemany, W. Lu, J. M. Tour, *ACS Nano* **2010**, *4*, 4806–4814.

[34] C. Mattevi, G. Eda, S. Agnoli, S. Miller, K. A. Mkhoyan, O. Celik, D. Mastrogiovanni, G. Granozzi, E. Garfunkel, M. Chhowalla, *Advanced Functional Materials* **2009**, *19*, 2577–2583.

[35] A. C. Ferrari, J. C. Meyer, V. Scardaci, C. Casiraghi, M. Lazzeri, F. Mauri, S. Piscanec, D. Jiang, K. S. Novoselov, S. Roth, et al., *Physical Review Letters* **2006**, *97*, 187401.

[36] F. Torrisi, T. Hasan, W. Wu, Z. Sun, A. Lombardo, T. S. Kulmala, G.-W. Hsieh, S. Jung, F. Bonaccorso, P. J. Paul, et al., *ACS Nano* **2012**, *6*, 2992–3006.

[37] R. Saito, A. Jorio, A. G. Souza Filho, G. Dresselhaus, M. S. Dresselhaus, M. A. Pimenta, *Physical Review Letters* **2001**, *88*, 27401.

[38] C. Thomsen, S. Reich, *Physical Review Letters* **2000**, *85*, 5214–5217.

[39] F. Tuinstra, *The Journal of Chemical Physics* **1970**, *53*, 1126.

[40] P. Zygouri, T. Tsoufis, A. Kouloumpis, M. Patila, G. Potsi, Z. Sideratou, H.

Katsaros, Fotios Charalambopoulou, Georgia, Stamatis, P. Rudolf, T. A. Steriotis, D. Gournis, *To be submitted* **.**

CHAPTER 5

Carbon Nanostructures containing Polyhedral Oligomeric Silsesquioxanes (POSS)

This review chapter describes the synthesis and properties of carbon nanostructures containing organic-inorganic cage-like polyhedral oligomeric silsesquioxane (POSS) nanoparticles. The physical and chemical functionalization of carbon nanomaterials such as graphene, graphene oxide, carbon nanotubes, and fullerenes with POSS towards the development of novel hybrid nanostructures is described in detail. Special emphasis is given to the potential impact of these hybrid nanostructures on various technological applications.

This Chapter is based on the invited mini review: Carbon Nanostructures containing Polyhedral Oligomeric Silsesquioxanes (POSS) by G. Potsi, A. Rossos, A. Kouloumpis, M. K. Antoniou, K. Spyrou, M. A. Karakassides, D. Gournis and P. Rudolf, Current Organic Chemistry, 20, (6), 662-673, 2016.

5.1. Introduction

Silsesquioxanes belong to the family of silicone resins[1] that have been used in a plethora of applications due to their exceptional properties such as thermal and photo stability, electric insulation, chemical stability and functionalities. Silsesquioxanes with a general formula $RSiO_{3/2}$ possess a pronounced aptitude to form three-dimensional (3-D) cage-like highly symmetric frameworks known as polyhedral oligosilsesquioxanes (POSS). Several structures are known for silsesquioxanes, including random, ladder, partially condensed and cage (*e.g*. T8, T10 and T12) types.[2] These cubic, hexagonal, octagonal, decagonal, dodecagonal or even open cage-like structures derive from hydrolytic condensation reactions of trifunctional organosilicon monomers[3] with formula $RSiOH_3$, where R is an organic group covalently attached to the silicon chain. POSS with the general formula $R_nSi_nO_{1.5n}$, where R is a vertex group including hydrogen or organic functional groups,[2],[4] consist of an inorganic silica-oxygen core and polar or non-polar organic substituents attached at the edges of the cage (see cubic analogue in Figure 5.1). This multiple functionality of POSS – in addition with their nanopore size that varies between 1-3 nm depending on the length of the R groups[5] - make them chemically compatible with many nanocomposite constituents like polymers, nanocarbons, inorganic layered materials, biological systems, or DNA.[6, 7, 8, 9, 10, 11, 12, 13, 14, 15] POSS can be attached to these systems[16] mainly via covalent linking on the surface or physical blending. After the discovery of the first POSS in 1946[17] a wide variety of stable 3-D polyhedral oligosilsesquioxane frameworks have been reported, with an immense variety of functional groups imparting new interesting properties to the silica cage structure.[18, 19]

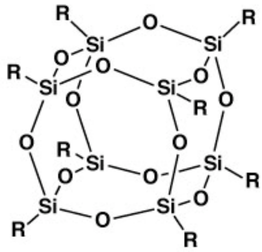

Figure 5.1. Molecular structure of a cubic polyhedral oligomeric silsesquioxane (POSS).

Polyhedral oligomeric silsesquioxanes appear highly promising candidates for the synthesis of hybrid nanomaterials suitable for a wide range of applications. The incorporation of POSS has been first applied into polymer matrices with the aim to improve the polymer properties in terms of higher thermal stability, mechanical stiffness and viscosity.[20] Moreover, immense efforts have been made worldwide over the last decade to incorporate 3D silsesquioxanes into carbon nanomaterials in order to enhance the characteristics of the resulting nanohybrids for various technological sectors such as energy storage,[21, 22] environmental applications[23] and biomedicine.[24, 25, 26] This mini-review focuses on the most recent experimental scientific endeavours to create novel materials combining cubic POSS (most common polyhedral structure) with carbon nanostructures such as graphene, carbon nanotubes and fullerenes. The design and development of these novel systems is of high importance for optical,[24, 27, 28, 29, 30] and thermal[31, 32, 33, 34] applications as well as in the fields of electronics[21, 29, 35, 36] and solar cells.[23, 37]

5.2. Fullerene functionalization with POSS and their derivatives

In 2008, David J. Clarke and coworkers[24] reported for the first time polyhedral oligomeric silsesquioxane bound to fulleropyrrolidines. These derivatives were proposed as suitable optical limiters, expected to find applications in various scientific, industrial, medical and military fields, where lasers are utilized. It is well known that the protection against pulsed tunable lasers is a great challenge. C_{60} solutions have been identified as effective optical limiters.[24] However, in order to extend the optical limiting behaviour of C_{60} to the solid phase (for example in a polymeric matrix), which is preferred for practical applications, David J. Clarke *et al*.[24] covalently linked fullerene derivatives to POSS even though these two nanoparticles are generally immiscible and own different molecular shapes. They proposed two quite long synthetic pathways[24] for the functionalization of fulleropyrrolidines with POSS as depicted in Figures 5.2 and 5.3. The characterization of the two POSS derivatives in solution confirmed the presence of the fulleropyrrolidines and an optical power limiting essentially identical to that of C_{60}. Since the optical properties of C_{60} were retained in the final compounds, the authors proposed that the incorporation of the POSS-C_{60} in a polymeric matrix through the synthesis of a N-functionalized amino glycine and its reaction with POSS-C_{60}. The combination of the two classes of material (POSS and C_{60}) leads to a successful integration of the properties of the two components in the new hybrid materials. Apart from the laser-focused applications proposed by the authors, the derived hybrids present important features for various nanotechnological fields including polymer reinforcement, solar cells, sensors, etc.

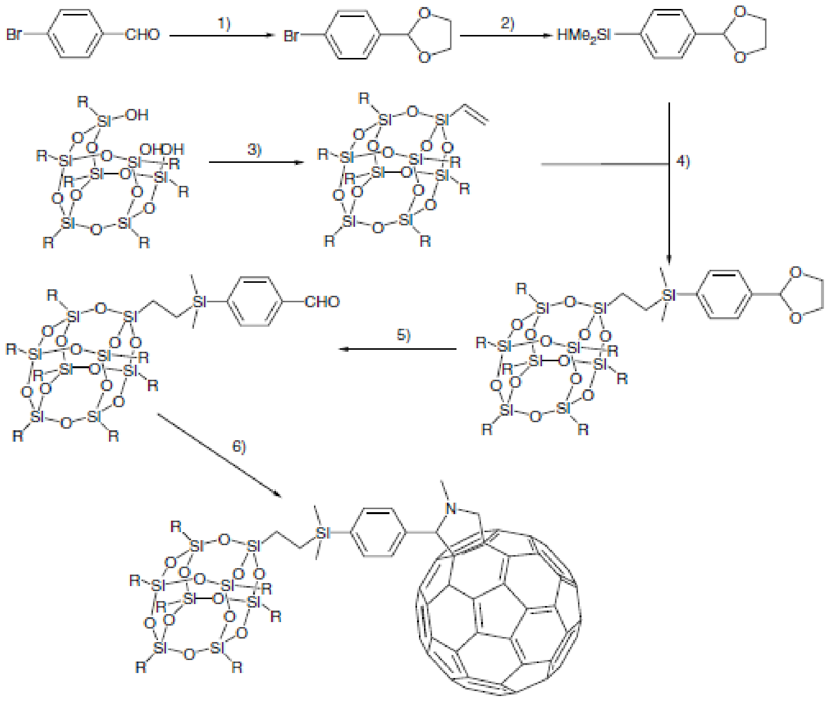

1) Ethylene Glycol, p-toluenesulfonic acid, C_6H_6; 2) Mg, $HSiMe_2Cl$, Et_2O; 3) CH_2=$CHSiCl_3$, Et_3N, Et_2O; 4) Karstedt's catalyst, 5) Et_2O; Pyridinium p-toluenesulfonate, acetone; 6) C_{60}, sarcosine, toluene
R = iBu, Ph

Figure 5.2. Synthesis of POSS/fulleropyrrolidines (synthetic pathway 1). (Reproduced with permission from Ref.[24])

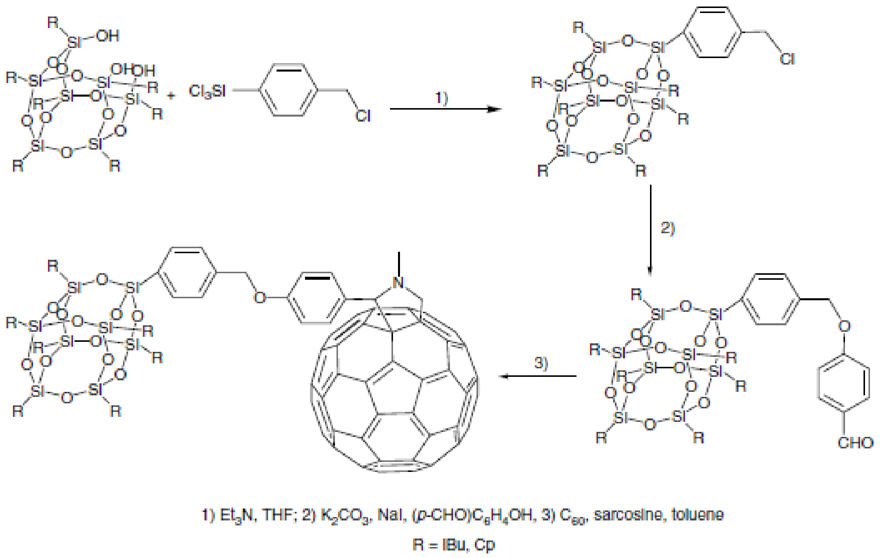

Figure 5.3. Synthesis of POSS/fulleropyrrolidines (synthetic pathway 2). (Reproduced with permission from Ref.[24])

To avoid the long synthetic route followed to obtain the POSS-fulleropyrrolidine described above, one year later, the same group of researchers synthesized and characterized a POSS-iminofullerene compound[27] shown in Figure 5.4. Their purpose was to prepare POSS-fullerene derivatives with short phenyl groups and optical limiting capacity, which could be incorporated into polymers. The study of the optical limiting properties of POSS-iminofullerene in solution showed that also in this case the optical power limiting of the compound was the same as that of C_{60}.

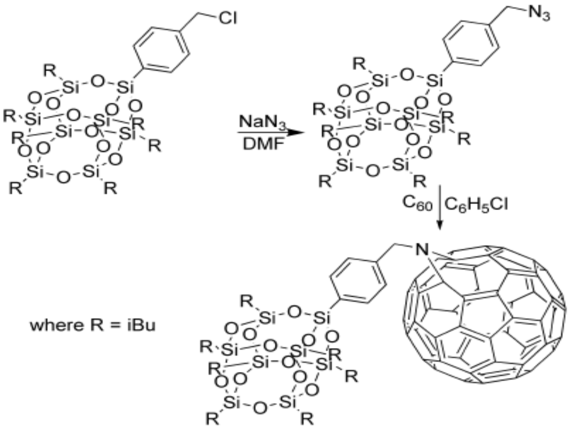

Figure 5.4. Synthesis of POSS/iminofullerene. (Reproduced with permission from Ref.[27])

Hao-Jan Sun *et al.*[21] synthesized and characterized a sphere-cubic shaped amphiphile composed of an inorganic-organic POSS-C_{60} dyad. Since POSS has insulating and C_{60} semiconducting properties in the solid state, crystals of this dyad can find application in nano-capacitors. POSS and C_{60} were connected with a short and single covalent linkage in order to prevent a macroscopic phase separation. More specifically, the POSS-C_{60} dyad was synthesized by Steglich esterification[21, 38] of a carboxylic acid-functionalized C_{60} and hydroxyl-functionalized POSS. The esterification was carried out in a mixed solvent of CH_2Cl_2/DMF. The resultant dyad exhibits polymorphism with two crystal lattices: orthorhombic and hexagonal. Both crystalline forms present a bi-layered structure, which contains double layers of C_{60} and double layers of POSS moieties. The C_{60}-C_{60} interaction is stronger in the case of the hexagonal lattice than in the orthorhombic one. A comparison between the two crystalline forms in terms of thermodynamic stability and structural formation kinetics showed that the hexagonal phase is thermodynamically more stable (higher melting point), while the orthorhombic phase was found to be kinetically more favourable and easier to form.

In 2012, Fafu Yang *et al.* claimed that the POSS-C_{60} derivatives with short phenyl groups are not favourable for homogeneous dispersion in polymers.[39] For this reason they designed and synthesized dumbbell-shaped POSS-C_{60} dyads where POSS and C_{60} are linked with long and flexible aliphatic spacers. These POSS-fullerene dyads possess great flexibility and compatibility with polymers. Figure 5.5 presents the synthetic route that was followed to obtain the POSS-C_{60} dyads in multiple steps with a total yield around 40 %.

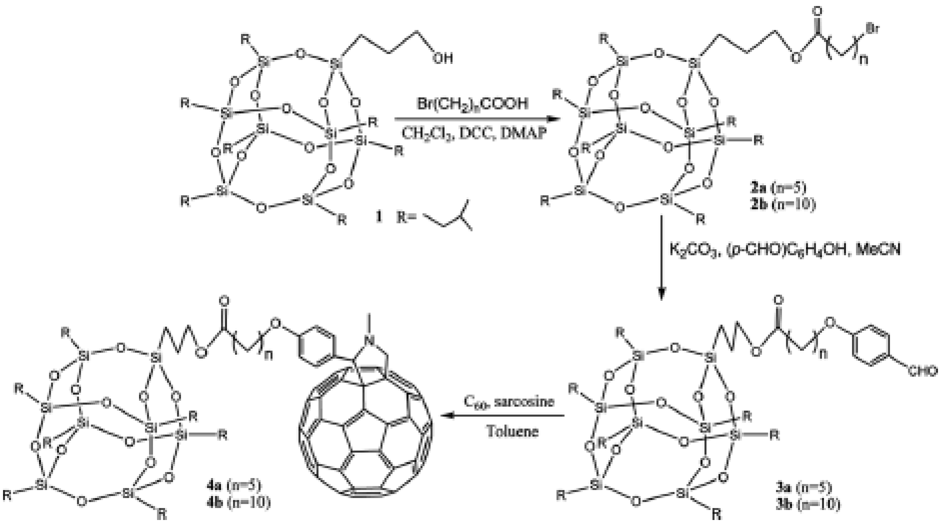

Figure 5.5. Synthesis of POSS-C_{60} dyads. (Reproduced with permission from Ref.[39])

Two years later, Cheng and his colleagues,[40] reported the design of an asymmetric giant amphiphile by combining two isobutyl POSS (BPOSS) and one C_{60}. This amphiphile is prepared by the Bingel reaction[41] and its structure consists of two different layer thicknesses of C_{60} and BPOSS, while the C_{60} layer is sandwiched between two BPOSS layers. After the coupling of the two BPOSS to the C_{60}, the total symmetry of the molecule reduces from I_h (C_{60}'s symmetry) to C_{2v} (diBPOSS-C_{60}).[42],[43] The possibility of altering the sizes and shapes of the molecular units which are used in order to obtain the giant amphiphiles, as well as the control of the thickness of the resulting layers, are two interesting characteristics that could lead to practical application as nano-capacitors.[44]

Important progress in the incorporation of POSS and fullerene into polymers was made in 2008 when Weihua Kai *et al.* succeeded in linking these compounds to both ends of the same polymer chains (poly(ε-caprolactone), PCL).[45] In this way, the poor solubility of C_{60} could be (partially) overcome and the final polymers presented improved optical limiting and thermomechanical properties. Inoue and coworkers prepared three different materials: a fullerene double end-capped PCL, a POSS single end-capped PCL and a fullerene and POSS double end-capped PCL (see Figure 5.6). They found that both POSS and C_{60} moieties aggregate in small particles onto the ends of the PCL chains creating a network structure. The confinement effect of POSS and C_{60} on the crystallization behaviour of PCL resulted in a decrease of the crystallization enthalpy (ΔH) from the DSC analysis (Table 5.1). As it is shown, the ΔH value of POSS single end-capped PCL is almost the same as that of double end-capped one, while that of fullerene and POSS double end-capped PCL decreases. Nevertheless, the value of such decrease is much smaller compared to that of PCL with fullerenes at both ends. This can be ascribed to the formation of the network structure by the aggregation of the fullerene moieties at both the ends of the PCL, while in the case of the fullerene and POSS double end-capped PCL the network structure is formed by two types of aggregates (fullerene and POSS moieties). Consequently, the confinement effect of the fullerene aggregates on the crystallization of PCL is stronger than that of POSS aggregates. Therefore, Weihua Kai *et al.* concluded that depending on the fullerene and POSS end cappings, it is possible to synthesize various kinds of aggregated polymeric materials with different network strengths.

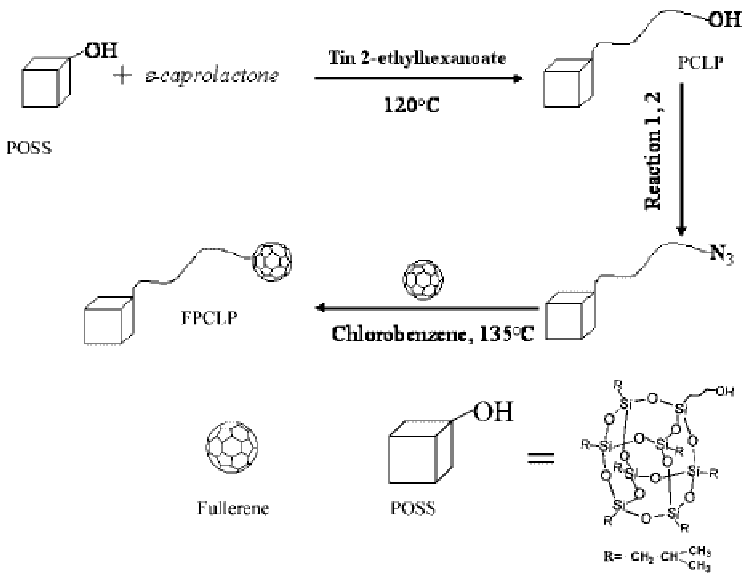

Figure 5.6. Synthetic pathway for fullerene and POSS double end capped PCL. (Reaction 1: Chlorobutyryl chloride, pyridine, room temperature; Reaction 2: Sodium azide, DMF, 65 °C. (Reproduced with permission from Ref.[45])

Table 5.1. Thermal properties of PCL and its fullerene (F) and POSS (P) capped derivatives.

Sample Code	DPCL	FPCLF	PCLP	FPCLP
ΔH (J g^{-1}) [a]	72.2	51.1	75.5	69.9
T_{mc} (°C) [a]	27.3	22.7	27.9	29.9
POSS content % [b]	-	-	10.0	10.0
Fullerene content % [c]	-	12.7	-	7.0

a. The crystallization enthalpy (ΔH) and melt crystallization temperature (T_{mc}) were determined from DSC and normalized with the PCL content b. The weight content of POSS calculated from TG results c. The fullerene weight content determined from the TG at a temperature about 600 °C.[45]

In 2012 Wen-Bin Zhang and coworkers[23] prepared and applied a POSS-C_{60} dyad as a novel electron acceptor for bulk heterojunction polymer solar cells with an inverted device configuration. The conducting polymer chosen to be mixed with POSS-C_{60} was poly[4,4’-bis(2-ethylhexyl)dithienol[3,2-b:2’,3’-d]silole)-2,6-diyl-*alt*-(4,7-bis(2-thienyl)-2,1,3-benzothiadiazole)-5,5’-diyl] (SiPCPDTBT). The incorporation of POSS into electro-active materials results in improved stability and device performance,[37] while C_{60} derivatives are commonly employed as electron acceptors in bulk heterojunction polymer solar cells. POSS-C_{60} dyads provide the benefits of both molecular moieties: electronic properties and versatile functionalization. Wen-Bin Zhang *et al.*[23] studied the ability of these bulk heterojunction materials to generate increased short circuit current and open circuit voltage for high power conversion efficiencies. The characterization of POSS-C_{60} with various techniques showed that the presence of POSS did not change the C_{60} electronic properties. The same group also studied the power conversion efficiencies of the bulk heterojunction polymer solar cells made by the same polymer (SiPCPDTBT) mixed with [6,6]-phenyl-C_{61}-butyric acid methyl ester (PCBM). To compare the difference in device performances between PCBM and POSS-C_{60}, bulk heterojunction polymer solar cells with an inverted device configuration were fabricated (Figure 5.7). The use of POSS-C_{60}

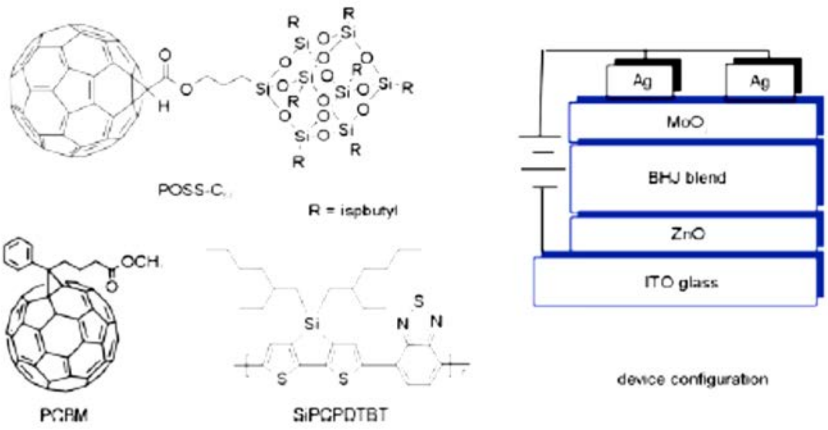

Figure 5.7. (right) Molecular structures of POSS-C_{60}, PCBM and SiPCPDTBT. (left) polymer solar cell device configuration. (Reproduced with permission from Ref.[23])

improved the performance and the overall device efficiency by increasing the short circuit current value by 2.22 mA cm^{-2} and the power conversion efficiencies by 0.58 % compared to PCBM. These results proved that POSS-C_{60} is a potentially useful electron acceptor in bulk heterojunction polymer solar cells.

5.3. Functionalization of carbon nanotubes with POSS and derived hybrids

In 2009, Jong-hwan Jeon *et al.*[46] developed a new approach for the preparation of hybrid nanocomposites of Pd nanoparticles and multi-walled carbon nanotubes (MWCNTs) destined to be used in hydrogen sensing devices.[46] The hybrid Pd-POSS and MWCNT-COOH nanocomposites were synthesized by a self-assembly method via ionic interaction between positively charged Pd-POSS and negatively charged MWCNT-COO^- as described in Figure 5.8. The palladium nanoparticles (Pd-POSS) were synthesized by using the cubic silsesquioxanes (POSS-NH_3^+) as a cross-linker for the self-organization of the isolated palladium nanoparticles.[46]

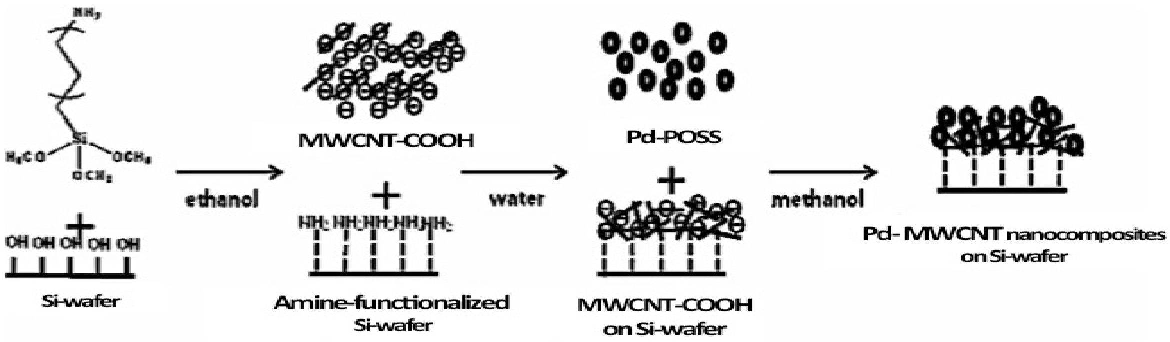

Figure 5.8. Experimental procedure of hybrid Pd-MWCNT nanocomposites. (Reproduced with permission from Ref.[46])

A year later, Anandhanatarajan Gomathi *et al.*[22] investigated the functionalization of MWNTs with POSS to enable their dispersion in polar solvents for polymer composite preparation and Qi-Fang Li *et al.*[29] synthesized composite fillers based on MCWNTs functionalized with POSS. More specifically MWCNTs were grafted with aminopropyl isooctyl-POSS, creating novel hybrids named MWCNT-g-POSS (g for grafted), as filler (Figure 5.9) for poly(L-lactide) (PLLA). The hybrid composites were studied for the optical transmittance, electrical, and electromagnetic interference shielding properties in comparison with PLLA/MWCNT composites.[29] The authors showed that for the hybrid PLLA/MWCNT-g-POSS composites the electrical threshold was 0.8 wt%, which was lower than that for composites without POSS (1.4 wt%). The PLLA/MWCNT-g-POSS composite also exhibited a better nanotube dispersion and less alignment of the nanotubes in the polymer, giving rise to better mechanical properties and to higher electrical conductivity and electromagnetic interference shielding.[29]

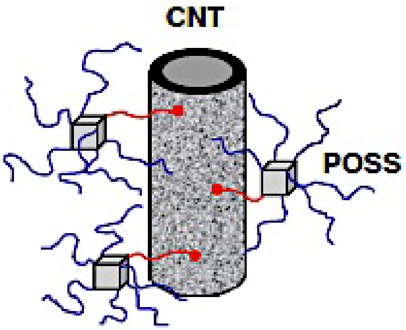

Figure 5.9. Functionalization of the MWCNT with POSS (Reproduced with permission from Ref.[29])

New hybrid reinforcements of carbon fiber with POSS-functionalized MWCNTs were fabricated by Feng Zhao and co-workers[47] in 2011. Octaglycidyldimethylsilyl POSS and MWCNTs were uniformly grafted on the carbon fiber surface to enhance the interfacial properties between carbon fibers and epoxy cast (Figure 5.10). Mechanical property test results demonstrated the improvement of the interlaminar shear strength and impact toughness.[47]

In 2012, Shahid Majeed *et al.*[48] created a hybrid system of pyrene and POSS which, when grafted onto MWCNTs, improves the dispersion of MWCNTs in organic solvents such as tetrahydrofuran, toluene, and n-hexane. The functionalized MWCNTs with pyrene-POSS (Figure 5.11) were used to fabricate polydimethylsiloxane (PDMS) nanocomposite membranes by solvent evaporation, reducing the likelihood of electrostatic discharges in gas separation applications.[48]

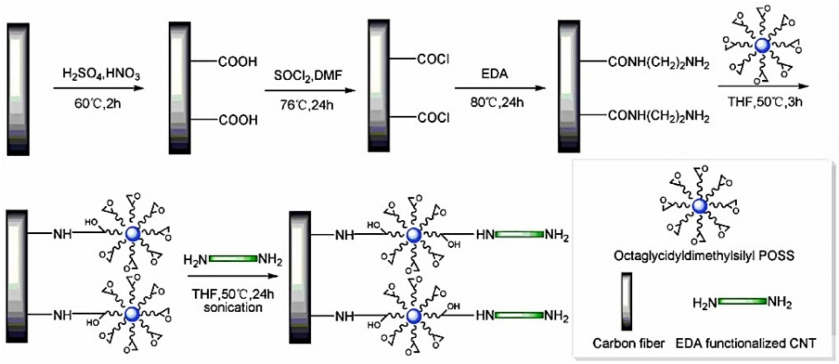

Figure 5.10. Experimental procedure for the realization of carbon fiber-POSS-MWCNT hybrids (Reproduced with permission from Ref.[47])

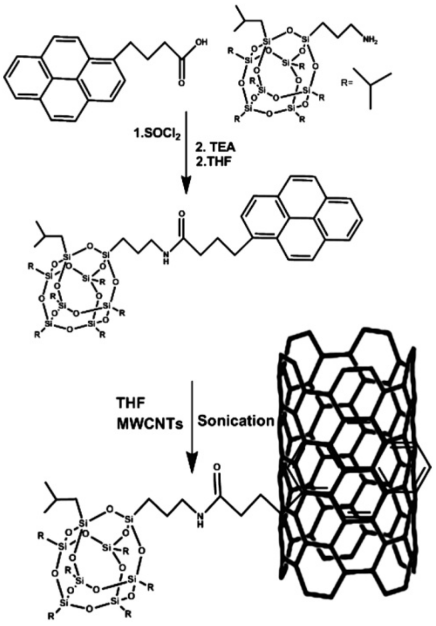

Figure 5.11. Functionalization of the MCWNT with pyrene-POSS. (Reproduced with permission from Ref.[48])

Aaron Tan *et al.*[49] in the same year, functionalized MWCNTs with a novel nanocomposite polymer of POSS and poly carbonate-urea (POSS-PCU) for biological and medical applications. A major concern for the use of carbon nanotubes in biological systems was their insolubility and their inherent toxicity. The amphiphilic nature of POSS-PCU increased the dispersibility of carbon nanotubes in biological systems as well as their biocompatibility. More importantly, when exposed to near-infrared radiation the nanocomposite increased the temperature and this effect was demonstrated to be exploitable in a biomedical setting to destroy cancer cells via photothermal ablation (Figure 5.12).[49] Apart from the biomedical purposes, these nanocomposites seem to have great potential for several other nanotechnological applications including nanoelectronics.

Yong Tang and coworkers[50] grafted POSS onto CNT's as to achieve *improved flame retardant* and super-hydrophobic properties in the resulting hybrid. Actually, this was a follow-up on their previous study where POSS and Carbon Nanofiber (CNF) were deposited to form a coating sheet on polymer composites in order to improve the latter's performance as a fire retardant; that combination turned out not to be efficient enough because of the aggregation and low thermal stability of POSS particles.[50] To improve this MWCNTs were used and POSS covalently attached on them, then the resulting hybrid material was processed into buckypaper, which improved the thermal stability of POSS particles.[50] The results reported so far are very promising and in this area there will be a growing interest in the near future toward efficient industrial use of these hybrid nanostructures.

Like C_{60} discussed above, also carbon nanotube suspensions exhibit optical limiting behaviour, which strongly depends highly on the concentration of MWCNTs. In this case functionalization with POSS can improve the solubility and hence the optical power limiting as shown by Bin Zhang *et al.*[30] These authors demonstrated that a hybrid MWCNT-POSS-NH_2 performs as active element in an optical limiter for nanosecond laser pulses at 532 nm. MWCNTs were treated with acids (HCl, H_2SO_4, HNO_3) in order to functionalize them with -COOH groups and then washed with excessive $SOCl_2$ for the -COCl groups to appear. Optical observation of the hybrid product in THF indicated that MWCNT-POSS with a POSS concentration 44 wt% gave rise to a black dispersion which was stable for at least one month.[30] Dispersions of the hybrid material show a pronounced nonlinear optical response - strong scattering at high intensities, followed by a decrease in transmission. Since POSS is a non-optically active material, it acts as a solubility promoter for the carbon nanotubes, responsible for the nonlinear optical response.

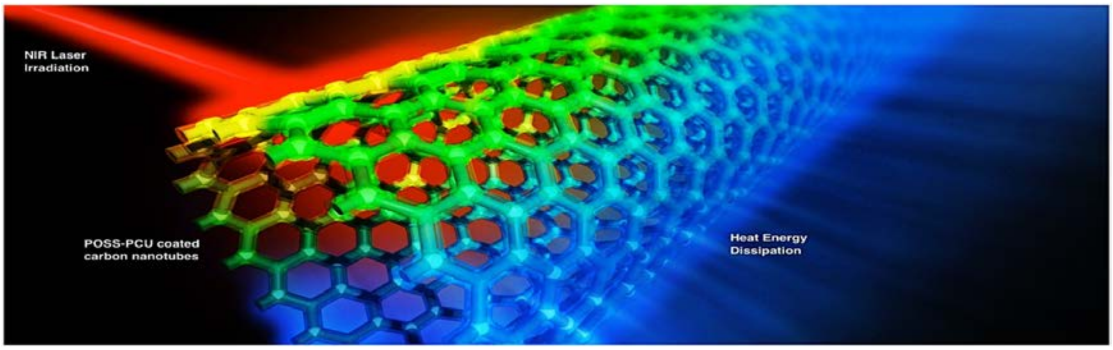

Figure 5.12. Illustration of photothermal ablation when MWCNTs functionalized with POSS-PCU are exposed to near infrared. (Reproduced with permission from Ref.[49])

The POSS functionalization of MWCNTs was also investigated by Guang-Xin Chen and Hiroshi Shimizu,[51] who first treated MWCNTs with acids in order to remove impurities and shorten them while grafting at the same time hydroxyl and carboxyl groups. They then reacted these nanotubes with excess of $SOCl_2$ to produce MWCNT-COCl, which they mixed with aminopropylisooctyl-POSS to obtain the MWCNT-g-POSS hybrid material. When this MWNT-g-POSS was dispersed in PLLA by solvent casting (chloroform) or simply by melt compounding, a homogeneous dispersion of MWNTs throughout the composite was obtained and the mechanical properties of the composite improved with respect to pure PLLA.[51]

An elegant new strategy to graft POSS onto MWCNTs by click-chemistry was developed by Santosh Kumar Yadav *et al.*[52] These authors first prepared azide moiety-functionalized POSS by a simple reaction with sodium azide in the presence of ammonium chloride and alkyne-functionalized MWCNTs via a solvent-free diazotization reaction and a coupling reaction between MWCNTs and *p*-aminophenyl propargyl ether. Then they linked the two via Cu(I)-catalyzed azide-alkyne cycloaddition with a product yield of 75-80 %.

Also POSS derivatives can be grafted on carbon nanotubes: Abdollah Omrani *et al.*[53] functionalized MWCNT and octa(phenol) octasilsesquioxane (OP-POSS) to fabricate a hybrid nanocomposite, by linking hydroxyl groups of OP-POSS and carboxyl acid groups of functionalized MWCNT–COOH. The hybrid MWCNTS/OP-POSS nanocomposite showed improved solubility and thermal stability compared to OP-POSS.

Celina Maria Damian and colleagues investigated the functionalization of MWCNTs with aminoethyl aminopropyl and POSS (POSS-NH_2) as reinforcing agent in epoxy nanocomposites.[54] The functionalization of MWNTs consisted in a three step reaction of oxidation, amidation and acylation with thionyl chloride (Figure 5.13). When the product was dispersed in a diglycidyl ether bisphenol (DGEBA) epoxy matrix, SEM studies showed that the POSS-functionalized MWNTs acted as fracture retardant within this nanocomposite material.[54]

A pilot procedure for coating MWCNTs with POSS was reported by Wenjing Zhang *et al.*[35] in 2014. This procedure combined the Diels−Alder cycloaddition with atom transfer radical polymerization. MWCNTs were functionalized with furfuryl-2-bromoisobutyrate (FBB) and used to induce the polymerization of octa-acrylate POSS on the MWCNT surface as described in Figure 5.14. Finally, the POSS-coated MWCNTs was dispersed in a polyvinylidene fluoride (PVDF) matrix to obtain a conductive composite with high dielectric constant and low dielectric loss.[35]

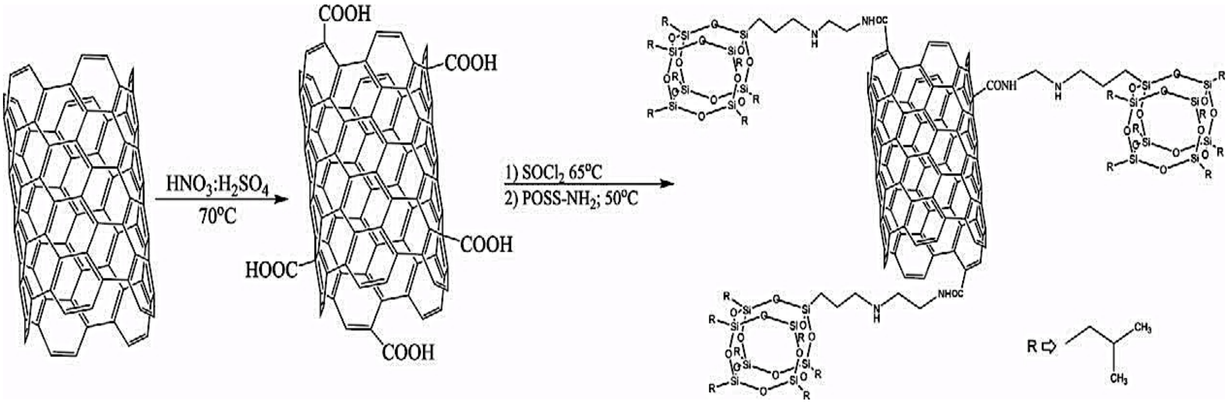

Figure 5.13. Functionalization of the MCWNT with POSS-NH$_2$. (Reproduced with permission from Ref.[54])

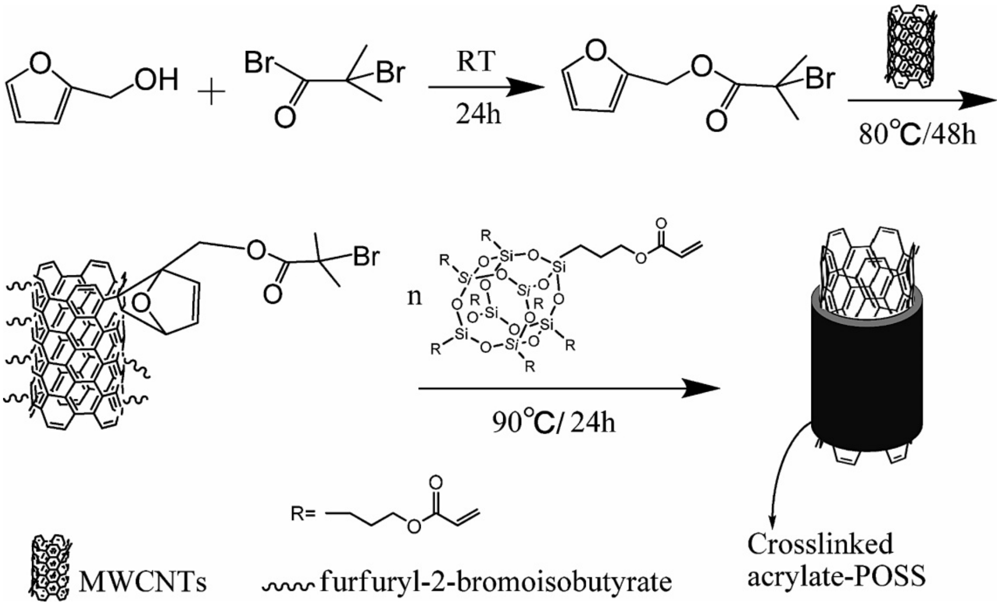

Figure 5.14. Functionalization of MCWNT with FBB and coating with octa-acrylate POSS. (Reproduced with permission from Ref.[35])

An alternative method for coating MWCNTs with Methacrylate-POSS by *in situ* free-radical polymerization was developed by Da Sun *et al.*[55] in the same year. The thickness of the POSS layer in the core−shell structure could be varied between 5 nm and 40 nm. The POSS-MWCNT hybrids showed excellent dispersion in organic solvents and also good electrical performance (from 0.75 Ω cm to 2505 Ω cm, depending on the thickness of the coating layer).[55] This synthetic method may become important for exploring and creating a rich variety of hybrid nanostructures for device applications.

To obtain new cobalt based materials, in 2013 Zhijun Ruan and co-workers,[56] used for the first time the solid-state pyrolysis (SSP) of POSS group-containing organometallic precursors to generate carbon nanotubes (MWCNTs) based nanocomposites for magnetic applications. With the presence of POSS and the control of $[Co_2(CO)_6]$ moieties the size and the shape of nanocomposites could be regulated.[56] However, many aspects (including a screening of various other metals) still have to be studied before the SSP method can be widely applied to produce CNT magnetic hybrid nanostructures.

POSS can also be used to synthesize MWCNT/SiO_2 hybrids. An interesting approach for the development of MWCNT/SiO_2 hybrids was proposed by Xu's group[57] by using a CVD method. Carbon nanotubes were grown from ethanol with the help of PSS-(2-(trans-3,4-cyclohexanediol)ethyl)-heptaisobutyl-substituted POSS acting as a metal-free catalyst. The two reagents were mixed, nebulized and brought inside the CVD reactor using hydrogen as carrier gas. Since POSS looses its ligands under CVD conditions, the produced CNTs were decorated with SiO_2 nanoparticles. Several parameters of the reaction such as growth temperature, concentration of POSS and amount of water in ethanol were examined with respect to their influence on the morphology of the produced MWCNTs and the SiO_2 nanoparticles attached to them.[57]

5.4. POSS immobilization on graphene and graphene oxide and resulting hybrids

The .functionalization of graphene with POSS was first investigated by Anandhanatarajan Gomathi, *et al*.[22] in 2010. Graphene, prepared by thermal exfoliation of graphitic oxide, was acid-treated to generate surface carboxyl and hydroxyl groups providing in this way the necessary environment for covalent binding of the POSS molecules. The graphene-POSS hybrid material was easily dispersed in polar solvents allowing for the preparation of polymer composites with polyvinyl alcohol and nylon-6,6. This method can be used for the deposition of any POSS derivative on a oxidized graphitic structure as long as the functional groups of the POSS derivatives are appropriate (mainly primary or secondary amines, or thiol groups) for covalent binding with the oxygen-containing groups decorating the graphene layers; it therefore has great potential for the functionalization of graphene-based materials with various POSS.

Just one year later, Xiaofang Shen and coworkers[58] described the preparation of an electrochemical sensor based on graphene oxide nanoribbons (GON) where, in order to overcome aggregation between graphene layers, they inserted octa(3-aminopropyl)octasilae quioxane octahydrochloride (OA-POSS) nanocages between the graphene layers. GON/OA-POSS films were used to modify an electrode for pre-concentrating and sensing of 1-hydroxypyrene (1-OHP), a metabolite of polycyclic aromatic hydrocarbons widely used as biomarker for the evaluation of human exposure to these molecules.[58]

The functionalization of graphene oxide (GO) with amine-functionalized POSS has been adopted by several groups.[59, 60, 61, 62] In that approach, POSS was linked via amide formation with the epoxy (via a ring opening reaction) and carboxyl groups of the graphene oxide sheets to change the chemical properties of GO, to separate the GO layers in a physical way or to enhance the *dispersibility of the sheets* in organic solvents, such as hexane, THF, chloroform, acetone and toluene. More specifically, POSS-graphene appears to be soluble in THF at a relatively high concentration of 30 mg/mL, without formation of precipitates.[59] The resulting hybrid could be prepared as a thin film (by solution casting),[59] which showed superhydrophobic properties with a water/air contact angle of ~157°. POSS-graphene powder was shown to form liquid freestanding marbles on hydrophobic or hydrophilic surfaces as a small reactor for different applications. When POSS-graphene hybrids were incorporated into PMMA at low percentage (1 wt%), the glass transition temperature T_g of the composite material increased by more than 10 °C, which identifies these hybrids as ideal reinforcing agents for polymer matrices.

Luca Valentini *et al.*[63] went one step further in the engineering of nanostructures by first immobilizing GO sheets on a (3-aminopropyl)triethoxysilane (APTES) layer on a Si substrate and then grafting POSS-NH_2 onto them. APTES layer was successfully self-assembled on the oxygen plasma-treated Si substrate as confirmed by IR spectroscopy. The reaction between the -NH_2 groups of POSS and the -COOH groups of GO, led to a change of the GO surface properties from hydrophilic to hydrophobic. Tribological measurements on the POSS-GO-APTES tri-layer revealed a reduced friction coefficient, making it suitable for application as lubricant coating.

In another report Luca Valentini *et al.* pursued the goal to graft POSS to the GO film when POSS is offered in the form of vapour.[64] The authors showed that amino-functionalized POSS can be brought in to the gas phase via thermal evaporation and easily interacts with GO's functional groups. A comparison of the morphology of the hybrids obtained by the evaporation of POSS-NH_2 and neat POSS onto GO evidenced clear differences in wrinkling and bending of the graphene sheets. Light ON/OFF tests on GO sheets treated with amino-functionalized POSS showed a variation of the conductivity under illumination. In a follow-up paper[65] the same group proved that when POSS-NH_2 was coupled with graphene oxide sheets in tetrahydrofuran (THF), a solvent capable of completely solubilizing the silsesquioxane molecules and dispersing GO, the photoconductivity response of the hybrid to visible-light stimulus was 50 times stronger.

In the same year Xin Wang and coworkers[66] developed a synthetic protocol for the functionalization and reduction of GO with octa-aminophenyl polyhedral oligomeric silsesquioxane (OapPOSS) by simple refluxing in THF, as described in Figure 5.15. When this hybrid was used incorporated in an epoxy resin, the thermal oxidative resistance and thermal stability improved as compared to the neat resin. The authors assigned this improvement to the good linkage between the OapPOSS-GO hybrid and the epoxy matrix and to the fact that graphene retards the permeation of heat and the escape of volatile degradation products. These experiments identified the novel hybrid material OapPOSS-rGO as an efficient graphene-based flame retardant additive for epoxy resin materials.[66] The results so far reported in this field are very promising, however, the properties of these new materials have been disclosed only partially.

The grafting of OapPOSS to GO was further developed by Wenqi Yu *et al.*[67] who employed a simple *in situ* reduction method for the surface functionalization of GO instead of exploiting the interaction between amino groups on POSS and carboxyl groups on the GO sheets as presented so far[59, 64, 68] (Figure 5.16).

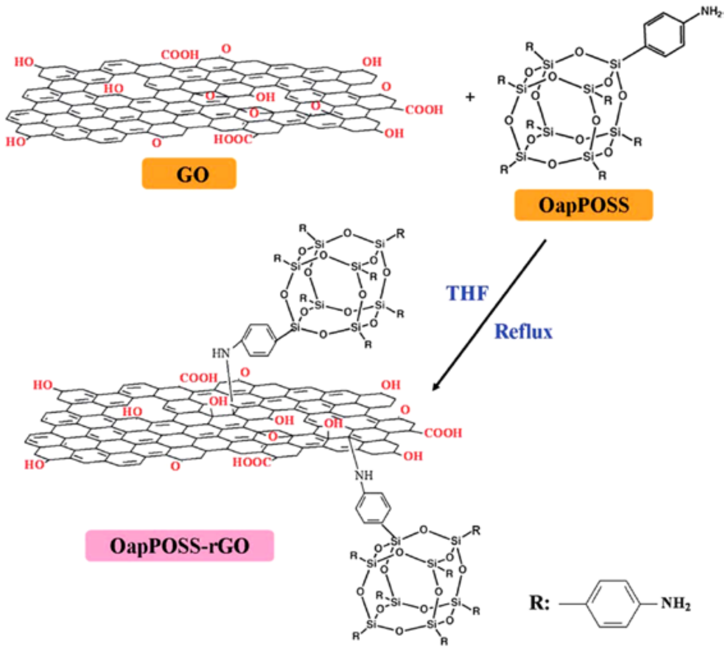

Figure 5.15. Schematic representation of graphene oxide reduction and functionalization with octa-aminophenyl polyhedral oligomeric silsesquioxane. (Reproduced with permission from Ref.[66])

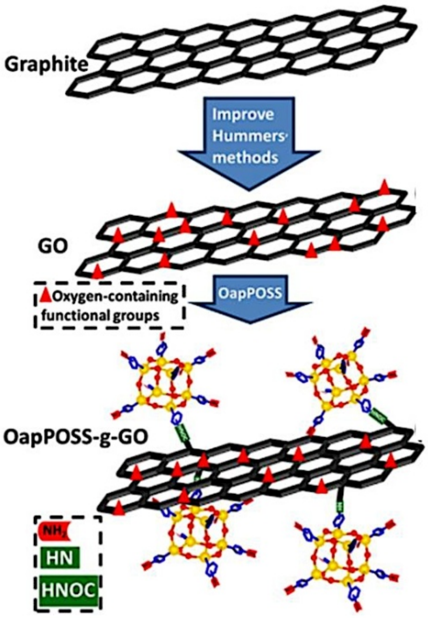

Figure 5.16. Schematic representation of the synthetic procedure from graphite to the reduced and functionalized graphene oxide (OapPOSS-g-GO). (Reproduced with permission from Ref.[67])

In the same year Kumari Pallathadka Pramoda and coworkers[34] prepared a polylactide (PLA)-based nanocomposite combining functionalized-GO nanosheets and oligomeric silsesquioxane (POSS) nanocages as nanofillers to enhance thermal and mechanical properties of PLA. The authors compared the structure-property relationship of PLA mixed with (1) functionalized GO, (2) functionalized POSS, (3) a physical mixture of functionalized GO and functionalized POSS, and (4) the GO-*g*-POSS (with eight hydroxyl groups) and demonstrated that the new GO-g-POSS hybrid nanocomposite exhibited a better/enhanced thermal and mechanical behaviour than the dispersed other nanofillers in PLA matrixes.[34]

Titash Mondal, Anil K. Bhowmick and Ramanan Krishnamoorti[69] went one step further by recently reporting a method towards covalent modification of graphene in order to produce novel inorganic-organic hybrid materials. Their purpose was to achieve the grafting of POSS to graphene in a scalable manner with a limited use of chemicals and in milder reaction conditions that the ones used when linking amine-terminated POSS to carboxylated graphene as described above. For this they decided to exploit the intrinsic topological defects of graphene, namely heptagons and pentagons situated close to the edges of the graphene layers; these defects show a higher reactivity because of the higher strain in these rings and their non-aromatic nature. Expanded graphite was brought in contact with n-butyl-lithium (n-BuLi), which attracts protons from the defects (nucleophilic attack) and produced anionic centers. The latter were reacted with epoxycyclohexylethyl-POSS with cyclopentane as substituent. Furthermore, a molar excess of n-BuLi also leads to a nucleophilic reaction between graphene sheets and butyl groups, resulting in bi-functionalized graphene where the covalently grafted butyl groups prevent the graphene layers from re-agglomeration. This functionalization protocol therefore has the added benefit of inducing exfoliation.

5.5. Conclusions

In conclusion, in this work we reviewed all the recent achievements concerning the grafting of polyhedral oligomeric silsesquioxanes (POSS) to carbon nanostructures including graphene, graphene oxide, nanotubes and fullerenes. The aim of this effort was to give a clear overview of all the synthetic procedures applied until now as well as to illustrate the improvements of chemical and physical properties that can be achieved by the combination of POSS with different carbon nanostructures. Thus, we reported improved solubility of carbon nanostructures through functionalization with POSS, as well as the utilization of the synthesized hybrid organic/inorganic nanostructures as nanofillers in polymers to attain enhanced thermal and mechanical behaviour, modify the electronic properties or, to improve flame retardancy. New frontiers are open taking advantage of new properties of these hybrid nanostructures that still under investigation.

References

*[1] Y. Kaneko, E. B. Coughlin, T. Gunji, M. Itoh, K. Matsukawa, K. Naka, International Journal of Polymer Science **2012**, 2012, 453821.*

*[2] D. B. Cordes, P. D. Lickiss, F. Rataboul, Chemical Reviews **2010**, 110, 2081-2173.*

*[3] R. H. Baney, M. Itoh, A. Sakakibara, T. Suzuki, Chemical Reviews **1995**, 95, 1409-1430.*

*[4] K. J. Shea, D. A. Loy, MRS Bulletin **2001**, 26, 368-376.*

*[5] S.-W. Kuo, F.-C. Chang, Progress in Polymer Science **2011**, 36, 1649-1696.*

*[6] D. Gnanasekaran, K. Madhavan, B. S. R. Reddy, Journal of Scientific & Industrial Research **2009**, 68, 437-464.*

*[7] J. Zhao, Y. Fu, S. Liu, Polymers & Polymer Composites **2008**, 16, 483-500.*

*[8] J.-H. Jeon, K. Tanaka, Y. Chujo, Organic & Biomolecular Chemistry **2014**, 12, 6500-6506.*

*[9] G. Z. Li, L. C. Wang, H. L. Ni, C. U. Pittman, Journal of Inorganic and Organometallic Polymers **2001**, 11, 123-154.*

*[10] F. Reno, F. Carniato, M. Rizzi, L. Marchese, M. Laus, D. Antonioli, Journal of Applied Polymer Science **2013**, 129, 699-706.*

*[11] K. Tanaka, Y. Chujo, Polymer Journal **2013**, 45, 247-254.*

*[12] Y.-Y. Yang, X. Wang, Y. Hu, H. Hu, D.-C. Wu, F.-J. Xu, ACS Applied Materials & Interfaces **2014**, 6, 1044-1052.*

*[13] D. Petridis, D. Gournis, M. A. Karakassides, Molecular Crystals and Liquid Crystals Science and Technology Section A: Molecular Crystals and Liquid Crystals **1998**, 311, 345-350.*

[14] *A. Szabo, D. Gournis, M. A. Karakassides, D. Petridis, Chemistry of Materials* ***1998****, 10, 639-645.*

[15] *G. Balomenou, P. Stathi, A. Enotiadis, D. Gournis, Y. Deligiannakis, Journal of Colloid and Interface Science* ***2008****, 325, 74-83.*

[16] *T. S. Haddad, R. Stapleton, H. G. Jeon, P. T. Mather, J. D. Lichtenhan, S. Phillips, Polymer Preprints* ***1999****, 40, 496-497.*

[17] *D. W. Scott, Journal of the American Chemical Society* ***1946****, 68, 356-358.*

[18] *F. J. Feher, T. A. Budzichowski, Journal of Organometallic Chemistry* ***1989****, 379, 33-40.*

[19] *F. J. Feher, T. A. Budzichowski, Polyhedron* ***1995****, 14, 3239-3253.*

[20] *G. Li, L. Wang, H. Ni, C. Pittman, Jr., Journal of Inorganic and Organometallic Polymers* ***2001****, 11, 123-154.*

[21] *H.-J. Sun, Y. Tu, C.-L. Wang, R. M. van Horn, C.-C. Tsai, M. J. Graham, B. Sun, B. Lotz, W.-B. Zhang, S. Z. D. Cheng, J. Mater. Chem.* ***2011****, 21, 14240-14247.*

[22] *A. Gomathi, K. Gopalakrishnan, C. N. R. Rao, Materials Research Bulletin* ***2010****, 45, 1894-1898.*

[23] *W.-B. Zhang, Y. Tu, H.-J. Sun, K. Yue, X. Gong, S. Z. D. Cheng, Sci China Chem* ***2012****, 55, 749-754.*

[24] *D. J. Clarke, J. G. Matisons, G. R. Simon, M. Samoc, A. Samoc, Appl. Organometal. Chem.* ***2008****, 22, 460-465.*

[25] *A. Tan, S. Y. Madani, J. Rajadas, G. Pastorin, A. M. Seifalian, Journal of Nanobiotechnology* ***2012****, 10.*

[26] *X. F. Shen, Y. Cui, Y. H. Pang, H. Qian, Electrochimica Acta* ***2012****, 59, 91-99.*

[27] *D. J. Clarke, J. G. Matisons, G. R. Simon, M. Samoc, A. Samoc, Appl. Organometal. Chem.* ***2010****, 24, 184-188.*

[28] *W. Kai, L. Hua, T. Dong, P. Pan, B. Zhu, Y. Inoue, Macromolecular Chemistry and Physics* ***2008****, 209, 1191-1197.*

[29] *Q. F. Li, Y. H. Xu, J. S. Yoon, G. X. Chen, Journal of Materials Science* ***2011****, 46, 2324-2330.*

[30] *B. Zhang, Y. Chen, J. Wang, W. J. Blau, X. D. Zhuang, N. He, Carbon* ***2010****, 48, 1738-1742.*

[31] *Y. Tang, J. H. Gou, Y. Hu, Polymer Engineering and Science* ***2013****, 53, 1021-1030.*

[32] *A. Omrani, Y. C. Yen, C. C. Cheng, F. C. Chang, Journal of Molecular Structure* ***2014****, 1056, 299-306.*

[33] *X. Wang, L. Song, H. Y. Yang, W. Y. Xing, B. Kandola, Y. Hua, Journal of Materials Chemistry* ***2012****, 22, 22037-22043.*

[34] *K. P. Pramoda, C. B. Koh, H. Hazrat, C. B. He, Polymer Composites* ***2014****, 35, 118-126.*

[35] *W. J. Zhang, Z. Zhou, Q. F. Li, G. X. Chen, Industrial & Engineering Chemistry Research* ***2014****, 53, 6699-6707.*

[36] *D. Sun, Q. F. Li, G. X. Chen, Materials Letters* ***2014****, 120, 90-93.*

[37] *S. Xiao, M. C. Nguyen, X. Gong, Y. Cao, H. B. Wu, D. Moses, A. J. Heeger, Adv. Funct. Mater.* ***2003****, 13, 25-29.*

[38] *B. Neises, W. Steglich, Angew. Chem.* ***1978****, 17, 522-524.*

[39] *F. Yang, C. Li, H. Guo, J. Ye, Z. Jiao, Synthetic Communications* ***2012****, 42, 3664-3669.*

*[40] M.-C. Lin, C.-H. Hsu, H.-J. Sun, C.-L. Wang, W.-B. Zhang, Y. Li, H.-L. Chen, S. Z. D. Cheng, Polymer **2014**, 55, 4514-4520.*

*[41] C. Bingel, Chemische Berichte **1993**, 126, 1957-1959.*

*[42] T. Hahn, International tables for crystallography, Vol. A, Dordrecht,Boston: Reidel Publishing Company, **1992**.*

*[43] W. Clegg, Crystal structure determination, Oxford, New York: Oxford University Press, **1998 (book)**.*

*[44] G. Shi, Y. Hanlumyuang, Z. Liu, Y. Gong, W. Gao, B. Li, J. Kono, J. Lou, R. Vajtai, P. Sharma, P. M. Ajayan, Nano Letters **2014**, 14, 1739-1744.*

*[45] W. Kai, L. Hua, T. Dong, P. Pan, B. Zhu, Y. Inoue, Macromol. Chem. Phys. **2008**, 209, 1191-1197.*

*[46] J. H. Jeon, J. H. Lim, K. M. Kim, Macromolecular Research **2009**, 17, 987-994.*

*[47] F. Zhao, Y. Huang, L. Liu, Y. Bai, L. Xu, Carbon **2011**, 49, 2624-2632.*

*[48] S. Majeed, V. Filiz, S. Shishatskiy, J. Wind, C. Abetz, V. Abetz, Nanoscale Research Letters **2012**, 7, 1-11.*

*[49] A. Tan, S. Y. Madani, J. Rajadas, G. Pastorin, A. M. Seifalian, Journal of Nanobiotechnology **2012**, 10, 34.*

*[50] Y. Tang, J. Gou, Y. Hu, Polymer Engineering & Science **2013**, 53, 1021-1030.*

*[51] G. X. Chen, H. Shimizu, Polymer **2008**, 49, 943-951.*

*[52] S. K. Yadav, S. S. Mahapatra, H. J. Yoo, J. W. Cho, Nanoscale Research Letters **2011**, 6, 122.*

*[53] A. Omrani, Y.-C. Yen, C.-C. Cheng, F.-C. Chang, Journal of Molecular Structure **2014**, 1056–1057, 299-306.*

*[54] C. M. Damian, C. C. Ciobotaru, S. A. Garea, H. Iovu, High Performance Polymers **2013**, 25, 566-575.*

*[55] D. Sun, Q. Li, G.-X. Chen, Materials Letters **2014**, 120, 90-93.*

*[56] Z. J. Ruan, C. Y. K. Chan, J. W. Y. Lam, Q. Wu, Q. Q. Li, J. G. Qin, B. Z. Tang, Z. Li, Journal of Materials Chemistry C **2014**, 2, 633-640.*

*[57] X. J. Xu, S. M. Huang, Y. L. Hu, J. D. Lu, Z. Yang, Materials Chemistry and Physics **2012**, 133, 95-102.*

*[58] X. Shen, Y. Cui, Y. Pang, H. Qian, Electrochim. Acta **2012**, 59, 91-99.*

*[59] Y. Xue, Y. Liu, F. Lu, J. Qu, H. Chen, L. Dai, The Journal of Physical Chemistry Letters **2012**, 3, 1607-1612.*

*[60] D. R. Dreyer, S. Park, C. W. Bielawski, R. S. Ruoff, Chemical Society Reviews **2010**, 39, 228-240.*

*[61] A. B. Bourlinos, D. Gournis, D. Petridis, T. Szabo, A. Szeri, I. Dekany, Langmuir **2003**, 19, 6050-6055.*

*[62] R. Y. N. Gengler, A. Veligura, A. Enotiadis, E. K. Diamanti, D. Gournis, C. Jozsa, B. J. van Wees, P. Rudolf, Small **2010**, 6, 35-39.*

*[63] L. Valentini, S. B. Bon, O. Monticelli, J. M. Kenny, Journal of Materials Chemistry **2012**, 22, 6213-6217.*

*[64] L. Valentini, S. B. Bon, M. Cardinali, O. Monticelli, J. M. Kenny, Chemical Physics Letters **2012**, 537, 84-87.*

*[65] L. Valentini, M. Cardinali, J. M. Kenny, M. Prato, O. Monticelli, Eur. J. Inorg. Chem. **2012**, 5282-5287.*

*[66] X. Wang, L. Song, H. Yang, W. Xing, B. Kandola, Y. Hua, Journal of Materials Chemistry **2012**, 22, 22037-22043.*

[67] W. Yu, J. Fu, X. Dong, L. Chen, L. Shi, Composites Science and Technology ***2014****, 92, 112-119.*

[68] A. Lerf, H. He, M. Forster, J. Klinowski, Journal of Physical Chemistry B ***1998****, 102, 4477-4482.*

[69] T. Mondal, A. K. Bhowmick, R. Krishnamoorti, Rsc Advances ***2014****, 4, 8649-8656.*

CHAPTER 6

Iron-substituted cubic silsesquioxane pillared clays: Synthesis, characterization and catalytic applications

Novel pillared structures were synthesized from the intercalation of iron-substituted cubic silsesquioxanes in a sodium and an acid-activated montmorillonite nanoclay and evaluated as acid catalysts. Octameric cubic oligosiloxanes were formed upon controlled hydrolytic polycondensation of the corresponding monomer (a diamino-alkoxysilane) and reacted with iron cations to form complexes that were intercalated within the layered nanoclay matrices. Upon calcination iron oxide nanoparticles are formed which are located on the silica cubes (pillars) and on the surfaces of the clay platelets. Acid activation of the nanoclay was performed in order to increase the number of acid active sites in the pristine clay and thus increase its catalytic activity. A plethora of analytical techniques including X-ray diffraction, thermal analyses, Fourier transform infrared, Raman, Mössbauer and X-ray photoelectron spectroscopies and porosimetry measurements were used in order to follow the synthesis steps and to fully characterize the final catalysts. The resulting pillared clays exhibit high specific area and show significant catalytic activity in the catalytic dehydration of isopropanol.

This chapter is based on the article: Iron-substituted cubic silsesquioxane pillared clays: Synthesis, characterization and catalytic applications by G. Potsi, A. K. Ladavos, D. Petrakis, A. P. Douvalis, Y. Sanakis, M. S. Katsiotis, S. Alhassan, D. Gournis and P. Rudolf, to be submitted.

6.1. Introduction

The field of engineering nanomaterials has a continuing need of well-defined building blocks that imbue functionality and allow for nanoparticle-by-nanoparticle assembly of a wide variety of materials with precise control over the nanoarchitecture.[1] [2] Silsesquioxanes possess a pronounced aptitude to form three dimensional cage-like highly symmetric frameworks known as polyhedral oligosilsesquioxanes (POSS) with cubic, hexagonal, octagonal, decagonal, dodecagonal or even open cage-like morphology.[3][4][5] Cubic silsesquioxanes (cubes), synthesized from the hydrolytic condensation of the corresponding trifunctional organo-silicon monomers, is the most common polyhedral structure and provide the opportunity to design and "construct" materials with extremely well-defined dimensions and behaviour. [3][6] [7][5] [4] [8] [9] [10] [11] [12] [13] In this context, cubic silsesquioxanes of the type $X_8Si_8O_{12}$ where X is $–(CH_3)_3NH_2$, $–(CH_3)_3NR_2$ and $–(CH_3)_3NH(CH_2)_2NH_2$ have been successfully employed as precursor reagents for pillaring inorganic layered solids such as clays,[14] [15] [16] [17] [18] [19] metal (IV) hydrogen phosphates,[20] [21] [22] photonic titanoniobates, [23] graphenes and graphene oxide,[3] [24] [25] [26] graphene oxide nanoribbons,[27] halloysite nanotubes[28] and perovskites.[29] Protonation of the amino groups generates oligomeric cationic species with expendable and bulky organic groups that can easily be inserted into the interlayer space of a phyllomorphous clay in amounts exceeding the cation exchange capacity of the mineral and can successively be removed by thermal treatment, resulting in silica pillared structures.[15] [14] This excess being in the form of physically adsorbed ion pairs influences the free distance between the layers and the surface area as well as the porosity of the silica-pillared composites.

On the other hand, these various mono- or bi-functional amino-silanes possess the ability to bind metal ions, M^{n+} (*e.g.* Cu^{2+}, Ni^{2+}, Co^{2+}, Fe^{3+}, Al^{3+}), yielding metal complexes, $M_x^{n+}[X_8Si_8O_{12}]_y$, and thus enabling the design and synthesis of metal complexes in which the redox active metal centre is coordinated to the functionalized group of the siloxane octamer.[22] The resulting cationic complexes are expected to be excellent pillaring precursors and may be further calcined to remove the organic side arms and produce cross-linked metal-substituted silica-pillared clays of high porosity and thermal stability. Upon calcination the metal ions may retain isolated as metal oxides located on both the clay surface and the pillar or may be integrated into the silica pillar. The clays pillared with metal oxide silica are solid acids with moderate or high Brønsted and Lewis acidity originating from acid sites located on the pillars and the clay surface; they can be used as acid catalysts in the range 100-600 ^{o}C, in which most catalytic reactions take place. Isopropyl alcohol decomposition is one example of a specific reaction where this type of pillared clay can be used as efficient catalyst. Furthermore the use of acid-activated clays instead of sodium-intercalated ones as efficient substrates for the synthesis of pillared structures could enhance the acid properties and subsequently their catalytic activity.[30] [31] [32] [33] [34] [35]

The first attempt to intercalate metal POSS in pillared structures was performed by Khattou *et al*.[36] [37] who intercalated a Cu^{2+}-octa(diaminoalkyl) siloxane complex into a-zirconium phosphate and examined the pillaring materials obtained after calcination by electron paramagnetic resonance (EPR) spectroscopy. In this case the metal ions act as probe for the determination of the evolution of local symmetry and structure during the pillaring process when using an element specific technique.

More recently Carniato *et al*.[38] demonstrated the intercalation of a bifunctional protonated titanium-containing aminopropyl isobutyl POSS, within the interlayer space of a synthetic sodium saponite and its use as filler in a polystyrene-based nanocomposite designed to enhance the thermooxidative properties. The same group[39] also intercalated Ti-containing aminopropylisobutyl polyhedral oligomeric silsesquioxane in synthetic saponite and investigated the catalytic activity of this composite in cyclohexene oxidation. Other catalysts based on clay-POSS hybrids include synthetic laponite clay first modified by octaaminopropyl polyhedral oligometric silsesquioxane and then used to support a nickel alpha-diimine late-transition-metal catalyst for ethylene polymerization;[40] laponite and montmorillonite functionalized with (3-aminopropyl)triethoxysilane and use both as supports for the vanadyl(IV) acetylacetonate catalysis[41] and POSS intercalated bentonites[42] for metal up take of copper, cadmium and lead.

In this work we report the intercalation of Fe^{3+}-substituted cubic silsesquioxanes in a sodium and an acid-activated montmorillonite to form novel catalytic pillared structures. A plethora of analytical techniques including X-ray diffraction (XRD), thermal analyses (DTA/TGA), Fourier transform infrared (FTIR), Raman, Mössbauer and X-ray photoelectron (XPS) spectroscopies and porosimetry measurements were used in order to follow the synthesis steps and to fully characterize the final catalysts. The resulting pillared clays exhibit high specific area and a narrow pore size distribution and show significant catalytic activity in the catalytic dehydration of isopropanol.

6.2. Results and Discussion

For the development of the catalytic pillared clays, a sodium montmorillonite (Na-T) and its acid activated form (HT) were used. Acid activation was performed in order to increase the number of acid active sites in the pristine clays and thus increase its catalytic activity during the dehydration of the isopropanol, which is an acid catalyzed reaction. For the pillaring solution, octameric cubic oligosiloxanes were formed upon controlled hydrolytic polycondensation of the corresponding monomer (EDAPTMOS) in an ethanol-water mixture and immediately reacted with ferrous cations to form complexes of the type $Fe^{2+}_x[X_8Si_8O_{12}]_y$. The colour of the solution changed from pale orange to dark green, indicative of the complexation of ferrous cations with the amino functional group of the corresponding siloxane molecules. When the pillaring solution was added to an aqueous dispersion of the clay an immediate flocculation of clay particles was observed due to the insertion of complex in the clay galleries by ion exchange. The colour of the slurry changed gradually within 1 h after the addition of iron-complex from green to orange, pointing to the oxidation of Fe(II) to Fe(III).

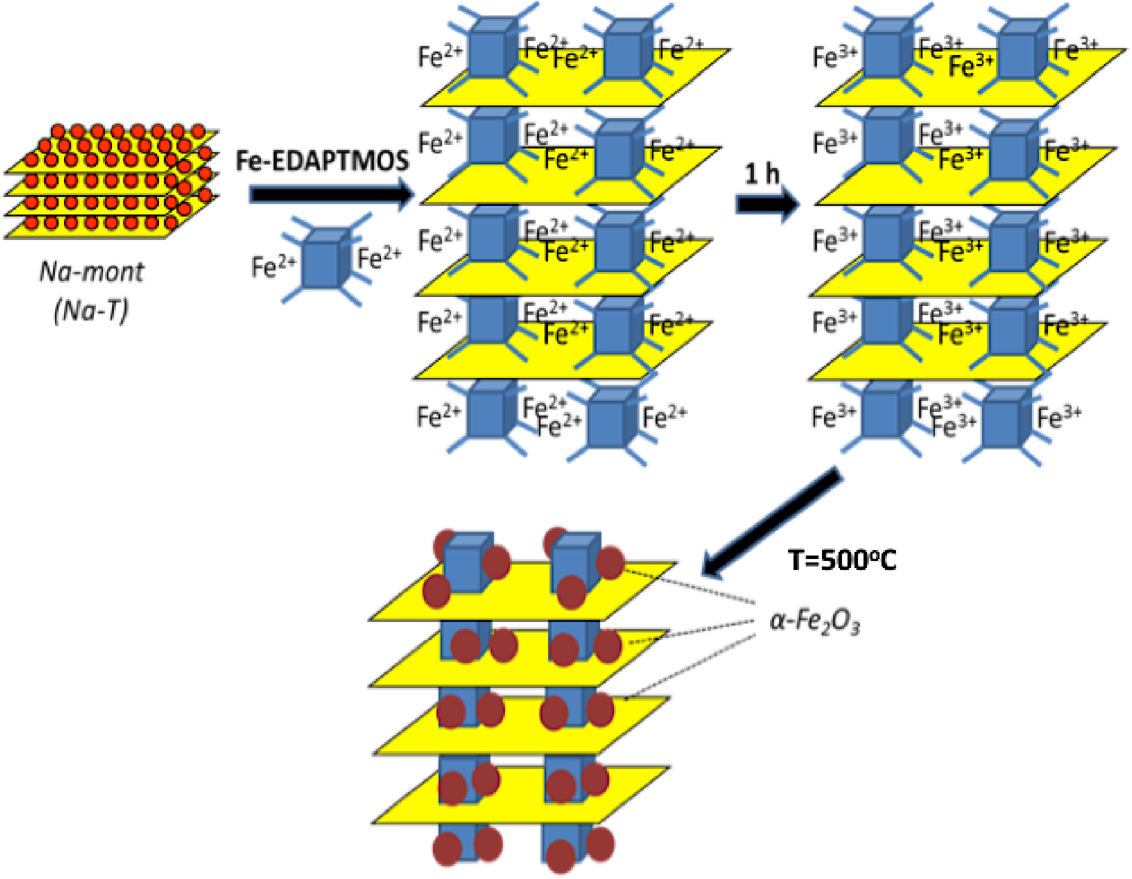

Figure 6.1. Schematic representation of experimental procedure.

Finally, intercalated samples were calcined at 500 °C in air to obtain pillared clays. The calcination procedure contributes to the removal of the organic chains of the organo-silane cubes and to the creation of iron oxide nanoparticles, which are immobilized on the silica cubes and on the surfaces of the clay platelets. A schematic representation of the experimental procedure is depicted in Figure 6.1.

X-ray diffraction was employed to reveal the successful intercalation of iron-silsesquioxane complexes as well as the formation of the pillared structures. [43] The XRD patterns of intercalated samples (for both Na-T and HT clays) before and after calcination at 500 °C are displayed in Figure 6 2. The insertion of iron-silsesquioxane complexes between the aluminosilicate layers increases the interlayer distance. More specifically, for TFeED obtained by intercalation in Na-T clay, the basal d_{001}-spacing, which is 12.6 Å in the initial montmorillonite clay, becomes 18.2 Å after the modification; this corresponds to an interlayer separation of 18.2–9.6 = 8.6 Å, where

9.6 Å represents the thickness of a clay layer.[43] [44] This value is reasonable if we consider that the edge of the siloxane cube (Si-O-Si distance) is 6.0 Å[14] and, due to complexation with the ferric cations, the flexible organic chains adopt a inclined orientation between the clay layers. Moreover, the interlayer distance of 8.6 Å is actually higher compared to the one observed (7.1 Å) upon clay intercalation with this particular aminosiloxane not complexed with ferric cations.[42] Similar results were obtained for the acid-activated montmorillonite. The XRD pattern of the HTFeED sample (Fig.6 2b) shows a d_{001} spacing of 17.2 Å, which corresponds to an interlayer separation of 7.6 Å. The interlayer distance in this case is slightly lower than for TFeED. However, a similar geometrical arrangement must be adopted in this case too with the flexible side chains of the siloxane cubes in an inclined orientation with respect to the aluminosilicate platelets. Upon calcination at 500 °C, the d_{001} spacing was decreased to 16.3 and 15.4 Å, for TFeED-500 and HTFeED-500 respectively, indicative of the removal of the side organic groups of the siloxane cubes and the subsequent reduction in the interlayer distance. Moreover, the absence of reflection peaks of the crystalline phase of iron oxides (see below) in the 2Θ region 2-80° indicates that iron oxide nanoparticles produced upon calcination are small enough and are not aggregated on the external clay surfaces but rather homogeneously dispersed in the clay matrix.

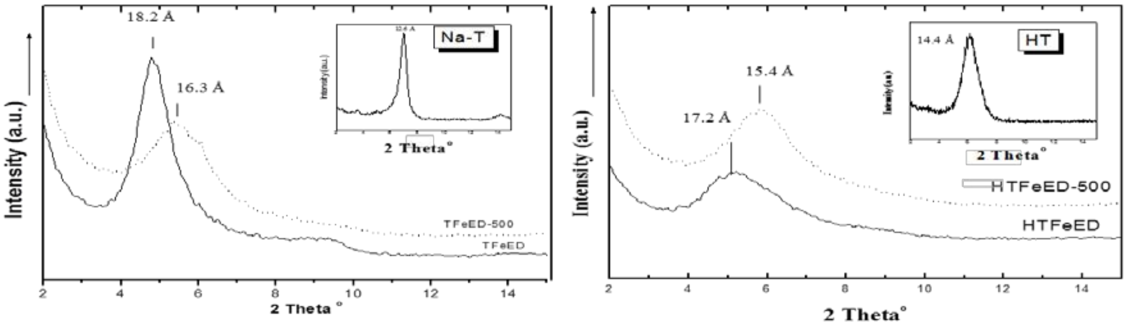

Figure 6.2. X-ray diffraction patterns of intercalated clay samples, TFeED and HTFeED, and the corresponding pillared structures produced upon calcination, TFeED-500 (left) and HTFeED-500 (right). Insets: pristine clays, Na-T and HT.

Figure 6.3 shows the infrared spectra of the pristine acid activated clay (HT) and of HTFeED and HTFeED-500; the spectrum of the Fe-EDAPTMOS complex which was obtained as solid (orange) after the centrifugation of the complex solution during the synthetic procedure, is also shown. The infrared spectrum of HT consists of three absorption bands at lower frequencies (below 1300 cm^{-1}); the first, at 1000-1200 cm^{-1} corresponds to stretching vibrations of Si-O-M bridges (where M= Si, Al, Mg, Fe), the second one at 800-1000 cm^{-1} to vibration modes of the OH groups of the octahedral layers and the third at 400-700 cm^{-1} to bending vibrations of the Si-O-Si and Si-O-Al bridges of the clay framework.[45] These same bands are also present in the spectrum of HTFeED. The NH_2 deformation of the aliphatic chains of the silicon cubes, expected at 1620 cm^{-1}, is superimposed on the broad band at 1650 cm^{-1}, which arises from the vibrations of interlayer water. Analogously the asymmetric stretching band of Si-O-Si linkages of the polysiloxane in the 1000-1200 cm^{-1} region (Fig. 3d) is not clearly distinguishable in the intercalated clay composites (Fig. 3b and c) due to the existence of the same type vibrations (Si-O-Si) of the clay framework in the same spectral region. The band at 690 cm^{-1} and the broad band at 1458 cm^{-1} observed in the spectrum of Fe-EDAPTMOS can be attributed to CH bending vibrations and NH wagging of the aliphatic chains of the EDAPTMOS cubes[14] [15] respectively. The appearance of these bands in the spectrum of HTFeED is indicative of the insertion of organosilicon cubes in the clay galleries. Both bands disappear upon calcination, as seen in the spectrum of HTFeED-500. Analoguous results were obtained for the samples based on sodium-montmorillonite, Na-T, TFeED and TFeED-500 (see supporting appendix).

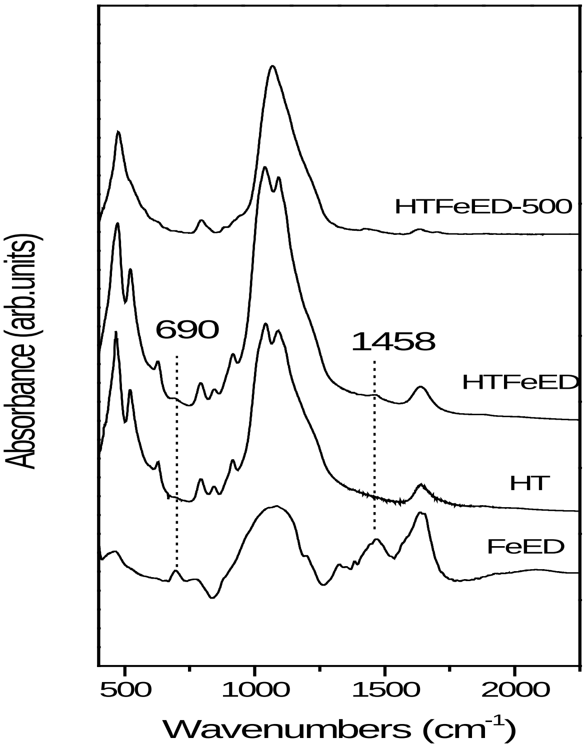

Figure 6.3. FTIR spectra of pristine HT, HTFeED and HTFeED-500; the spectrum of the Fe-EDAPTMOS complex (FeED) is added for comparison.

Figure 6.4 shows typical Mössbauer spectra of the pillared hybrid materials after calcination at 500 °C. Both quadrupole and magnetically split components are observed in the spectra and their resonant lines possess some degree of broadening. In addition the absorption area of the magnetic components increases at 10K (-263.15 °C), relative to that observed at 300K (26.85 °C), at the expense of the area of the quadrupole split component. The IS, quadrupole splitting (QS), quadrupole shift (2ε) and hyperfine magnetic field (B_{hf}) values (listed in Table S.I, see Appendix), correspond to Fe^{3+} high spin (S=5/2) ions in α-Fe_2O_3 (hematite) nanoparticles [46][47][48] These nanoparticles acquire a distribution of particle sizes and are subjected to superparamagnetic relaxation phenomena.[49][50]

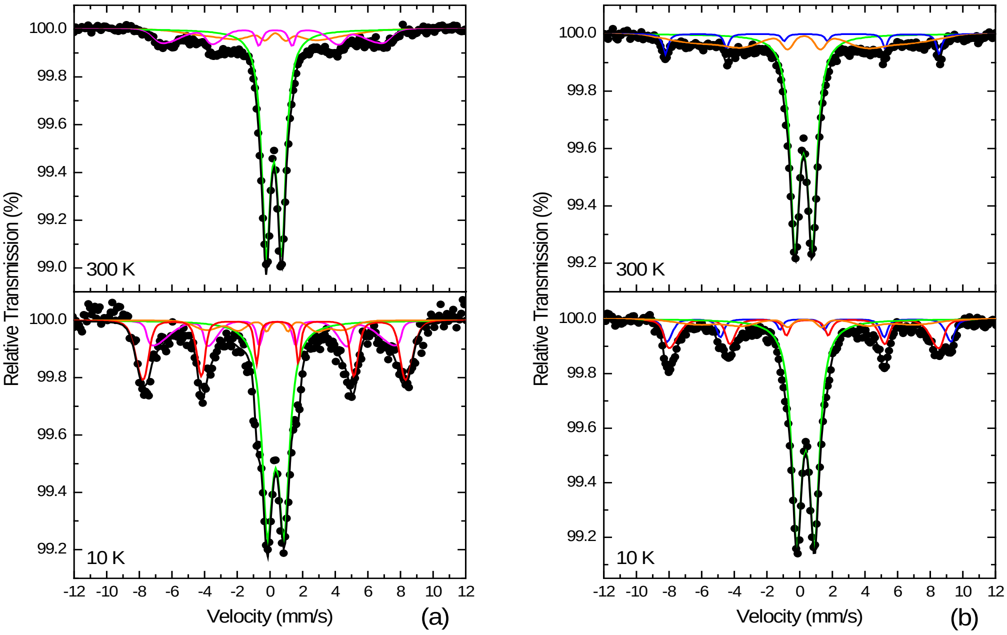

Figure 6.4. Mössbauer spectra of TFeED-500 (a) and HTFeED-500 (b) samples recorded at different temperatures.

XPS spectroscopy was also used to identify the constituents of TFeED and HTFeED and to verify the successful incorporation of the iron complexes in the montmorillonite matrices. In every survey spectrum (see Appendix) iron peaks were observed at the expected binding energies (Fe2$p_{3/2}$ at 710 eV and Fe2$p_{1/2}$ at 723 eV). To identify which iron and nitrogen species are present we fitted the core level spectra shown in Figure 6.5. In the case of iron we followed the approach of Grosvenor, *et al.*[51] For both TFeED and HTFeED five iron components are present, Fe(O)OH, $FeCl_2$ being the most dominant ones. Additionally, the nitrogen spectra reveal two nitrogen components, a first one peaked at around 401 eV binding energy, which accounts for 55% and 51% of the total N1*s* intensity for TFeED and HTFeED respectively, and which we attribute to protonated terminal amines of the silsesquioxane moieties and a second one at 399 eV, which makes up 45% and 51% of

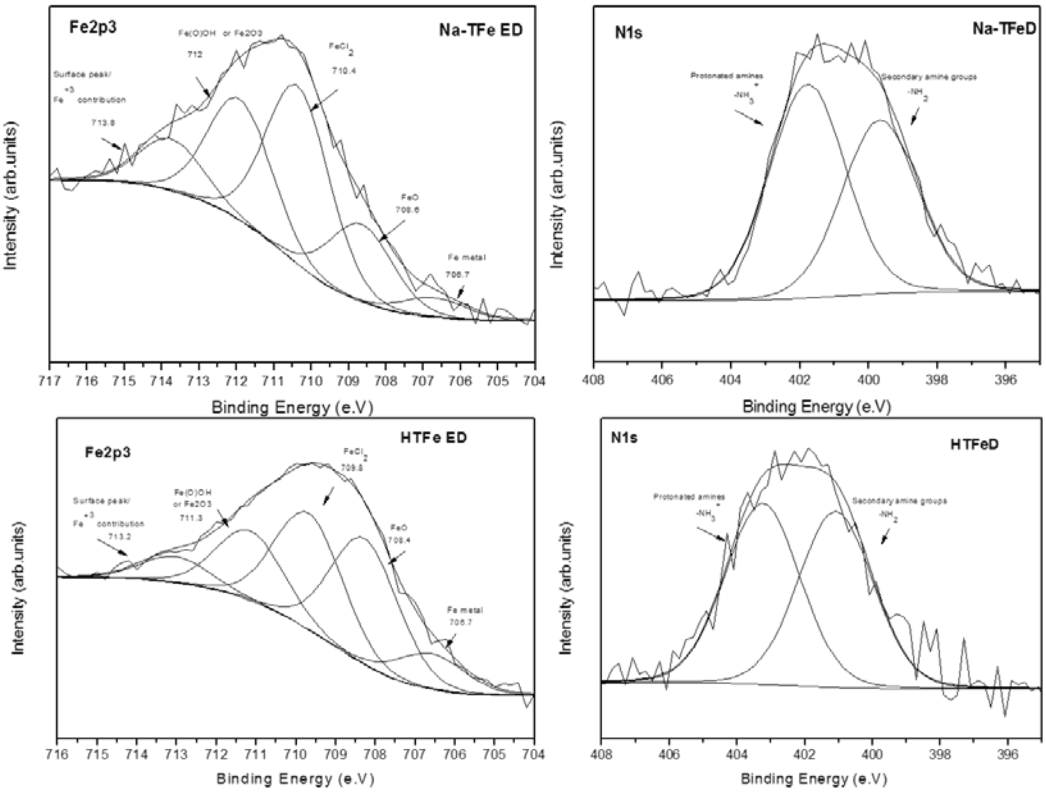

Figure 6.5. X-ray photoemission spectra of the Fe2*p*3/2 (left) and N1*s* (right) core level regions of TFeED and HTFeED

the total N1*s* intensity for **TFeED** and **HTFeED** respectively) and which is due to secondary amine groups of the same moieties.[52] Finally the intensity ratio silicon Si2p /aluminum Al2s increased from 2.6 for **Na-T** to 4.9 and 4.5 for **TFeED** and **HTFeED** respectively. This increase is due to the extra silicon stemming from the incorporation of silsesquioxanes and confirms, together with the FTIR spectra and the XRD data discussed above, the successful intercalation of the iron complexes in the clay matrices.

Figure 6.6 shows the DTA-TGA curves, of the intercalated hybrid HTFeED and of the pristine acid-activated montmorillonite, HT. HT shows a 10% weight loss up to 120 °C, related to the removal of the intercalated water. The amount of adsorbed water is considerably lower (6 wt%) in the case of HTFeED revealing the less hydrophilic

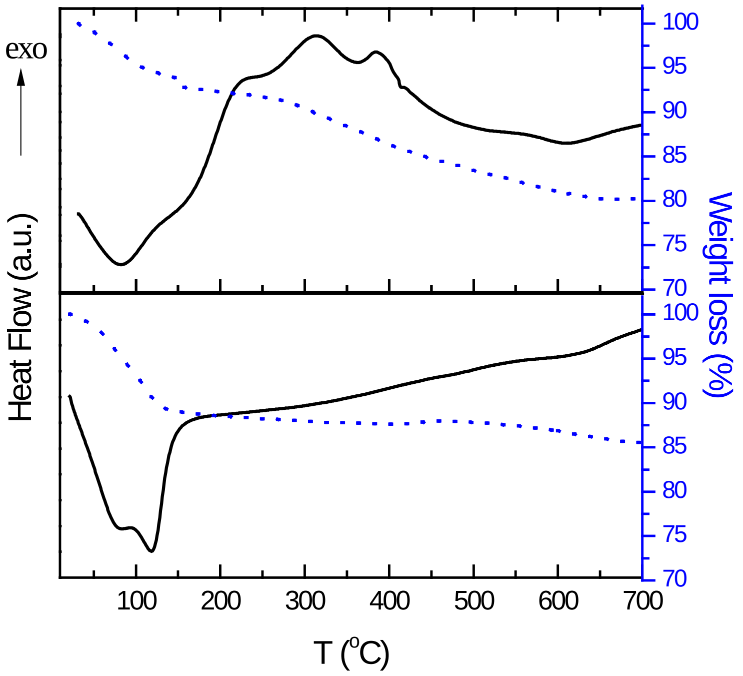

Figure 6.6. DTA-TGA curves of pristine HT (bottom) and of HTFeED (top).

character of this hybrid structure. Moreover, HTFeED presents three exothermic peaks between 150 and 420 °C accompanied by an approximately 10% weight loss. Considering the mass percentage, these signals must correspond to the removal of the organic chains of the silsesquioxane cubes, which takes place in three exothermic steps. Consequently, considering an octahedral complex of the type $Fe^{3+}{}_{8/3}[X_8Si_8O_{12}]$, where X is $H_2N(CH_3)_2NH(CH_2)_3$-, the amount of Fe-EDAPTMOS incorporated within the clay is estimated to account for 17 % of the total mass. Analogous results were obtained for TFeED. In this case, the organic part of intercalated moieties was found to correspond to about 15 wt% of the total mass (see Supporting Information) and thus the percentage of the organosilicon cubes to about 25 wt%.

Nitrogen adsorption-desorption measurements at 77K (-196.15 °C) were performed on both pillared clays in order to determine the porosity in each case. We not only obtained the specific-surface-areas (S_{BET}) obtained from the isotherms through BET analysis, but, in order to distinguish between the external plus mesoporous surface area and micropore volume, we also made use of the a_s-plot method.[53] [54] The a_s plots, defined as $a_s=(n_s/n_{0.4})_{ref}$ where n_s, $n_{0.4}$ are the amounts of N_2 adsorbed by a reference solid at P/P_o=s and P/P_o=0.4, have been proposed[53] [54] as a very valuable tool to investigate the porosity of solids. According to Gregg and Sing[53] it is convenient to set a_s=1 at P/P_o=0.4, since monolayer coverage and microporous filling occur at P/P_o<0.4, while capillary condensation takes place at P/P_o>0.4. In the present study two treatments with two different reference solids were carried out. As reference material Na-T, heated at 800 °C for 3 hs to eliminate the pores, with a specific surface area of 5 m^2g^{-1} was employed. The slope of the linear part of the V-a_s plot gives the meso+external surface area, $S_{m,e}$=2.87xV_{ads}/a_s, while the positive intercept gives the microporous volume, $V_{\mu p}$, after conversion of the gas volume adsorbed at 77 K: $V_{\mu p}$=V_{ads}(STP)x0.001547.

The values of specific surface area (S_{BET}) and total pore volume (V_p) from the experimental measurements as well as the mesoporous plus external surface ($S_{m,e}$), the micropores volume ($V_{\mu p}$) and micropores surface area ($S_{\mu p}$) calculated as described above are reported in Table I.

Table I. Results from a_s analysis, using as reference material **Na-T,** heated to 800 °C to eliminate the pores.

Sample	S_{BET} (m^2g^{-1})	V_p (cm^3g^{-1})	$S_{m,e}$ (m^2g^{-1})	$V_{\mu p}$ (cm^3g^{-1})	100($S_{m,e}$/S_{BET}) %	100($V_{\mu p}$/V) %
TFeED-500	248.8	0.256	107.4	0.068	43.2	26.6
HTFeED-500	230.2	0.263	102.7	0.061	44.6	23.2
Hat	107.8	0.151	67.3	0.022	62.4	14.6
Na-T	61	0.126	54.8	0.006	89.8	4.8

As obvious from the values of Table I, the BET specific surface area (S_{BET}) of the pristine clay increased after the acid activation. In addition TFeED-500 and HTFeED-500 hybrids show a significant increase in S_{BET} as compared to the pristine clay materials. More specifically the S_{BET} of TFeED-500, 248 m^2g^{-1}, amounts to 4 times the value of Na-T (61 m^2g^{-1}) while in the case of HTFeED-500 the S_{BET} was almost double (230 m^2g^{-1} as compared to 107 m^2g^{-1} for HT). Moreover $S_{m,e}$ also increased for the intercalated hybrids (in the case of TFeED-500 $S_{m,e}$ doubled) while the values of $V_{\mu p}$ for both hybrids (0.068 cm^3g^{-1} for TFeED-500 and 0.061 cm^3g^{-1} for HTFeED-500) are indicative of pillared structures.

6.3. Isopropanol decomposition.

The total degrees of conversion of isopropanol (Fig. 6.7a) as well as the selectivity towards propene and diisopropylether (Fig. 6.7b) are depicted as a function of reaction temperature. The data in Fig. 9(a) clearly indicate that both samples show a high catalytic activity due to the presence of acid sites on the surface. Since the decomposition of isopropanol is an acid catalyzed reaction, which is favored by catalysts with large number of acid sites, it is not surprising that HTFeED-500, which has been prepared using as starting material acid-activated clay, shows a higher activity. Moreover, as evidenced from Fig. 9(b) the selectivity to diisopropylether of TFeEDW-500 slightly predominates the selectivity to propene up to 105 ^oC, while in the case of HTFeED-500, the selectivity to propene starts from the values around 75%, and remains constant up to 105 ^oC.

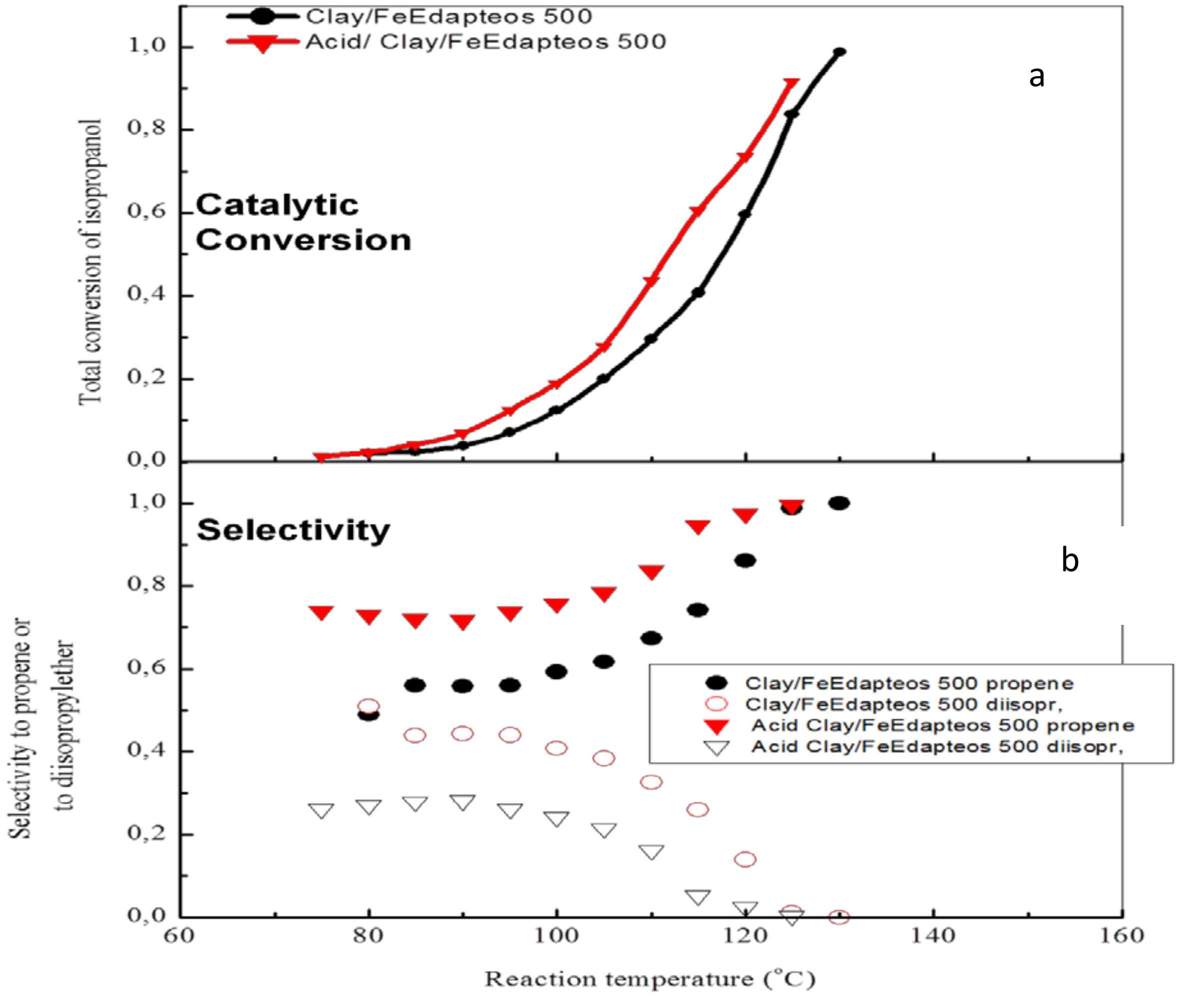

Figure 6.7. (a)The total degrees of conversion of isopropanol and (b) the selectivity towards propene (dark symbols) and diisopropylether (open symbols) as a function of reaction temperature for TFeED-500 and HTFeED-500 pillared clays.

Generally, the product profiles show that both propene and diisopropylether are present from the onset of the reaction, indicating that both reaction products are formed by direct dehydration; *i.e.*, they are primary reaction products coming from isopropanol through a parallel reaction network. According Campelo *et al.*[55] the pathway of formation of both products from 2-propanol conversion on $AlPO_4$ catalysts is a combination pathway of parallel and consecutive reactions presented in Figure 6.8.

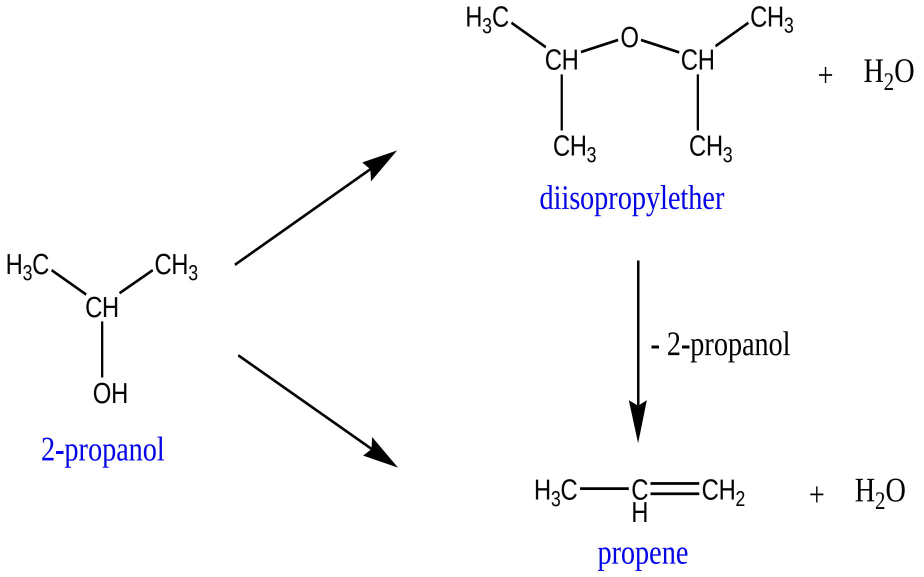

Figure 6.8. Schematic representation of parallel and consecutive reactions during from 2-propanol conversion.

Therefore, propene is a primary plus secondary reaction product while diisopropylether is a primary unstable product. In our case, it is clear that for all samples, the production of propene predominates at high reaction temperature and reaches 100% above 130 °C, independently of how many intermediates may be involved in its formation. On the other hand the differentiation on the onset selectivity to diisopropylether for the examined samples might be connected to stereochemical parameters. Thus the selectivity for the larger product (diisopropylether) is favoured on the catalyst with higher d-spacing (TFeED-500).

6.4. Conclusions

Intercalation of Fe^{3+}-substituted cubic silsesquioxanes in layered aluminosilicate nanoclays resulted in the formation of novel catalytic pillared structures. Octameric cubic oligosiloxanes, formed upon controlled hydrolytic polycondensation of the corresponding bi-functional amino-silane monomer (EDAPTMOS), were reacted with iron cations to form iron-siloxane complexes. These cationic complexes were intercalated in a sodium and an acid activated nanoclay and the resulting intercalated structures were further calcined to remove the organic side arms and produce cross-linked metal-substituted silica-pillared clays of high porosity and thermal stability. XRD measurements revealed the successful intercalation of iron-silsesquioxane complexes within the clay interlayers as well as the formation of the pillared structures upon calcination. The absence of reflection peaks of the crystalline phase of iron oxides indicates that iron oxide nanoparticles produced upon calcination are small enough and are not aggregated on the external clay surfaces but rather homogeneously dispersed in the clay matrix. The incorporation of the organosilicon cubes in the clay galleries was confirmed by infrared and X-ray photoelectron spectroscopies. The amount of the iron-silicon cubane complexes incorporated within the clay was estimated by thermal analysis between 17% and 25% of the total mass. Mössbauer spectra of the pillared materials after calcination at 500 °C, showed the existence of α-Fe_2O_3 (hematite) nanoparticles in the final hybrid systems. Nitrogen adsorption-desorption measurements showed that the specific surface area (S_{BET}) of the calcined intercalated clays was increased up to four times compared with that of pristine clays while the pore characteristics as estimated by the a_s-plot method are indicative of pillared structures. Finally, pillared clays showed high catalytic activity for isopropanol decomposition due to the presence of acid sites on the surface. In fact, pillared clay prepared using acid-activated clay as starting material showed a higher activity due to the large number of acid sites. The selectivity to diisopropylether of the pillared clay prepared from sodium-clay, slightly predominates the selectivity to propene up to 105 °C, while in the case of acid activated pillared clay, the selectivity to propene starts from the values around 75%, and remained constant up to 105 °C. This differentiation on the onset selectivity is a to stereochemical parameters. The resulting pillared clays exhibiting high specific areas and narrow pore size distribution could also be used as catalysts in many catalytic reactions in organic synthesis.

References

[1] A. Sellinger, R. M. Laine, *Chemistry of Materials* **1996**, *8*, 1592–1593.

[2] A. Sellinger, R. M. Laine, *Macromolecules* **1996**, *29*, 2327–2330.

[3] G. Potsi, A. Rossos, A. Kouloumpis, M. K. Antoniou, K. Spyrou, M. A. Karakassides, D. G. and P. Rudolf, *Current Organic Chemistry* **2016**, *20*, 662–673.

[4] D. B. Cordes, P. D. Lickiss, F. Rataboul, *Chemical Reviews* **2010**, *110*, 2081–2173.

[5] Y. Kaneko, E. B. Coughlin, T. Gunji, M. Itoh, K. Matsukawa, K. Naka, *International Journal of Polymer Science*, ***2012*****, (book)**.

[6] D. W. Scott, *Journal of the American Chemical Society* **1946**, *68*, 356–358.

[7] S. H. Phillips, T. S. Haddad, S. J. Tomczak, *Current Opinion in Solid State and Materials Science* **2004**, *8*, 21–29.

[8] R. Tamaki, Y. Tanaka, M. Z. Asuncion, J. Choi, R. M. Laine, *Journal of the American Chemical Society* **2001**, *123*, 12416–12417.

[9] R. M. Laine, J. Choi, I. Lee, *Advanced Materials* **2001**, *13*, 800–803.

[10] C. Zhang, T. J. Bunning, R. M. Laine, *Chemistry of Materials* **2001**, *13*, 3653–3662.

[11] C. Zhang, F. Babonneau, C. Bonhomme, R. M. Laine, C. L. Soles, H. A. Hristov, A. F. Yee, *Journal of the American Chemical Society* **1998**, *120*, 8380–8391.

[12] R. M. Laine, M. F. Roll, *Macromolecules* **2011**, *44*, 1073–1109.

[13] W. J. Yao Min Gu Xueping, Feng Lianfang, *Progress in Chemistry* **2012**, *24*, 405–413.

[14] A. Szabó, D. Gournis, M. A. Karakassides, D. Petridis, *Chemistry of Materials*

1998, *10*, 639–645.

[15] D. Petridis, D. Gournis, M. A. Karakassides, *Molecular Crystals and Liquid Crystals Science and Technology Section A Molecular Crystals and Liquid Crystals* **1998**, *311*, 345–350.

[16] G. Fetter, D. Tichit, P. Massiani, R. Dutartre, F. Figueras, *Clays & Clay Minerals* **1994**, *42*, 161–169.

[17] L. M. Johnson, T. J. Pinnavaia, *Langmuir* **1991**, *7*, 2636–2641.

[18] J. Ahenach, P. Cool, E. Vansant, O. Lebedev, J. Van Landuyt, *Physical Chemistry Chemical Physics* **1999**, *1*, 3703–3708.

[19] R. M. Barrer, *Journal of Inclusion Phenomena* **1986**, *4*, 109–119.

[20] J. Roziere, D. J. Jones, T. Cassagneau, *Journal of Materials Chemistry* **1991**, *1*, 1081–1082.

[21] T. Cassagneau, D. J. Jones, J. Roziere, *The Journal of Physical Chemistry* **1993**, *97*, 8678–8680.

[22] P. Olivera-Pastor, P. Maireles-Torres, E. E. Rodríguez-Castellón, A. Jiménez-López,, T. Cassagneau, D. J. Jones, J. Rozière, *Chemistry of Materials* **1996**, *8*, 1758–1769.

[23] W. Hou, J. Ma, Q. Yan, X. Fu, *Journal of the Chemical Society, Chemical Communications* **1993**, 1144–1145.

[24] D. R. Dreyer, S. Park, C. W. Bielawski, R. S. Ruoff, *Chemical Society Reviews* **2010**, *39*, 228–240.

[25] A. B. Bourlinos, D. Gournis, D. Petridis, T. Szabo, A. Szeri, I. Dekany, *Langmuir* **2003**, *19*, 6050–6055.

[26] A. Gomathi, K. Gopalakrishnan, C. N. R. Rao, *Materials Research Bulletin* **2010**,

45, 1894–1898.

[27] X. Shen, Y. Cui, Y. Pang, H. Qian, *Electrochimica Acta* **2012**, *59*, 91–99.

[28] S. Jana, S. Das, *Rsc Advances* **2014**, *4*, 34435–34442.

[29] S. Kataoka, S. Banerjee, A. Kawai, Y. Kamimura, J.-C. Choi, T. Kodaira, K. Sato, A. Endo, *Journal of the American Chemical Society* **2015**, *137*, 4158–4163.

[30] U. Flessner, D. J. Jones, J. Rozière, J. Zajac, L. Storaro, M. Lenarda, M. Pavan, A. Jiménez-López, E. Rodríguez-Castellón, M. Trombetta, et al., *Journal of Molecular Catalysis A, Chemical* **2001**, *168*, 247–256.

[31] A. K. Ladavos, F. Kooli, S. Moreno, S. P. Skaribas, P. J. Pomonis, W. Jones, G. Poncelet, *Applied Clay Science* **1998**, *13*, 49–63.

[32] V. N. Stathopoulos, A. K. Ladavos, K. M. Kolonia, S. P. Skaribas, D. E. Petrakis, P. J. Pomonis, *Microporous and Mesoporous Materials* **1999**, *31*, 111–121.

[33] A. K. Ladavos, P. N. Trikalitis, P. J. Pomonis, *Journal of Molecular Catalysis A: Chemical* **1996**, *106*, 241–254.

[34] F. Tomul, *Chemical Engineering Journal* **2012**, *185–186*, 380–390.

[35] R. Issaadi, F. Garin, C.-E. Chitour, *Catalysis Today* **2006**, *113*, 166–173.

[36] F. Khattou, G. Aptel, J.-V. Zanchetta, D. J. Jones, B. Deroide, J. Roziere, *Journal of Materials Chemistry* **1999**, *9*, 2453–2458.

[37] F. Khattou, G. Aptel, D. J. Jones, B. Deroide, J. Rozière, J.-V. Zanchetta, *Microporous and Mesoporous Materials* **2001**, *47*, 231–241.

[38] F. Carniato, C. Bisio, G. Gatti, E. Boccaleri, L. Bertinetti, S. Coluccia, O. Monticelli, L. Marchese, *Angewandte Chemie* **2009**, *121*, 6175–6177.

[39] F. Carniato, C. Bisio, G. Gatti, M. Guidotti, L. Sordelli, L. Marchese, *Chemistry-an Asian Journal* **2011**, *6*, 914–921.

[40] F. A. He, L. M. Zhang, *Nanotechnology* **2006**, *17*, 5941–5946.

[41] C. Pereira, A. R. Silva, A. P. Carvalho, J. Pires, C. Freire, *Journal of Molecular Catalysis a-Chemical* **2008**, *283*, 5–14.

[42] G. Balomenou, P. Stathi, A. Enotiadis, D. Gournis, Y. Deligiannakis, *Journal of colloid and interface science* **2008**, *325*, 74–83.

[43] D. Gournis, A. Lappas, M. A. Karakassides, D. Többens, A. Moukarika, *Physics and Chemistry of Minerals* **2008**, *35*, 49–58.

[44] BKG. Theng, *The Chemistry of Clay Organic Reactions*, London: Adam Hilger, **1974 (book)**.

[45] P. Falaras, F. Lezou, *Journal of Electroanalytical Chemistry* **1998**, *455*, 169–179.

[46] W. Kündig, H. Bömmel, G. Constabaris, R. H. Lindquist, *Physical Review* **1966**, *142*, 327–333.

[47] F. Bødker, M. F. Hansen, C. B. Koch, K. Lefmann, S. Mørup, *Physical Review B* **2000**, *61*, 6826–6838.

[48] F. Bødker. and S. Mørup, *EPL (Europhysics Letters)* **2000**, *52*, 217.

[49] J.-M. Greneche, in *Mössbauer Spectroscopy: Tutorial Book* (Eds.: Y. Yoshida, G. Langouche), Springer Berlin Heidelberg, Berlin, Heidelberg, **2013**, pp. 187–241.

[50] T. Tsoufis, A. Tomou, D. Gournis, A. P. Douvalis, I. Panagiotopoulos, B. Kooi, V. Georgakilas, I. Arfaoui, T. Bakas, *Journal of Nanoscience and Nanotechnology***.**, **200*8***, 8, 11, 5942–5951.

[51] A. P. Grosvenor, B. A. Kobe, M. C. Biesinger, N. S. McIntyre, *Surface and Interface Analysis* **2004**, *36*, 1564–1574.

[52] X. Song, Y. Ma, C. Wang, P. M. Dietrich, W. E. S. Unger, Y. Luo, *The Journal of Physical Chemistry C* **2012**, *116*, 12649–12654.

[53] S. J. Gregg, K. S. W. Sing, *Adsorption, Surface Area, and Porosity TT -*, Academic Press, London ;, **n.d.**

[54] A. Lecloux, J. P. Pirard, *Journal of Colloid and Interface Science* **1979**, *70*, 265–281.

[55] J. M. Campelo, A. Garcia, J. F. Herencia, D. Luna, J. M. Marinas, A. A. Romero, *Journal of Catalysis* **1995**, *151*, 307–314.

Appendix

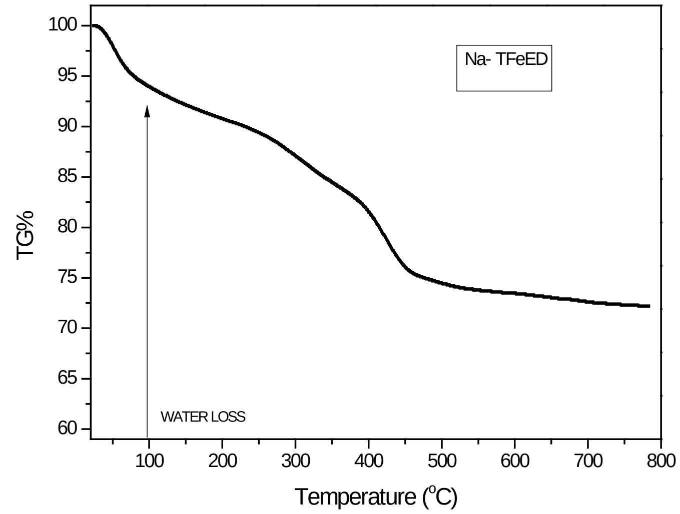

Figure S1. Thermogravimetric analysis: weight loss in % for the intercalated hybrid TFeED.

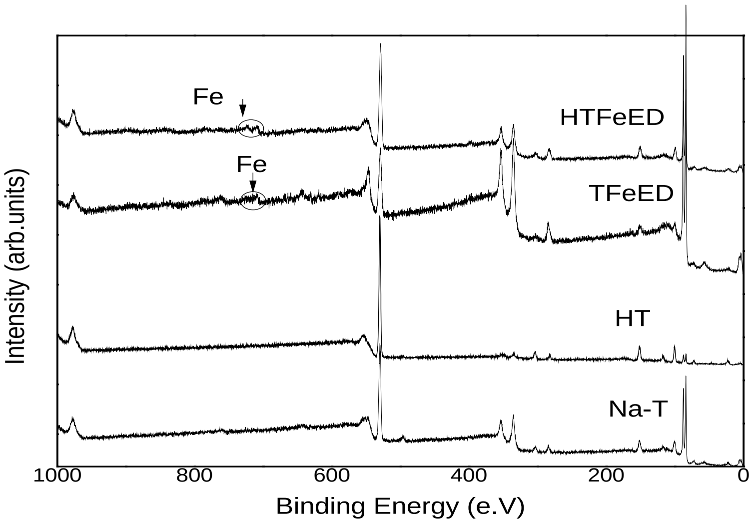

Figure S2. X-ray photoemission survey spectra of the pristine clays HT and Na-T as well as of the intercalated hybrids TFeED and HTFeED.

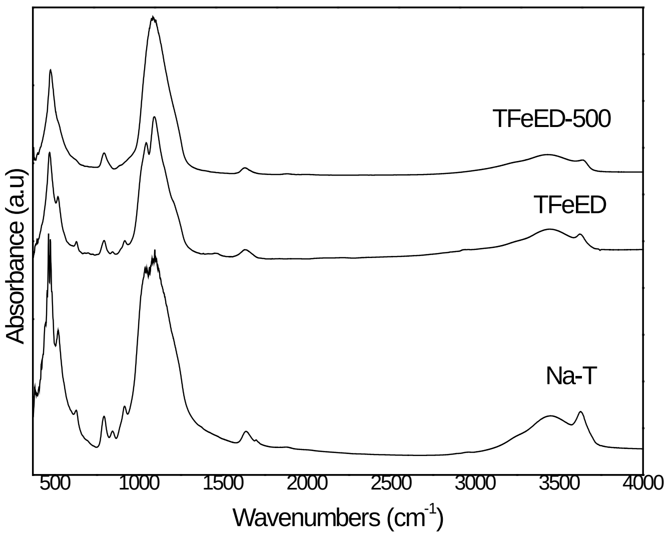

Figure S3. FT-IR spectra of the pristine Na-T clay, the intercalated hybrid TFeED and the pillared clay TFeED-500.

Table S.I. Mössbauer hyperfine parameters as resulting from the best fits of the Mössbauer spectra of the TFeED-500 and HTFeED-500 samples recorded at 26,85 °C and -263.15 °C. *IS* is the isomer shift (relative to a-Fe at 26,85 °C), *Γ/2* is the half line-width, *QS* is the quadrupole splitting, *2ε* is the quadrupole shift, B_{hf} is the central value of the hyperfine magnetic field, ΔB_{hf} is the hyperfine magnetic field spreading (symmetric in single column, or asymmetric denoted by the < and > symbols in the relative columns) around B_{hf} and *A* is the relative spectral absorption area of the components used to fit the spectra. Typical errors are ±0.02 mm/s for *IS*, *Γ/2*, *2ε* and QS, ±0.3 T for B_{hf} and ±5 % for A.

Sample	**T**	**IS**	**Γ/2**	**QS or 2ε**	**B_{hf}**	**ΔB_{hf}**	**$\Delta B_{hf} < B_{hf}$**	**$\Delta B_{hf} > B_{hf}$**	**Area**
	(K)	**mm/s**	**mm/s**	**mm/s**	**kOe**	**kOe**	**kOe**	**kOe**	**%**
TFeED-500	300	0.35	0.32	0.94	-	-	-	-	66
		0.35	0.14	-0.21	424	-	34	14	19
		0.35	0.14	-0.20	242	90	-	-	15
	10	0.47	0.40	1.02	-	-	-	-	48
		0.47	0.14	-0.20	257	43	-	-	8
		0.48	0.15	-0.20	497	-	7	12	26
		0.47	0.15	-0.21	482	-	34	0	18
HTFeED-500	300	0.35	0.35	1.06	-	-	-	-	66
		0.38	0.18	-0.21	521	3	-	-	7
		0.32	0.15	-0.10	392	108	-	-	27
	10	0.48	0.37	1.08	-	-	-	-	60
		0.48	0.20	0.41	541	-	10	0	10
		0.48	0.23	-0.20	528	-	16	0	19
		0.49	0.15	0.12	409	83	-	-	11

CHAPTER 7

Fabrication of highly ordered Cu^{2+}/Fe^{3+} substituted POSS thin films, a case study of structure influenced by metal coordination

In this chapter we introduce a layer-by-layer protocol to grow metal-decorated organic-inorganic cage-like polyhedral oligomeric silsesquioxanes (POSS) thin films with possible application in the field of quantum computers.[1][2]Our key strategy is to use metal ions (Cu^{2+} or Fe^{3+}) as linker for the ammonium-functionalized cage-like POSS which are self-assembled between arachidic acid to form highly ordered structures by using the Langmuir–Schaefer method.

7.1. Introduction

As it is described in Chapter 5 silsesquioxanes ($RSiO_{3/2}$) form three-dimensional (3D) cage-like highly symmetric frameworks known as polyhedral oligosilsesquioxanes (POSS). These formations derive from hydrolytic condensation reactions of organosilicon monomers[3] ($RSiOH_3$), where an organic group is covalently attached to the silicon chain. Moreover (POSS) have the ability to bind metal ions forming metal substituted silsesquioxanes[4][5][6] and can be used as components during the synthesis of hybrid materials suitable for catalytic applications such as natural gas separation[7] or hydrogen catalysis.[8]

POSS attracted significant attention over the past few decades and provided a versatile platform for innovative research and diverse applications in aerospace,[9] dentistry,[10][11] protective coatings,[3] microelectronics[12] and catalysis,[13][14] energy storage, environmental, drug delivery and biomedicine.[4] However, the insertion of cage-like units into suitable host systems remains a major challenge in current materials science and technology.

In most cases, POSS hybrids are usually synthesized by conventional chemical copolymerization, crosslinking, physical blending[15] or can be used as cores for dendrimer synthesis.[16] While most of the research refers mainly studies concern bulk synthesis of polymer nanocomposites[17][18][19][20] and hybrid materials,[21][22] there are fewer reports using a thin film approach, in particular the Langmuir-Blodgett (LB)[23][24][25][26][27][28] or Langmuir Schaefer[25] (LS) methods. Recently, POSS derivatives have been found to self-assemble as monolayers at the air/water interface.[29][30] In POSS the OH groups that are attached to the cage are hydrophilic so they can rest on the subphase, while the R groups are hydrophobic and take up positions away from the water surface. This amphiphilic properties of POSS allow the formation of Langmuir thin films.[25] [31]

Synthesis methods like LB and LS permit to form complex structures of desirable thickness and architecture. Additionally these methods overcome a major problem in the preparation of POSS hybrids which is the tendency of POSS to segregate and form aggregates causing inhomogeneity during film formation.[27] Controlling a structure using LB or LS deposition provides homogeneity as well as better reproducibility of the hybrid systems and hence warrants a better management of the materials' properties.[26][29]

This work focuses on using the Langmuir–Schaefer method as a means to control the structure of thin metal-decorated (Cu^{2+} or Fe^{3+}) POSS thin films using a simple surfactant such as arachidic acid (AA). Our aim was to investigate the final structure of hybrid thin films as well as to prove that using metal ions with different coordination[32][33][34] one can tailor the architecture of the thin film. In fact, during the synthesis of the metal substituted silsesquioxanes, the arrangement of copper (II) chloride trans square planar molecules is governed by weak intermolecular Cu-Cl interactions. Moreover Cu (II) complexes containing N- and O- donors are very common and usually in aqueous solutions only four ligands are replaced.[35],[16] On the other hand, iron in complexes usually exist in octahedral coordination, while during the formation of Fe-N complexes six nitrogen ligands are present.[32][33][34] These differences are expected to translate into a different thin film structure.

7.2. Method of preparation

The thin films were fabricated via two synthetic routes illustrated in Scheme 7.1. Following the first route, initially a AA Langmuir film is transferred to the substrate (step 1), then a monolayer of metal- decorated (Cu^{2+} or Fe^{3+})-POSS is self-assembled on it by dipping into a solution of the metal-substituted silsesquioxanes (step 2) and then again a AA monolayer is added by a LS deposition (step 3). Repeating the sequence to obtain a multilayer structure

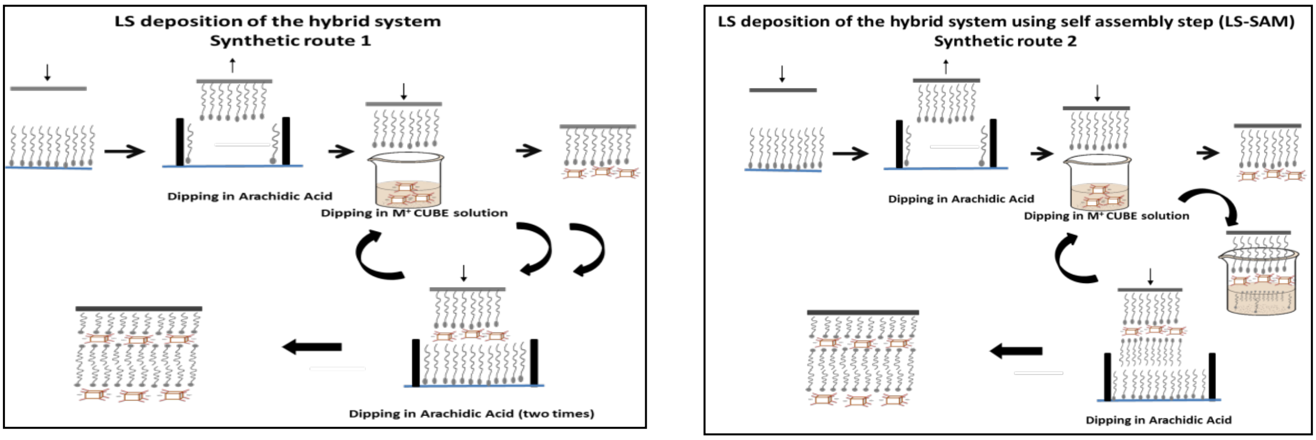

Scheme 7.1. Preparation of the Layered Structure of the Hybrid metal-decorated ((Cu^{2+} or Fe^{3+}) organic-inorganic cage-like POSS by two modified Langmuir-Schaefer deposition protocols which differ in the deposition of the arachidic acid on top of the POSS: Synthetic Route 1 (left panel) proceeds with assembly via Langmuir-Schaefer deposition and Synthetic Route 2 (right panel) via self-assembly from solution. Both should give rise to the same film structure as sketched in the lower left corner of each panel.

one expects an alternation between 2 AA layers assembled tail-to-tail and a metal-decorated (Cu^{2+} or Fe^{3+})-POSS monolayer, as sketched in the lower left corner of the left panel in Scheme 7.1. Following the second synthesis route, steps 1 and 2 are identical to synthetic route 1 but then an extra layer of AA is deposited by self-assembly (step 3) by dipping into a solution of AA. Also in this case, when repeating the sequence to obtain a multilayer structure, one expects an alternation between 2 AA layers assembled tail-to-tail and a metal-decorated (Cu^{2+} or Fe^{3+})-POSS monolayer, as sketched in the lower left corner of the right panel in Scheme 7.1. The purpose of following two different routes was to determine which one leads to better structural order in the final multilayer LS films.

A series of analysis techniques were employed to investigate the structural properties of these films and confirm the specific architecture.

7.3. Results and Discussion

7.3.1. Characterization of the deposition of AA- Metal (Cu^{+2},Fe^{+3}) POSS hybrid films

The van der Waals interactions between the hydrophobic part of POSS and the hydrophobized substrate (surface of substrates was modified with octadecyltrichlorosilane) initiate the film formation.[36][23] Prove of the transfer of AA comes from Figure 7.1 which displays the time dependence of the total trough area covered by the monolayer of arachidic acid that can be transferred to the substrate[37] as well as the surface pressure during the deposition of AA-Cu POSS and AA-Fe POSS hybrid films following synthetic routes 1 and 2. During each deposition process the pressure remains stable over time thereby attesting for the stability of the depositions. Studying further the shape of the trough area and pressure curves, it is possible to gain information about the amount of material deposited: The air-water interface is fully covered by a stable monolayer at the beginning. When the substrate is dipped into the subphase, one layer is transferred from the trough to the substrate, giving rise to sharp step on the curve of the trough area versus time and a sharp downward peak on the curve of the pressure versus time. The transfer ratio is 1 if the step height on the trough area curve is same as the surface area of substrate; then the surface is 100 % covered by a monolayer at each dip into the subphase. If transfer ratio is more than 1, this indicates that more than one layer was transferred; if it is less than 1 the layer was not entirely transferred. From the curves in Figure 7.1, and knowing that the substrate surface area is close to 2.5 cm^2 it can be seen that the transfer ratio is larger than 1 (1.5-1.7) throughout the deposition, indicating that the transfer at each dip cost more AA molecules than expected to cover the whole substrate area. However, control studies on pure LB and LS deposition of AA have shown that for identical conditions, the film produced by LS always has a transfer ration superior to one by ~ 60 %. We attribute this effect to be due to excess material carried in a droplet that forms at the surface of the substrates when breaking the meniscus after every dip.

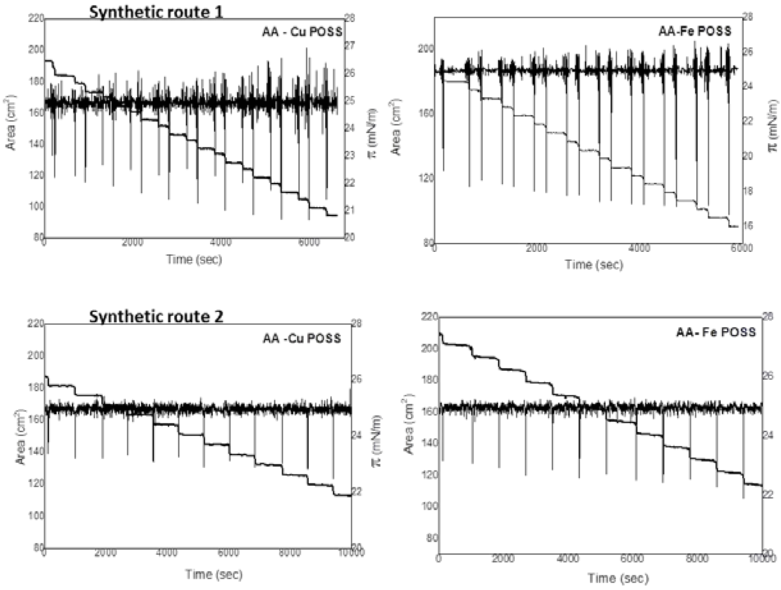

Figure 1. Upper panel: The LS deposition of AA-Cu POSS hybrid films following synthetic route 1 (a) and synthetic route 2 (b); Lower panel: The LS deposition of AA-Fe POSS hybrid films following synthetic route 1 (c) and synthetic route 2 (d).

7.3.2. XRR Patterns of AA-POSS-Metal hybrid films

X-ray reflectance (XRR) is a usefull method for the characterization of thin films focusing in film properties such as film thickness, periodical fringes, density and surface roughness.[38] In our case measurements were performed in order to reveal information about the structure properties of the films depending on the metal that was used in the silsesquioxane substitution. X-ray reflectivity measurements were carried out on 20-layer thick hybrid films at ambient conditions. Figures 7.2a and 7.2b show XRR patterns for films prepared with copper or iron substituted silsesquioxanes following Synthetic route 1 and 2.

Comparing the XRR results for the two synthetic routes in both cases (Figure 7.2c) it is obvious that Synthetic route 2 that includes the self-assembly of AA step leads to more ordered films since the d_{001} diffraction peak is sharper and well-shaped than when synthetic route 1 was followed. That means that molecules of AA are better organized when the second layer of the surfactant is created through contacting the surface of the AA solution and a self-assembled monolayer (SAM) is formed spontaneously at the substrate surface.

Additionally, LB films synthesized using copper substituted silsesquioxanes exhibit the 001 diffraction peak at 2.3 degrees, which translates to a d_{001} value of 37.7 Å. On the other hand for LS films that were synthesized using iron substituted silsesquioxanes the diffraction peak appears at much lower angles (1.4 degrees) corresponding to d_{001} = 68 Å. The length of AA monolayer can vary from 25 to 15 Å depending on the tilt angle in the film structure.[39]Assuming that the AA layer in both cases is tilted in the same way, the 30 Å difference in d_{001} can be explained by the different conformation of the metal substituted silsesquioxanes layer when using different metals. According to Szabo *et al.,*[40] G. Balomenou *et al.*[21] and Kataoka *et al.*[41] that studied the intercalation of silsesquioxanes into layered structures the dimensions of the silsesquioxanes are 6.6-7.1 Å, (horizontal orientation) and 11.2-17.6 Å (vertical orientation) shown in Figure 7.3.

Moreover, while copper usually forms usually planal (four coordinated) complexes, the metal coordination of iron is octahedral and six ligands can be replaced during the formation of the metal substituted silsesquioxanes solution. This fact could explain the increased unit distance since it is highly possible that during the formation of the iron substituted silsesquioxanes solution a second silsesquioxane is attached due to the 2 free ligands of iron particle, which is bonded on the silsesquioxanes Fig 7.3.

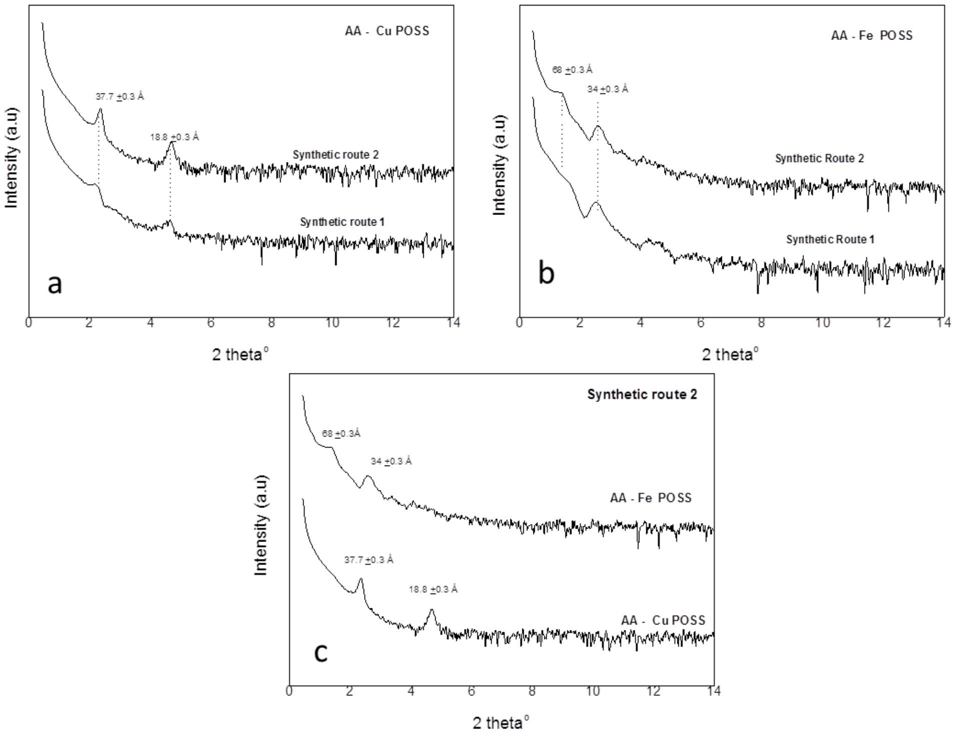

Figure 7.2. X-ray reflectivity patterns of 20 layer thick hybrid films of (a) AA-Cu POSS and (b) AA-Fe POSS deposited following synthetic routes 1 and 2; (c) comparison of the X-ray reflectivity patterns of 20 layer thick hybrid films of AA-Cu POSS and AA-Fe POSS synthesised with synthetic route 2.

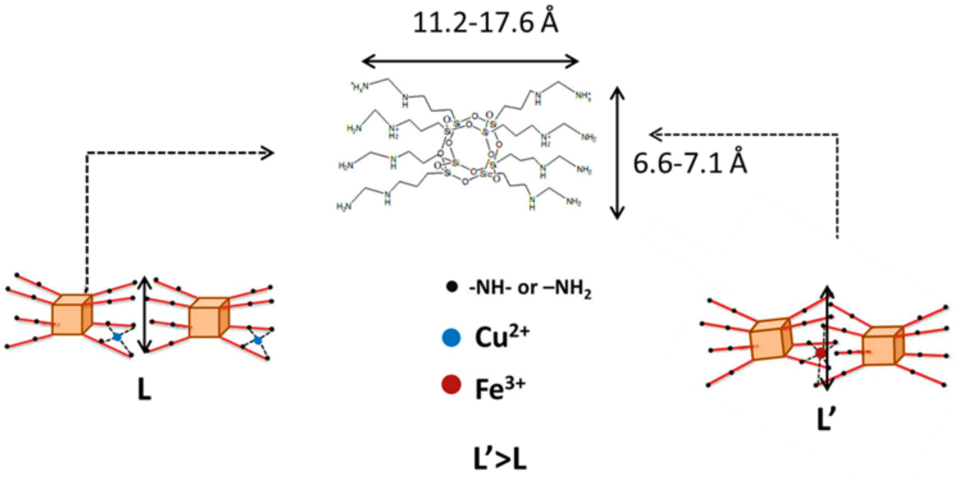

Figure 7.3. Possible arrangements of the metal (Cu^{2+}, Fe^{3+}) decorated POSS in the hybrid AA-M (Cu^{2+}, Fe^{3+}) POSS films.

After the lift from the metal substituted POSS solution, the outer surface of the layer is positively charged and hydrophilic. The AA monolayer on the water surface is terminated by alkyl chains and hence hydrophobic. That allows to hydrophilic POSS surface interact with the hydrophobic alkyl chains of AA monolayer and give rise to the X-type structure.[42] However, this type of film is stable only for non-polar molecules.[43] For this reason, a "flip over" mechanism has been proposed to form the more stable Y-type structure.[44] [45] [42] In our case, the "flip over" occurs in every step 3 of the cycle, no matter if AA deposition occurs from the LB trough (synthetic route 1) or from the AA solution of ethanol (synthetic route 2).

7.3.3. Probing the surface of AA-Metal POSS hybrid films by XPS

To verify our model, XPS measurements were performed on films prepared following a different synthetic route, described as synthetic route 3 in Scheme 7.2. The route was introduced to investigate the nature of the topmost surface of hybrid AA-metal POSS thin films in order to confirm the attachment of the AA layer. It consists in producing a hybrid film in 2-step cycles: initially a AA Langmuir film is transferred to the substrate (step 1), then a monolayer of metal-decorated (Cu^{2+} or Fe^{3+})-POSS is self-assembled on it by dipping into a solution of the metal-substituted silsesquioxanes (step 2) and then the cycle is repeated. XPS can be used for identifying the surface elemental composition of materials. Using a 37° electron take-off angle, 95 % of the XPS signal comes from a depth of ~ 1.1 nm, the remaining 5% comes from deeper in the sample.[45][46] Figure 7.4(a) shows XPS spectra of the C1*s* (used as reference), N1*s*, Si2*p*, and Cu2*p* core level regions collected from AA-Cu-POSS hybrid films and Figure 7.4(b) those of the C1*s*, N1*s*, Si2*p*, and Fe2*p* core level regions collected from AA-Fe-POSS hybrid films. From Figure 7.4 (a), it can be clearly seen that the Cu, N, Si peak intensities change in alternate layers. Layers with odd number have a larger amount of Cu, N, Si at the topmost surface than layers with even number. Since Cu, N and Si come from the Cu-decorated POSS layers, this observation confirms the successful attachment of AA layers. During the deposition, every layer of AA will be attached to the Cu-decorated POSS layer, inducing the alternate predominance of C (from the AA surfactant) or of Cu-N-Si (from Cu-decorated POSS layer) in topmost surface. From Figure 7.4 (b) It is obvious that the N, Si peaks vary in the same way as in Figure 7.4(a), while the Fe peak intensity is always constant with alternate layers. In consideration with the 6-coordinated Fe, we assume that the silsesquioxanes surrounding iron prevent fluctuation at peak intensity. As can be seen from Figure 7.3, for AA-Fe-POSS hybrid films, even when the Fe-decorated POSS layer is on the topmost surface, Fe is still covered by the POSS and the intensity of Fe peak does not show alternate change. So the attachment of every AA layer exists also during the deposition of AA-Fe-POSS hybrid films.

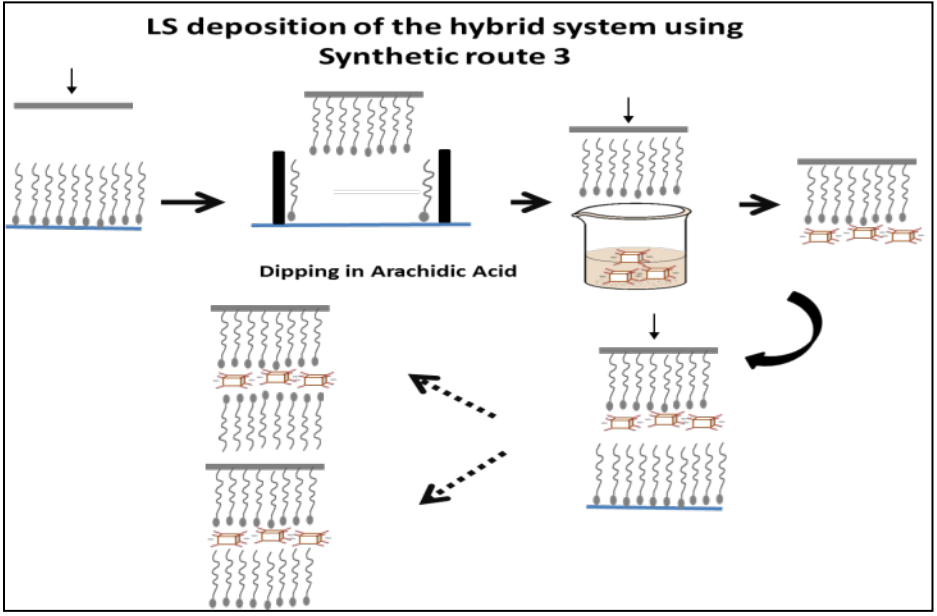

Scheme 7.2. Langmuir-Schaefer method synthetic route 3 (dip one time into the trough in every cycle).

.

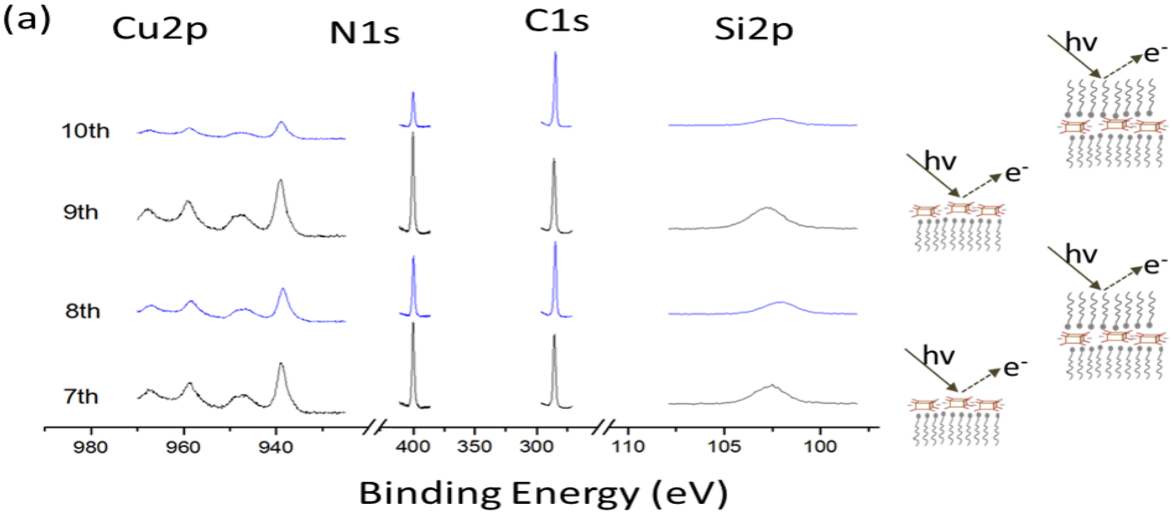

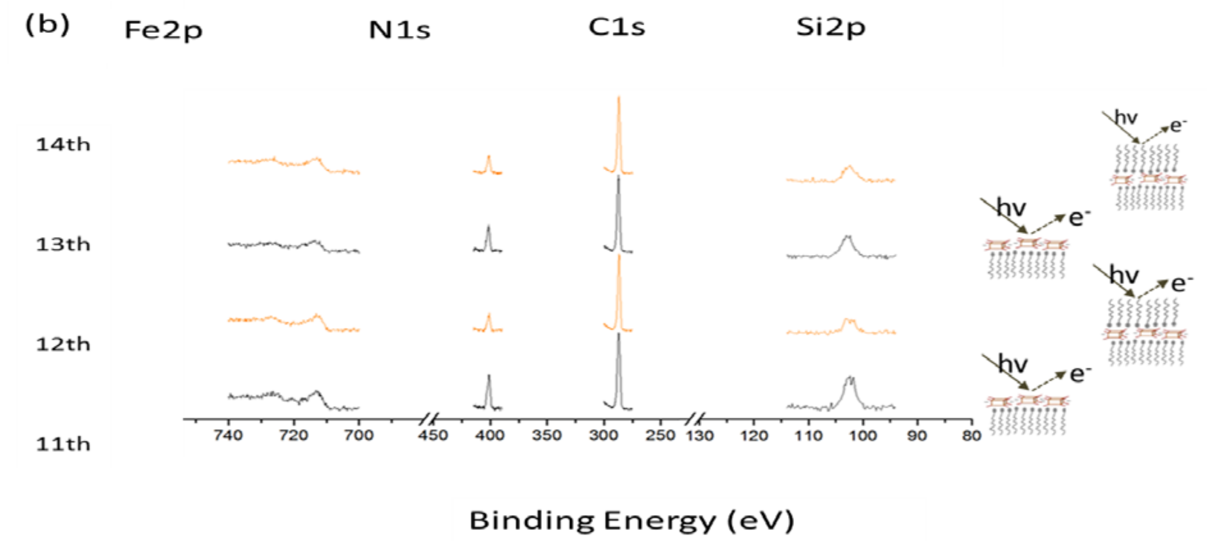

Figure 7.4. X-ray photoemission spectra of the indicated core level regions of (a) AA-Cu POSS hybrid films collected after the deposition of layers 7, 8, 9 to 10 and (b) AA- Fe POSS hybrid films collected after the deposition of layers 11, 12, 13 and 14.

7.4. Perspectives

In order to verify the metal coordination of iron and copper in our systems Grazing-Incidence Small-Angle X-ray Scattering (GI-SAXS) and Extended X-ray Absorption Fine Structure (EXAFS) experiments are ongoing the present time. These sets of measurements will allow us to have a clear view on the exact metal coordination as well as the oxidation state of the metals in our hybrid AA – metal POSS films.

7.5. Conclusion

We successfully fabricated multilayer films of well-ordered metal-decorated (Cu^{2+} and Fe^{+3}) polyhedral oligomeric silsesquioxanes (POSS) using two modified Langmuir-Schaefer deposition protocols which both start with LS deposition of arachidic acid followed by self-assembly of a monolayer of metal- decorated (Cu^{2+} or Fe^{3+})-POSS by dipping into a solution of the metal-substituted silsesquioxanes but differ in the deposition of the arachidic acid on top of the POSS: Synthetic Route 1 proceeds with assembly via Langmuir-Schaefer deposition and Synthetic Route 2 via self-assembly from solution. An XPS study revealed the successful attachment of AA layers during the deposition, leading to a periodically repeated AA-Metal (Cu^{2+} and Fe^{+3})-POSS-AA unit. XRD results showed that the interlayer distance between the units is affected by the metal coordination of the metal ions. Additionally, it was shown that the hybrid films deposited following Synthetic route 2 (involving self-assembly process) lead to a better ordered structures than Synthetic route 1. Future experiments using GISAXS and EXAFS are expected to prove the metal coordination as well as the oxidation state in the film systems.

References

*[1] G. Aromi, D. Aguila, P. Gamez, F. Luis, O. Roubeau, Chemical Society Reviews **2012**, 41, 537–546.*

*[2] G. Mitrikas, Y. Sanakis, C. P. Raptopoulou, G. Kordas, G. Papavassiliou, Physical Chemistry Chemical Physics **2008**, 10, 743–748.*

*[3] R. H. Baney, M. Itoh, A. Sakakibara, T. Suzuki, Chemical Reviews **1995**, 95, 1409–1430.*

*[4] G. Potsi, A. Rossos, A. Kouloumpis, M. K. Antoniou, K. Spyrou, M. A. Karakassides, D. G. and P. Rudolf, Current Organic Chemistry **2016**, 20, 662–673.*

*[5] Y. Kaneko, E. B. Coughlin, T. Gunji, M. Itoh, K. Matsukawa, K. Naka, International Journal of Polymer Science, **2012,(editorial book).***

*[6] D. B. Cordes, P. D. Lickiss, F. Rataboul, Chemical Reviews **2010**, 110, 2081–2173.*

*[7] F. Li, Y. Li, T.-S. Chung, S. Kawi, Journal of Membrane Science **2010**, 356, 14–21.*

*[8] A. Maiti, R. H. Gee, R. Maxwell, A. P. Saab, Chemical Physics Letters **2007**, 440, 244–248.*

*[9] S. H. Phillips, T. S. Haddad, S. J. Tomczak, Current Opinion in Solid State and Materials Science **2004**, 8, 21–29.*

*[10] M. S. Soh, A. S. and A. U. J. Yap, Current Nanoscience **2006**, 2, 373–381.*

*[11] H. Fong, S. H. Dickens, G. M. Flaim, Dental Materials **2005**, 21, 520–529.*

*[12] Y.-T. Chang, C.-F. Shu, C.-M. Leu, K.-H. Wei, Journal of Polymer Science Part A: Polymer Chemistry **2003**, 41, 3726–3735.*

[13] F. Carniato, C. Bisio, G. Gatti, E. Boccaleri, L. Bertinetti, S. Coluccia, O. Monticelli,

*L. Marchese, Angewandte Chemie **2009**, 121, 6175–6177.*

*[14] N. N. Ghosh, J. C. Clark, G. T. Eldridge, C. E. Barnes, Chemical Communications **2004**, 856–857.*

*[15] W. Zhang, A. H. E. Müller, Macromolecules **2010**, 43, 3148–3152.*

*[16] K. Naka, M. Fujita, K. Tanaka, Y. Chujo, Langmuir **2007**, 23, 9057–9063.*

*[17] K. J. Shea, D. A. Loy, Chemistry of Materials **2001**, 13, 3306–3319.*

*[18] S.-W. Kuo, F.-C. Chang, Progress in Polymer Science **2011**, 36, 1649–1696.*

*[19] G. Li, L. Wang, H. Ni, C. U. Pittman, Journal of Inorganic and Organometallic Polymers, **2001**,11, 123–154.*

*[20] H.-J. Sun, Y. Tu, C.-L. Wang, R. M. Van Horn, C.-C. Tsai, M. J. Graham, B. Sun, B. Lotz, W.-B. Zhang, S. Z. D. Cheng, Journal of Materials Chemistry **2011**, 21, 14240–14247.*

*[21] G. Balomenou, P. Stathi, A. Enotiadis, D. Gournis, Y. Deligiannakis, Journal of colloid and interface science **2008**, 325, 74–83.*

*[22] Y. Xue, Y. Liu, F. Lu, J. Qu, H. Chen, L. Dai, The Journal of Physical Chemistry Letters **2012**, 3, 1607–1612.*

*[23] W. Yin, J. Deng, A. R. Esker, Langmuir **2009**, 25, 7181–7184.*

*[24] W. Lee, S. Ni, J. Deng, B.-S. Kim, S. K. Satija, P. T. Mather, A. R. Esker, Macromolecules **2007**, 40, 682–688.*

*[25] A. Wamke, K. Dopierała, K. Prochaska, H. Maciejewski, A. Biadasz, A. Dudkowiak, Colloids and Surfaces A: Physicochemical and Engineering Aspects **2015**, 464, 110–120.*

[26] A. C. Kucuk, J. Matsui, T. Miyashita, Journal of Colloid and Interface Science

__2011__, 355, 106–114.

[27] *M. Mitsuishi, F. Zhao, Y. Kim, A. Watanabe, T. Miyashita, Chemistry of Materials __2008__, 20, 4310–4316.*

[28] *M. K. Ferguson-McPherson, E. R. Low, A. R. Esker, J. R. Morris, The Journal of Physical Chemistry B __2005__, 109, 18914–18920.*

[29] *J. R. Hottle, H.-J. Kim, J. Deng, C. E. Farmer-Creely, B. D. Viers, A. R. Esker, Macromolecules __2004__, 37, 4900–4908.*

[30] *J. Deng, B. D. Viers, A. R. Esker, J. W. Anseth, G. G. Fuller, Langmuir __2005__, 21, 2375–2385.*

[31] *A. R. Esker, H. Yu, in (Eds.: J.M. Owen, R.P. Dvornic), Springer Netherlands, Dordrecht, __2012__, pp. 195–228(__book section__).*

[32] *M. Balamurugan, P. Vadivelu, M. Palaniandavar, Dalton Transactions __2014__, 43, 14653–14668.*

[33] *D. M. Collins, R. Countryman, J. L. Hoard, Journal of the American Chemical Society __1972__, 94, 2066–2072.*

[34] *E. L. Rue, K. W. Bruland, Marine Chemistry __1995__, 50, 117–138.*

[35] *C. Housecroft, No TitleHousecroft Inorganic Chemistry, 3/E, Prentice Hall, __2007(book)__.*

[36] *M. K. Ferguson-McPherson, E. R. Low, A. R. Esker, J. R. Morris, Langmuir __2005__, 21, 11226–11231.*

[37] *J. A. Spink, Journal of Colloid and Interface Science __1967__, 23, 9–26.*

[38] *J. Fanton, C. Uhrich, L. Koppel, __2002 (book)__.*

[39] *N. Akhtar, G. R. Blake, R. Felici, H. Amenitsch, T. T. M. Palstra, P. Rudolf, Nano*

*Research **2014**, 7, 1832–1842.*

[40] *A. Szabó, D. Gournis, M. A. Karakassides, D. Petridis, Chemistry of Materials **1998**, 10, 639–645.*

[41] *S. Kataoka, S. Banerjee, A. Kawai, Y. Kamimura, J.-C. Choi, T. Kodaira, K. Sato, A. Endo, Journal of the American Chemical Society **2015**, 137, 4158–4163.*

[42] *Y. Umemura, Y. Onodera, A. Yamagishi, Thin Solid Films **2003**, 426, 216–220.*

[43] *G. Decher, Angewandte Chemie **1992**, 104, 498–499.*

[44] *R. Y. N. Gengler, D. Gournis, A. H. Aimon, L. M. Toma, P. Rudolf, Chemistry – A European Journal **2012**, 18, 7594–7600.*

[45] *L. M. Toma, R. Y. N. Gengler, E. B. Prinsen, D. Gournis, P. Rudolf, Physical Chemistry Chemical Physics **2010**, 12, 12188–12197.*

[46] *K. L. Mittal, R. Kohli, Developments in Surface Contamination and Cleaning - Vol 2 , 1st Edition Particle Deposition, Control and Removal, Elsevier, **2009**.*

Summary

The field of layered nanostructured hybrid materials focuses on the synthesis and possible applications of materials that combine the properties of building blocks of nanometer size dimensions. Bringing together the building blocks can enhance their properties or generate new properties not present in either of the constituents alone.

The aim of this thesis centred on layered nanostructured hybrid materials for environmental, medical, energy and catalytic applications, is to describe the synthesis, characterization and possible applications of a number of hybrid layered materials based on carbon allotropes or different inorganic matrices like clay minerals.

Chapter 3 presents the synthesis of multi-functional pillared layered materials synthesized by the intercalation of adamantylamine into the interlayer space of graphite oxide and layered aluminosilicate nanoclays. Different characterization techniques demonstrated the successful intercalation of adamantylamine and showed that the final pillared materials have an increased specific surface area. In addition these hybrids were found to be capable of adsorbing significant quantities of organic pollutants, which entails a great potential for environmental remediation applications. Moreover they were found to present improved cytotoxic activity on A549 cancer cells, whilst the cytotoxicity towards MRC-5 cells (normal) was minimal, a fact that renders them suitable as antiproliferative agents in biomedical applications.

Chapter 4 describes the chemical oxidation of carbon nanodiscs, industrially prepared via the so-called pyrolytic Kværner Carbon Black & H_2 process, towards the formation of a hydrophilic analogue. The detailed

characterization of the pristine and the oxidized material is described and the study of the cytotoxic properties of the oxidized nanodiscs is reported. Besides resulting in the separation of carbon nanodiscs from the mixed nanodiscs/nanocones/soot starting material, the oxidation treatment causes the attachment of oxygen-containing functional groups (epoxy, hydroxyl and carboxyl groups) on the nanodisc surface, improving the solubility in polar solvents and thereby the use in various applications. The study of the cytotoxicity properties showed that the oxidized nanodiscs can act as cytotoxic agent and promises well for their future use in nanobiocatalytic systems.

Chapter 5 presents a review of various experimental studies of the synthesis and properties of carbon nanostructures containing organic-inorganic cage-like polyhedral oligomeric silsesquioxane (POSS) nanoparticles The aim is to illustrate the improvements of chemical and physical properties that can be achieved by the combination of POSS with different carbon nanostructures focusing on the potential impact of these hybrid nanostructures on various technological applications.

Chapter 6 reports the intercalation of iron substituted (Fe^{+3}) cubic silsesquioxanes in a sodium and an acid-activated montmorillonite to form novel catalytic pillared structures. A variety of characterization techniques was applied to prove the successful intercalation of the cubic silsesquioxanes into the clay matrices as well as the formation of pillared structures after calcination. The final pillared hybrids possess high specific area and contain α-Fe_2O_3 (hematite) nanoparticles as verified by Mössbauer spectroscopy. Catalytic measurements showed that the final hybrid pillared materials catalyse the conversion of isopropanol to diisopropylether and propene due to high specific area and presence of acid sites on the surface; the selectivity is affected by stereochemical parameters.

Chapter 7 presents the fabrication of metal (Cu^{2+} and Fe^{+3}) decorated POSS thin films via the Langmuir –Schaefer method or via a combination of this method with self-assembly, using a simple surfactant such as arachidic acid (AA). Characterization with different techniques proofed the successful deposition of the layers, leading to a periodically repeated AA-Metal (Cu^{2+} and Fe^{+3})-POSS-AA unit. Moreover the interlayer distance between the units was found to be affected by the coordination of the metal ions. Additionally, comparison of the two fabrication protocols showed that the hybrid films deposited following synthetic route involving self-assembly process lead to better ordered structures.

Samenvatting

Het veld van gelaagde nanogestructureerde hybride materialen richt zich op de synthese en mogelijke toepassingen van materialen die de eigenschappen van bouwstenen van nanometer afmetingen combineert. Het samenbrengen van bouwstenen kan hun eigenschappen verbeteren of nieuwe eigenschappen genereren die niet aanwezig waren in de afzonderlijke bestandsdelen.

Het doel van dit proefschrift is de toepassing van gelaagde nanogestructureerde materialen voor milieu, medische, energie en katalytische doeleinden, beschrijving van de synthese, karakterisering en toepassingsmogelijkheden van een aantal gelaagde hybride materialen gebaseerd op koolstof allotropen of verschillende anorganische matrixen, zoals kleimineralen.

Hoofdstuk 3 beschrijft de synthese van multifunctionele gepilaarde en gelaagde materialen gesynthetiseerd door middel van intercalatie van adamantylamine in de ruimte van de tussenlaag van grafietoxide en gelaagde aluminosilicaat nanokleien. Verschillende karakterisatie technieken demonstreren de succesvolle intercalatie van adamantylamine en tonen aan dat de uiteindelijke gepilaarde materialen een verhoogd specifiek oppervlakte hebben. Hierbij is bevonden dat deze hybriden in staat zijn om significante hoeveelheden van organische verontreinigingen te adsorberen, dit heeft grote potentie voor milieu saneringstoepassingen. Bovendien bleken zij verbeterde cytotoxische activiteit te vertonen op A549 kankercellen, terwijl de cytotoxiciteit richting MRC-5 cellen (normaal) minimaal was. Dit maakt ze geschikt als antiproliferatieve middelen in biomedische toepassingen.

Hoofdstuk 4 beschrijft de chemische oxidatie van koolstof nanoschijven, industrieel bereid via de zogenoemde pyrolytische Kværner Carbon Black & H_2 proces, naar de formatie van een hydrofiele analoog. De gedetailleerde karakterisering van het ongerepte en het geoxideerde materiaal is beschreven en het onderzoek naar de cytotoxische eigenschappen van de geoxideerde nanoschijven gerapporteerd. Naast de resulterende afscheiding van de koolstof nanoschijven uit het gemengde nanoschijven/nanokegels/roet uitgangsmateriaal, veroorzaakt de oxidatiebehandeling ook de bevestiging van zuurstofhoudende functionele groepen (epoxy-, hydroxyl-, en carboxylgroepen) aan het nanoschijf oppervlak., Dit leidt tot een betere oplosbaarheid in polaire oplosmiddelen waardoor het bruikbaar wordt voor verschillende toepassingen. Het onderzoek naar de cytotoxiciteit eigenschappen toont aan dat de geoxideerde nanoschijven op kunnen treden als cytotoxisch middel, wat veelbelovend is voor toekomstig gebruik in nanobiokatalytische systemen.

Hoofdstuk 5 geeft een overzicht weer van verschillende experimentele studies naar de synthese en eigenschappen van koolstof nanostructuren welke organische-anorganische kooi-achtige veelhoekige oligomeer silsesquioxaan (POSS) deeltjes bevatten. Het doel is om te demonstreren welke verbeteringen van chemische en fysische eigenschappen kan worden behaald door POSS met verschillende koolstof nanostructuren te combineren, gericht op de mogelijke impact van deze hybride nanostructuren op verschillende technische toepassingen.

Hoofdstuk 6 beschrijft de intercalatie van ijzer gesubstitueerde (Fe^{3+}) kubische silsesquioxanen in een natrium en zuur geactiveerd montmorilloniet om nieuwe katalytische gepilaarde structuren te vormen. Verschillende karakterisatietechnieken zijn toegepast om de succesvolle intercalatie van de kubische silsesquioxanen in de kleimatrixen en de vorming van gepilaarde structuren na calcinatie aan te tonen. De uiteindelijke gepilaarde hybrides bezitten een hoog specifiek oppervlakte en bevatten α-Fe2O3 (hematiet) nanodeeltjes, wat geverifieerd is door middel van Mössbauerspectroscopie. Katalytische metingen tonen aan dat de uiteindelijke gepilaarde hybride materialen de omzetting van isopropanol naar diisopropylether en propeen katalyseren vanwege de hoge specifieke oppervlakte en de aanwezigheid van zure groepen op het oppervlak; de selectiviteit wordt beïnvloed door stereo-chemische parameters.

Hoofdstuk 7 beschrijft de fabricage van metaal (Cu^{2+} en Fe^{3+}) gedecoreerde POSS dunne lagen door middel van de Langmuir-Schaefer methode of door een combinatie van deze methode met zelfassemblage, gebruik makend van een eenvoudige oppervlakteactieve stof zoals arachidonzuur (AZ). Karakterisering met verschillende technieken heeft bewezen de depositie van de lagen, wat tot een periodiek herhalend AA-Metaal (Cu^{2+} en Fe^{3+})-POSS-AA eenheid leidt. Bovendien is bevonden dat de tussenlaag afstand tussen de eenheden beïnvloed wordt door de coördinatie van de metaalionen. Daarnaast toonde vergelijking tussen beide fabricage protocollen aan dat de gedeponeerde hybride lagen gevolgd door de synthetische route, welke het zelfassemblage proces bevatte, leidde tot beter geordende structuren.

Περίληψη

Ο τομέας των φυλλόμορφων νανοδομημένων υβριδικών υλικών επικεντρώνεται κυρίως στη σύνθεση και στις πιθανές εφαρμογές υλικών που συνδυάζουν τις ιδιότητες των δομικών τους μονάδων σε κλίμακα νανομέτρων. Συνδυάζοντας αυτές τις δομικές μονάδες μπορούμε να βελτιώσουμε ή και να δημιουργήσουμε νέες ιδιότητες οι οποίες δεν ήταν παρούσες στα επιμέρους αρχικά μας υλικά. Στόχος της παρούσας διατριβής είναι ο σχεδιασμός και η ανάπτυξη ολιγοστρωματικών νανοδομημένων υβριδικών υλικών για περιβαλλοντικές, βιο-ιατρικές ενεργειακές και καταλυτικές εφαρμογές. Πιο συγκεκριμένα, στο πόνημα αυτό περιγράφεται η σύνθεση, ο χαρακτηρισμός και οι πιθανές εφαρμογές μια πληθώρας υλικών που έχουν σαν βάση αλλοτροπικές δομές του άνθρακα ή άλλα ανόργανα υλικά όπως οι φυλλόμορφοι άργιλοι.

Το κεφάλαιο 3 περιγράφει την σύνθεση πολυλειτουργικών υποστυλωμένων υλικών τα οποία έχουν αναπτυχθεί μέσω της ενσωμάτωσης μορίων αμινοαδαμαντίνης στον ενδοστρωματικό χώρο οξειδίου του γραφίτη και φυλλόμορφων αργιλοπυριτικών αργίλων. Οι διάφορες τεχνικές χαρακτηρισμού που χρησιμοποιούνται αποδεικνύουν την επιτυχή ενσωμάτωση της αμινοαδαμαντίνης καθώς και ότι τα τελικά υποστυλωμένα υλικά παρουσιάζουν αυξημένη ειδική επιφάνεια. Επιπροσθέτως τα υβριδικά υλικά βρέθηκαν να έχουν σημαντική προσροφητική ικανότητα οργανικών ρύπων γεγονός που τα καθιστά κατάλληλα για χρήση σε περιβαλλοντικές εφαρμογές. Επιπλέον παρουσιάζουν βελτιωμένη κυτταροτοξική ικανότητα σε καρκινικά κύτταρα (A549) σε σχέση με υγιή κύτταρα (MRC-5) στα οποία η δράση τους είναι ελάχιστη γεγονός που τα καθιστά κατάλληλα να χρησιμοποιηθούν ως ανασταλτικοί παράγοντες ανάπτυξης σε βιο-ιατρικές εφαρμογές.

Στο κεφάλαιο 4 περιγράφεται η χημική οξείδωση νανοδίσκων άνθρακα που έχουν παραχθεί βιομηχανικά μέσω της πυρολυτικής διαδικασίας Kværner Carbon Black & H_2 και ο σχηματισμός ενός υδρόφιλου αναλόγου. Περιγράφεται ο λεπτομερής χαρακτηρισμός τόσο του αρχικού όσο και του οξειδωμένου υλικού καθώς και μελέτη των κυτταροτοξικών ιδιοτήτων του οξειδωμένου υλικού. Κατά την οξείδωση των νανοδίσκων επιτυγχάνεται ο διαχωρισμός τους από το μίγμα νανοδίσκων/νανοκώνων/καταλοίπων του αρχικού υλικού και η δημιουργία λειτουργικών ομάδων οξυγόνου (επόξυ-, υδρόξυ-, καρβόξυ-) στην επιφάνεια τους βελτιώνοντας την διαλυτότητα τους σε πολικούς διαλύτες ώστε να μπορούν να χρησιμοποιηθούν σε διάφορες εφαρμογές. Η μελέτη των κυτταροτοξικών ιδιοτήτων τους έδειξε ότι οι οξειδωμένοι νανοδίσκοι δρουν ως κυτταροτοξικοί παράγοντες και αποτελούν ένα πολλά υποσχόμενο υλικό για την ανάπτυξη νανο βιοκαταλυτικών συστημάτων.

Στο κεφάλαιο 5 παρουσιάζεται μια ανασκόπηση διαφόρων πειραματικών μελετών πάνω στην σύνθεση και τις ιδιότητες νανοδομών άνθρακα που περιέχουν οργανικά-ανόργανα πολυεδρικά ολιγομερή σιλοξάνια (POSS) (cage-like). Στόχος είναι να τονιστεί η βελτίωση των φυσικοχημικών ιδιοτήτων που επιτυγχάνεται με προσθήκη τους επικεντρώνοντας στον αντίκτυπο που μπορεί να έχουν τα υβριδικά αυτά υλικά σε διάφορες τεχνολογικές εφαρμογές.

Στο κεφάλαιο 6 αναφέρεται η ενσωμάτωση υποκατεστημένων κυβικών σιλοξανίων του σιδήρου (Fe^{+3}), σε νατριούχο μοντμοριλλονίτη καθώς και στο όξινα ενεργοποιημένο ανάλογό του με σκοπό την δημιουργία καινοτόμων καταλυτικών υποστυλωμένων δομών. Μια πληθώρα τεχνικών χαρακτηρισμού εφαρμόστηκε ώστε να αποδειχθεί η επιτυχής ενσωμάτωση των σιλοξανίων στις αργιλικές μήτρες καθώς και ο σχηματισμός υποστυλωμένων δομών μέσω τις θέρμανσης τους. Τα τελικά παραγόμενα υλικά βρέθηκαν να διαθέτουν μεγάλη ειδική επιφάνεια ενώ η παρουσία νανοσωματιδίων αιματίτη (α-FeO_3) επιβεβαιώθηκε μέσω της φασματοσκοπία Mössbauer. Καταλυτικές πειραματικές μετρήσεις έδειξαν ότι τα τελικά υβριδικά υλικά καταλύουν την αφυδάτωση της ισοπροπανόλης σε προπένιο και διισο-προπυλαιθέρα λόγω της μεγάλης ειδικής επιφάνειας και των ενεργών καταλυτικών κέντρων στην επιφάνεια τους ενώ η εκλεκτικότητα προς την διάσπαση της ισοπροπανόλης επηρεάζεται από στερεοχημικές παραμέτρους

Στο κεφάλαιο 7 παρουσιάζεται η δημιουργία λεπτών ολιγοστρωματικών υμενίων υποκατεστημένων με μέταλλα (Cu^{2+} και Fe^{+3}) πολυεδρικών ολιγομερικών σιλοξανίων (POSS) μέσω της μεθόδου Langmuir –Schaefer ή με συνδυασμό της με τη μέθοδο αυτο-οργάνωσης (self-assembly) με τη χρήση μιας απλής τασιενεργής ένωσης όπως το αραχιδικό οξύ (AA). O χαρακτηρισμός με διάφορες τεχνικές απέδειξε την επιτυχή εναπόθεση των στρωμάτων της τασιενεργής με αποτέλεσμα την δημιουργία περιοδικών δομικών μονάδων που αποτελούνται αντίστοιχα από στρώματα αραχιδικού οξέος και υποκατεστημένων με μέταλλα (Cu^{2+} και Fe^{+3}) POSS. Επιπλέον, η ενδοστρωματική απόσταση μεταξύ των δομικών μονάδων εξαρτάται από την γεωμετρία και τον αριθμό ένταξης των μεταλλικών ιόντων. Επιπροσθέτως η σύγκριση των δύο πειραματικών πρωτοκόλλων σύνθεσης έδειξε ότι τα υβριδικά υμένια που έχουν εναποτεθεί με τη συνδυασμένη συνθετική διαδικασία που περιλαμβάνει το στάδιο της αυτό-οργάνωσης των μορίων οδηγούν σε καλύτερα οργανωμένες δομές.

Acknowledgements

This PhD thesis is the result of an effort that started 4 years ago at the Ceramics and Composites Laboratory in University of Ioannina and was continued at the Zernike Institute for Advanced Materials in University of Groningen. During this time I had the chance to meet and work with a lot of people that contributed not only in scientific manner in this thesis but also helped me to adjust more smoothly in the different working and living environments .At this point I would like to express my gratitude to my 2 supervisors Prof Petra Rudolf and Prof Dimitrios Gournis.

Petra I remember the first day that we met in your office when I had just arrived at Groningen. Everything felt new and the truth is that I was a bit in panic. I want to thank you for making me feel welcomed. I also want to thank you for helping and advising me especially during the time I spent in your group. I learned a lot from you and I have to say that you are an inspiration for all of us.

Next I would like to thank Prof Dimitrios Gournis who guided me not only during my PhD but also during my Master studies. He was the person that convinced me to continue in science, and who taught me how to work and behave in a lab. The most important thing for me though is that after all these years I consider him family since he is always there for every member of his group.

Thanks to Prof.Meike Stöhr and Prof Michael Karakassides for their valuable contribution during my studies

I wish also to thank the members of the reading committee Prof. Francesco Picchioni, Prof. Marcella Bonchio, Prof. Alkiviadis Paipetis and Prof. George Froudakis for their willingness to read my thesis and their valuable comments and suggestions. Moreover I would like to thank the rest members of the

committee in Greece, Prof. M. Karakassides, Prof. A. Bourlinos, Prof., A. Douvalis, and Prof. H. Stamatis.

Many thanks also to Yvonne Nagelghout who makes our lives easier in such many ways and Dr. Regis Gengler who was the daily supervisor during my time in Zernike. Thanks as well to the technicians of the group Mihaela and Jos, your role as you know is always crucial.

I would also like to acknowledge Jos Noteboom and Dr.Esther Vertelaman. for translating and correcting the Dutch summary in this thesis

I would also want to thank all the collaborators during the last 4 years. Thanks to: Prof. Alexios. Douvalis, Prof. Athanasios Ladavos, Prof. Dimitrios Petrakis, Prof Dimitrios Bikiaris, Prof. Athanasios Bourlinos, Prof.H. Stamatis,.Prof. T. A. Steriotis, Prof. Angelos M. Evangelou, Prof. Yiannis Deligiannakis, Prof.Gustaaf Van Tendeloo, Prof. Yiannis Sanakis, Prof .Graeme Blake, Prof. *Bart* J. *van* Wees, Prof. Giussepe Portale, Prof. Bart Crielaard**,** Dr. Marios S. Katsiotis , Dr. Saeed Alhassan, Dr. T. Tsoufis, Dr. M. Patila, Dr. Z. Sideratou, Dr. F. Katsaros, Dr. G. Charalambopoulou, Dr. Andreas Rossos, Dr. Myrsini Antoniou, Dr. Ke Xiaoxing, Dr. Ioannis Verginadis, Dr. Anastasia Velalopoulou, Karolin Romhild and Eleni Seristratidou.

Thanks a lot to the members (or former members) of the 2 groups that beside collaborators are most of them now also good friends: Souzana, Fouli, Apostoli, Maria M., Afroditi, Maria A., Kosta V, Kosta D., Kosta S., Giouli, Vasili, Klairi, Christina, Lefteri, Eleni P., Kyriakh ,Lena, Theodosi, Niko, Ali, Leonid, Jiquan, Sumit, Tashfeen, Martina, Peter, Bey, Ahn, Juan Carlos, Jun Li, Lam, Nico, Florian, Madhu and Stefano.

Special thanks to Antonis that supported me and helped me to overcome every difficulty during the last years.

I should also thank my friends in Groningen: Aggeliki, Eygenia, Giorgo, Thanasi, Amanda, Kosta, Mino, Sofokli for making feel more like home.

I would also like to acknowledge the European Union (European Social Fund – ESF) and Greek national funds through the Operational Program "Synergasia" and the Ubbo Emmius Programme for funding me during my studies

Last I wish to thank my family for always supporting and believing in me.

List of Publications

1. Spyrou K.*, **Potsi G.***, Diamanti E.K.*, Ke X., Serestatidou E., Verginadis I., et al. Towards Novel Multifunctional Pillared Nanostructures: Effective Intercalation of Adamantylamine in Graphene Oxide and Smectite Clays. Adv Funct Mater [Internet]. 2014; 24 (37):5841–50.
2. Zygouri P., **Potsi G.**, Mouzourakis E., Spyrou K., Gournis D., Rudolf P.. Non-covalent interactions of graphene with polycyclic aromatic hydrocarbons. Curr Org Chem. 2015; 19 (18).
3. **Potsi G.**, Rossos A., Kouloumpis A., Antoniou M.K., Spyrou K., Karakassides M.A., et al. Carbon Nanostructures Containing Polyhedral Oligomeric Silsesquioxanes (POSS) [Internet]. Vol. 20, Current Organic Chemistry. 2016. p. 662–73.
4. Simari C., **Potsi G.**, Policicchio A., Perrotta I., Nicotera I. Clay–Carbon Nanotubes Hybrid Materials for Nanocomposite Membranes: Advantages of Branched Structure for Proton Transport under Low Humidity Conditions in PEMFCs. J Phys Chem C [Internet]. 2016 Feb 11; 120 (5):2574–84.
5. Terzopoulou Z., Bikiaris D.N., Triantafyllidis K.S., **Potsi G.**, Gournis D., Papageorgiou G.Z., et al. Mechanical, thermal and decomposition behavior of poly(ε-caprolactone) nanocomposites with clay-supported carbon nanotube hybrids. Thermochim Acta. 2016; 642.
6. Madhushankar B. N., Kaverzin A., Giousis T., **Potsi G.**, Gournis D., Rudolf P., Blake G.R.,Van Der Wal C.H, Van Wees B.J. Electronic properties of germanane field-effect transistors (submitted)
7. **Potsi G.**, Ladavos A.K, Petrakis D., Douvalis A.P, Sanakis Y., Katsiotis M.S., Alhassan S., Gournis D., Rudolf P., Iron-substituted cubic silsesquioxane pillared clays: Synthesis, characterization and catalytic applications (to be submitted)
8. Zygouri P., Tsoufis T., Kouloumpis A., Patila M., **Potsi G.**, Sideratou Z., Katsaros F., Charalambopoulou G., Stamatis H, Rudolf P., Steriotis T.A., Gournis D., Hydrophilic oxidized carbon nanodiscs: A promising multifunctional nanocarbon for bioapplication (to be submitted)

*__Equal contribution__